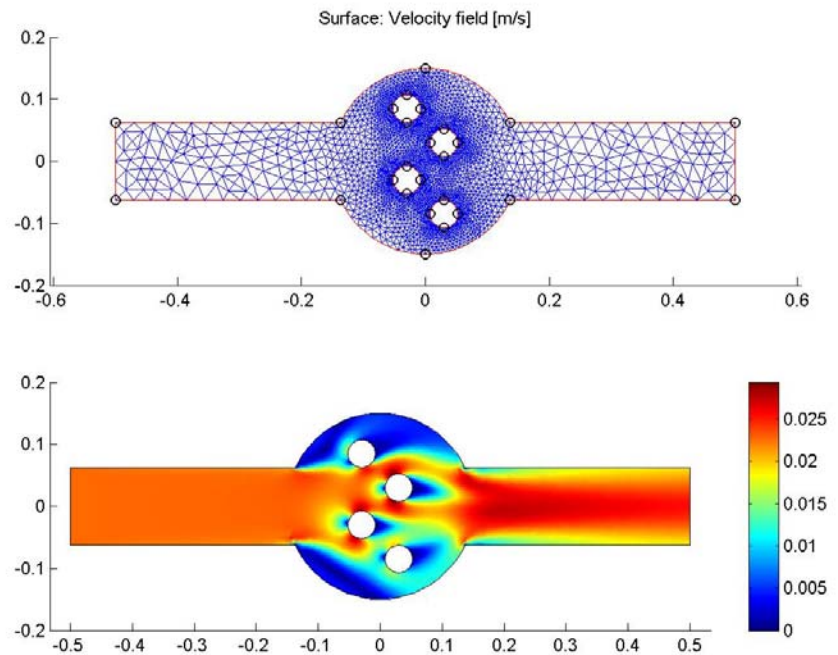
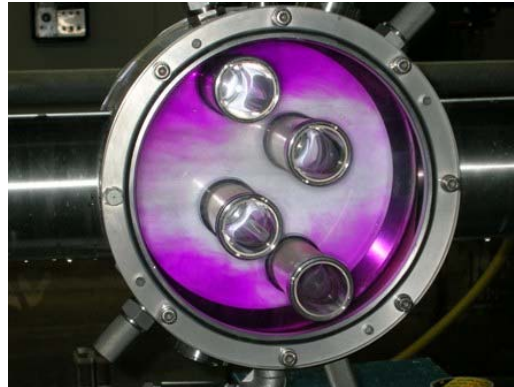


Degradation of 4TBP by AOP, UV Reactor Modeling and Validation

July, 2007

Lanzhu Shao



Department of Water Management
Sanitary Engineering Section



Degradation of 4TBP by Advanced Oxidation Process, CFD Modeling and Validation for UV Reactor

Lanzhu Shao
Student number 1284509
July, 2007

A dissertation submitted in partial fulfillment of the requirements for the degree of
Master of Science in Civil Engineering, specialization Water Management

Examination Committee:

Prof.ir.J.C.Van Dijk

Delft University of Technology, Faculty of Civil Engineering and
Geosciences, Section Water Management

Dr.ir.L.C.Rietveld

Delft University of Technology, Faculty of Civil Engineering and
Geosciences, Section Water Management

Dr.ir.J.A.M.H.Hofman

Kiwa Water Research, Section of Integrated Water Treatment

Dr.ir.W.S.J.Uijttewaal

Delft University of Technology, Faculty of Civil Engineering and
Geosciences, Section Environmental Fluid Mechanics



ACKNOWLEDGEMENTS

The present report is the result of the research project undertaken in order to obtain the degree of Master of Science in Civil Engineering at Delft University of Technology. During a period of two months, experimental research has been executed at Tongji University, Shanghai, China. Afterwards, months of model building up and validation work have been done at Kiwa Water Research and Delft University of Technology in the Netherlands. The research has been supported by a lot of institutions and people. I would like to thank them all here.

Two months stay in China appeared to be a great study and a very valuable experience. I would like to thank all the members who attended the workshop in Shanghai for developing a new alternative treatment scheme for drinking water. I would like to thank Professor Naiyun Gao and teachers as well as students at Tongji University who helped me to conduct the lab work there.

I would like to thank Kiwa Water Research and TU Delft, who provided this research project and supported me during this study. And my thanks also go to the hydraulic engineering laboratory at TU Delft and the staff working there for their fast and great support during my experiments.

I would like to thank you my great professor, Prof.ir.J.C.van Dijk, for his great encourage and support during my study, I learned a lot from him for how to be a good civil engineer. I would also like to thank my supervisors, Dr. J.A.M.H.Hofman and Dr.ir.L.C. Rietveld, for giving me the opportunity to work with them, also for their supervisory skills and encouragement during my research. Many thanks also go to Ir.B.A.Wols for the knowledge he had to share on CFD modeling.

I also would like to thank you my graduation committee Prof.ir.J.C.van Dijk, Dr.ir.L.C. Rietveld, Dr. J.A.M.H.Hofman, Dr.ir.W.S.J.Uijtewaal for their kind cooperation, enthusiasm and feedback on this research project.

Special thanks for Mr. Koichi Domoto for all the encouragements I have got from him during all my master study.

Delft, July 2007
Lanzhu Shao

ABSTRACT

Advanced Oxidation Processes (AOPs) are innovative, cost-effective, catalyzed chemical oxidation processes for treating pollutants in low or high concentration from contaminated soil, sludge and water. The common used AOPs in drinking water treatment include UV/H₂O₂ process, UV/Ozone Process, UV/Titanium Dioxide and Fenton's Reagent. AOPs are ultraviolet driven, which share predominance from photochemical technology, and often, give the clients dual benefit of both environmental contaminant treatment and disinfection.

Endocrine Disrupting Chemicals (EDCs) are very disturbing contaminants measured in natural waters. Phenols and their tert-butyl derivatives are important contaminants belonging to EDCs. After a successful workshop for developing alternative drinking water treatments at Shanghai, AOPs with UV/H₂O₂ technology are chosen to remove 4-tert-butylphenol (4TBP) from Shanghai water. The kinetics of reaction was studied in the first part of this thesis. The results show that UV/H₂O₂ process can effectively decrease 4TBP concentration than hydrogen peroxide alone. Good free oxidation radical production can be achieved within UV dose range from 0 to 200mJ/cm² by a low pressure mercury lamp. The 4TBP degradation process fits with pseudo first order equation for UV-dose and H₂O₂-dose. However, at very high H₂O₂-doses, the scavenging of hydroxyl-radicals needs to be taken into account.

Computational Fluid Dynamics (CFD) modeling of UV reactor and validation of CFD model were studied in the second part of this thesis work in order to provide an applicable UV reactor design for the 4TBP treatment and also give possible reactor improvement suggestions. The CFD model used in this study is a 2-D model developed using software Comsol, V3.3a, based on a current UV reactor design at Kiwa Water Research, the Netherlands. The developed UV dose model includes three parts, a k-ε flow model, a UV intensity model and a random walk model. Different feed flow rates and different lamp configurations were studied by the model. The calculation results show that a higher feed flow rate contributes to a relative narrow UV dose distribution than the lower flow rate. With three lamp configurations, position 0 is the best among the three with the highest average UV dose as well as the narrowest dose distribution pattern. Model also predicted low pressure lamps have about 8% higher power output to UV dose efficiency than medium pressure lamps.

Validation of the flow model was helped by flow measurements at Delft University of Technology. Experimental studies of velocity measurements by Laser Doppler Velocity Meter were conducted together with salt and dye dose experiments. After comparisons of model predictions and experimental measurements, it was found that the k-ε CFD flow model demonstrated generally good qualitative prediction of flow

inside the reactor but failed to give correct prediction of recirculation zones behind the quartz tubes. There are dead zones of water at the top and bottom near the inlet of the reactor. Bigger areas exist behind the quartz tubes that have water recirculation than the model predicted, which may result 25% of more UV dose prediction by the model. And differences caused by 2-D model and 3-D measurements may result about 20% less UV dose model prediction.

Current UV reactor design at Kiwa Water Research, position 0 and low pressure mercury lamps applied at a feed flow rate of $4.1\text{m}^3/\text{h}$ appears to be an applicable design for advanced oxidation treatment of 4TBP by UV/H₂O₂ in Shanghai. High roughness quartz tubes walls and relative smaller ratio of reactor to feed pipe diameters are recommended to improve reactor performance in the recirculation and dead zones with current design. Further investigations of the dose model and UV-sensitive dyed microspheres particle tracking experiments are recommended.

ACKNOWLEDGEMENTS	i
ABSTRACT	ii
CHAPTER 1	- 1 -
INTRODUCTION	- 1 -
1.1 Background	- 1 -
1.2 Research Motivation and Objective	- 2 -
1.3 Outline of Thesis	- 3 -
CHAPTER 2	- 4 -
THEORY AND LITERATURE REVIEW OF AOPs	- 4 -
2.1 UV Photolysis Basics	- 4 -
2.1.1 Background	- 4 -
2.1.2 UV radiation	- 4 -
2.1.3 Propagation of UV light	- 5 -
2.1.4 UV Dose and Dose Distribution	- 6 -
2.1.5 Different UV lamp types	- 7 -
2.1.6 UV Reactor	- 8 -
2.2 Advanced Oxidation Processes	- 9 -
2.2.1 Introduction	- 9 -
2.2.2 Transition State Theory	- 10 -
2.2.3 Chemical Kinemics	- 10 -
2.2.4 UV/H ₂ O ₂ Process	- 12 -
2.2.3 Fenton's Reagent	- 15 -
2.2.4 Ultraviolet/Ozone	- 16 -
2.2.5 UV/Titanium Dioxide	- 16 -
2.3 Byproducts of Direct UV Irradiation and AOPs	- 16 -
2.4 Parameters Impacting AOPs Efficiency	- 17 -
CHAPTER 3	- 19 -
DEGRADATION OF 4TBP BY UV/H ₂ O ₂ TREATMENT	- 19 -
3.1 Background	- 19 -
3.1.1 Organic Contaminants in Natural Water Environment	- 19 -
3.1.2 Endocrine Disrupting Substances	- 19 -
3.1.3 Application of AOPs	- 20 -
3.2 Materials and Methods	- 20 -
3.2.1 Water	- 20 -
3.2.2 Reagent	- 21 -
3.2.3 Photolysis Equipment-Collimated Beam	- 21 -
3.2.4 Analysis Apparatus-Liquid Chromatograph	- 23 -
3.3 Advanced Oxidation Experimental Procedure	- 24 -
3.4 Results and Discussions	- 24 -
3.4.1 Degradation of 4TBP with H ₂ O ₂ Only	- 24 -
3.4.2 Degradation of 4TBP with UV/H ₂ O ₂ Process	- 26 -

3.5 Conclusions and Recommendations	- 31 -
CHAPTER 4	- 32 -
THEORY OF CFD MODELLING AND VALIDATION	- 32 -
4.1 Introduction.....	- 32 -
4.2 Introduction of CFD.....	- 32 -
4.2.1 What is CFD?.....	- 32 -
4.2.2 Elements of CFD.....	- 33 -
4.2.3 Problem solving with CFD	- 34 -
4.3 Modeling for UV based water treatment processes	- 34 -
4.4 CFD Validation	- 36 -
CHAPTER 5	- 37 -
THE CFD MODEL FOR UV DOSE CALCULATION	- 37 -
5.1 Introduction.....	- 37 -
5.2 Problem Geometry and Formulation	- 37 -
5.3 Mesh of the Model.....	- 38 -
5.4 Building up of Flow Model.....	- 39 -
5.4.1 Reynolds Averaged Navier-Stokes Equations.....	- 39 -
5.4.2 k- ϵ model.....	- 40 -
5.4.3 Boundary condition settings	- 41 -
5.4.4 Flow model predictions	- 42 -
5.5 Building up of UV irradiation model.....	- 44 -
5.5.1 UV intensity without reflection and refraction	- 44 -
5.5.2 Refraction and Snell's Law	- 46 -
5.5.3 Reflection and the Fresnel laws	- 47 -
5.5.4 Factor setting for the UV intensity model.....	- 47 -
5.5.5 UV intensity model prediction.....	- 48 -
5.6 UV dose model	- 48 -
5.6.1 Random-walk theory.....	- 48 -
5.6.2 Calculation of UV dose.....	- 50 -
5.6.3 UV dose model prediction	- 50 -
5.7 Conclusions.....	- 59 -
CHAPTER 6	- 61 -
FLOW MODEL VALIDATION	- 61 -
6.1 Introduction.....	- 61 -
6.2 Experiment Apparatus and Materials.....	- 61 -
6.3 Flow Velocity Measurements.....	- 62 -
6.3.1 Theory	- 62 -
6.3.2 Experimental set-up	- 64 -
6.3.3 Experiment Procedures	- 66 -

6.4 Flow Velocity Measurements.....	- 67 -
6.4.1 Measurement cross sections.....	- 67 -
6.4.2 Velocity vectors comparisons	- 68 -
6.4.3 Well predicted area.....	- 70 -
6.4.4 Poorly predicted area	- 71 -
6.4.5 Failed prediction of circulation behind the quartz tubes.....	- 72 -
6.4.6 2-D model with 3-D flow measurements.....	- 73 -
6.4.7 Possible influences on the UV dose prediction.....	- 74 -
6.5 Salt dosing experiment.....	- 75 -
6.5.1 Theory	- 75 -
6.5.2 Experimental set-up and procedures.....	- 76 -
6.5.3 Results for salt dosing experiments	- 77 -
6.6 Dye experiment.....	- 78 -
6.6.1 Experimental set-up and procedures.....	- 78 -
6.6.2 Results and discussions of dye experiment.....	- 79 -
6.7 Conclusions and Recommendations	- 81 -
6.7.1 Conclusions.....	- 81 -
6.7.2 Recommendations.....	- 81 -
CHAPTER 7	- 84 -
CONCLUSIONS AND RECOMMENDATIONS.....	- 84 -
7.1 Introduction.....	- 84 -
7.2 Conclusions.....	- 84 -
7.3 Recommendations.....	- 85 -
REFERENCE	- 86 -

CHAPTER 1

INTRODUCTION

1.1 Background

The enormous diversity of toxic and organic pollutants of various chemical compositions eliminates the possibility of using a universal treatment method and has led to the fast development of special treatment methods for decontamination [Yu. M, 2005]. Among the most promising emerging chemical oxidation processes, Advanced Oxidation Processes (AOPs) have provided innovative, cost-effective, catalyzed chemical oxidation for treating pollutants in low or high concentration from contaminated soil, sludge and water [Parsons, 2004]. Four types of Advanced Oxidation Processes have been widely applied until now, which are UV/ H₂O₂, UV/O₃, UV/Fenton and UV/Titanium Dioxide. These UV driven processes are primarily based on utilizing the photolyzing power of ultraviolet light to generate extremely reactive intermediate oxidizing species, such as the hydroxyl radical, through the direct photolysis of hydrogen peroxide (H₂O₂), or through photo-induced processes as in the photo-Fenton type reactions or photocatalysis. An obvious advantage of this method is that it is ultraviolet driven, which shares predominance from photochemical technology, and often, gives the clients dual benefit of both environmental contaminant treatment and disinfection.

Since the late 1960s, Ultraviolet/hydrogen peroxide process (UV/H₂O₂) has been used by numerous researchers to oxidize various organic substances from groundwater, drinking water, and municipal and industrial wastewaters. This method has an advantage over traditional treatments, such as aeration and granular activated carbon, in that the contaminant in question can be degraded into other compounds possibly removing from the environment. In addition to its environmental friendly aspect, other advantages are that no bromate is formed in this process compared with UV/ozone and that the application itself is quite clean and simple [IJpelaar, 2002].

The design for the UV/ H₂O₂ water treatment operations has been traditionally relying on empirical guidelines, and hence a systematical approach into process optimization has been difficult. Because of non-uniformities in the UV irradiation intensity and flow patterns, micro-organisms traveling through a UV system will experience a broad distribution of dose, which of course, will affect the performance of the whole treatment process. Over the years, numerical models have been

developed to evaluate the effectiveness of UV systems. Perhaps the most promising numerical technique for UV system analysis is Computational Fluid Dynamics (CFD). With improved understanding of fundamental process dynamics and the development of computer flow dynamics models, process prediction and optimization becomes less time-consuming and more attractive. Several researchers have used CFD for analyzing and improving the hydraulics through UV systems [Crittenden et al., 1999; Buffle et al., 2000].

1.2 Research Motivation and Objective

In September 2006, thirty-three water treatment experts from Shanghai and The Netherlands met at a workshop in Shanghai for developing new alternative treatment processes for the future drinking water supply of Shanghai. An ambition for the alternative treatment is to guarantee safe drinking water without taste and odour. As a result of the workshop at Shanghai, Advanced Oxidation Process with UV/ H₂O₂ ended up as a promising choice.

In spite of the commercial success of the UV/H₂O₂ process, the chemistry, kinetics and engineering principles associated with this process have not been elucidated adequately, especially when the process is applied to various water qualities. Phenols and their tert-butyl derivatives are very disturbing contaminants found worldwide [Furuichi, 2004; Ce'spedes, 2005]. The first part of this study attempts to add to the existing literature through an experimental investigation of the effect of the UV/ H₂O₂ process parameters on the process performance in term of oxidation rate of 4-tert-phenol (4TBP), which is a new contaminant that will be listed in the Chinese Drinking Water Guideline 2007.

A good performance of advanced oxidation in real applications asks for a well designed UV reactor. The objective of UV reactor design is to approach a uniform UV dose distribution through the total treatment volume. However, the direct calculation of UV dose distribution is difficult because of complicated hydrodynamic of reactor and there is no method until now to measure that directly within a continuous flow reactor. In order to find an applicable UV reactor design for the 4TBP treatment in Shanghai with a known dose prediction, the extensive work of the second part of this study was brought, focusing on Computational Flow Dynamic model which helps calculate the dose distribution of an existing UV reactor design and validation of this model. After the model validation, improvements of the existing design are suggested.

1.3 Outline of Thesis

Chapter 1 is the introduction and layout of this study, which explained the background, research motivation and objectives.

Chapter 2 gives a comprehensive review of the theory of Ultraviolet Photolysis, focusing on Advanced Oxidation Technology. Kinetics and Mechanism of AOPs processes are provided, for the four main kinds of AOPs. In the last part of this chapter information is provided about UV by-product formation.

In Chapter 3, the collimated beam UV/H₂O₂ experimental study at Tongji University, Shanghai, People's Republic of China is presented. The kinetics for the treatment was studied using low pressure mercury lamp to remove 4-tert-butylphenol from local Shanghai water got from Taihe Water Plant.

Chapter 4 introduces the theory and literature review of Computational Flow Dynamics, which is so called CFD. History of CFD applications was reviewed, and elements of building up a CFD model were also introduced.

Chapter 5 presents the CFD model built for AOPs application in this study, which is composed of a flow model, a UV intensity field model and a free walk model. The model ends up with a prediction of UV dose distribution.

Chapter 6 is the experimental study of flow measurements for validation of CFD flow model developed in Chapter 5. Velocity measurements, salt dose and dye inject experiments were conducted.

Finally, Chapter 7 provides conclusions of the research and recommendations for further research on this topic.

CHAPTER 2

THEORY AND LITERATURE REVIEW OF AOPs

2.1 UV Photolysis Basics

2.1.1 Background

Over the past two decades, there has been a growing interest in the application of photochemical technologies, particularly driven by the overall public concern about the removal of pollutants from contaminated environment [USEPA, 2003]. Photochemical technology is simple and clean, cost-effective in many applications, and, often, has disinfection benefit. UV light has been widely used to disinfect effluent from wastewater treatment facilities, especially those ones that reused for irrigation purpose. Disinfection by means of UV irradiation has already been used widely in North America [Lyn et al., 1999]. Researchers found that UV photolysis can effectively inactivate *Cryptosporidium* at low dosage [Buhkari et al., 1999]. Before Buhkari's study, it was widely known that UV could effectively inactivate bacteria, and at higher dose, inactivate viruses. To inactivate parasites such as *Cryptosporidium* by the way of UV was not even considered and thought to be impractical. The work of Buhkari largely changed all the old thinking and gave UV a wider application. UV technology has improved significantly over the past decade and UV system is now well defined and can offer versatile and realizable performance at relatively low costs. In UV direct photolysis, the contaminant must adsorb radiation and undergo degradation starting from its excited state. Because normally low concentrations of contaminants are present in the polluted water and photolysis efficiency is low, direct UV photolysis is not applied as much in commercial use as UV driven advanced oxidation processes (AOPs).

2.1.2 UV radiation

UV radiation is usually defined as the electromagnetic spectrum of wavelength between 10 and 400 nm [CRC Handbook, 1991] according to other sources, between 4 and 400 nm [Koller, 1965], covering the gap between visible light and X-ray regions. For UV photolysis application in water treatment, the UV spectrum range of interest is the UVC (200-280nm) [Phillips, 1983]. There is also UVB within 280-320 nm range. Figure 2.1 shows the electromagnetic spectrum from 100 to 1000nm. From

the figure, Vacuum UV (100-200nm), UVC (200-280nm), UVB (280-315nm), and UVA (315-400nm) form the whole UV range [Parson, 2004].

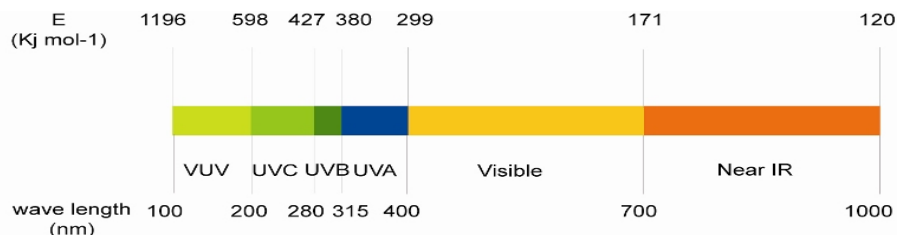
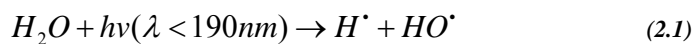


Figure 2.1 Spectrum of the electromagnetic radiation [Phillips, 1983]

Besides UVC, the vacuum UV (VUV) region (100-200 nm) is also interesting for AOPs, since these radiations are adsorbed by water and generate highly reactive species for oxidation of pollutants in the water.



In order to activate reaction, the energy carried by UV radiation should be larger than the dissociation energy of the compound.

2.1.3 Propagation of UV light

UV light will undergo absorption, scattering, reflection and refraction when it propagates from its source and interacts with materials it enters. Absorption and scattering theory is given here and the reflection and refraction aspects will be explained later in Chapter 5 when discussing the building up of the CFD flow model.

Absorption is the transformation of light to other forms of energy as it passes through a substance. UV absorption of a substance varies with the light wavelength. Scattering of light is the change in direction of light propagation caused by interaction with a particle. Particles can cause scattering in all directions. When assessing water quality, UV absorption or UV transmittance is the parameter which incorporates absorption and scattering. UV absorption is widely used to define the decrease in the amount of incident light as it passes through a sample over a specified distance or path-length. UV transmittance (UVT) is used to characterize the absorption, by

$$\%UVT = 100 \times 10^{-A_{254}} \quad (2.2)$$

where

UVT=UV transmittance at a specified wavelength (e.g.,254nm) and path-length (e.g.,1cm)

A₂₅₄=UV absorbance at specified wavelength (e.g. 254nm) and path-length (e.g., 1 cm)

When applied for water treatment, the light absorption capacity of background water is very important because the UV light intensity the pollutants really get will be affected a lot from the absorption of background water.

2.1.4 UV Dose and Dose Distribution

UV dose is defined as UV energy per unit area that is incident on a surface. UV dose is the product of the average intensity acting on a microorganism from all directions and the exposure time. And the UV dose in a batch system can be determined by multiplying the calculated average intensity by specific exposure time. Dose delivery in a continuous-flow reactor is subject to hydrodynamic irregularities and a variable UV intensity distribution and is a function of the UV absorbance of the water, the quartz over the UV lamps, the flow rate through the reactor, the UV output from the lamps, and the hydraulic characteristics within the reactor. As such, it is difficult to calculate directly the UV dose over the reactor. Numerical modeling is often used for calculations of UV dose within a continuous-flow reactor. The difference in UV dose experienced by microorganisms in a flowing reactor is best characterized by a dose distribution.

A UV dose distribution is the probability distribution of UV doses that microorganisms receive in a flow through reactor. Some microorganisms move through the reactor more quickly than others, and some of them travel circuitous paths.

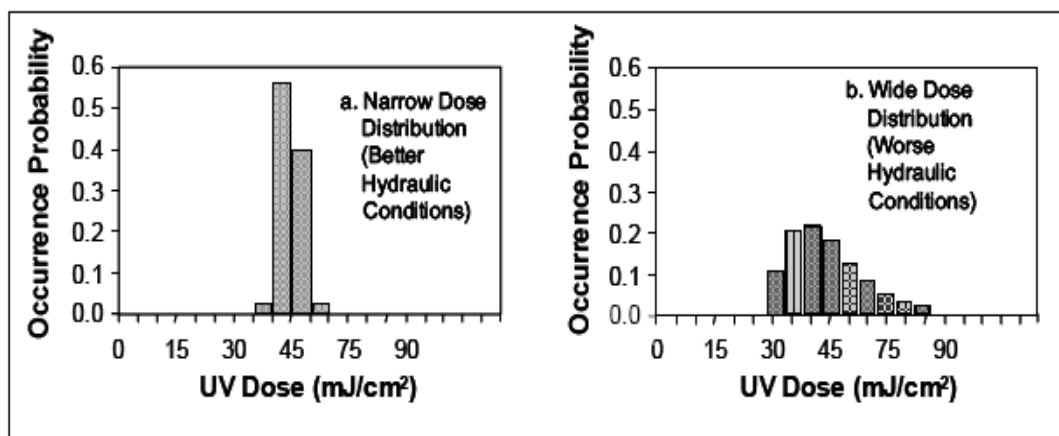


Figure 2.2 Hypothetical dose distribution for two reactors with differing hydraulics

A narrow dose distribution indicates more ideal hydrodynamic conditions. A wider distribution indicates less efficient reactor performance and results in a greater degree of ‘overdosing’ to ensure that the minimum dose needed is achieved for the microorganisms at the lower end of dose distribution.

2.1.5 Different UV lamp types

There are two kinds of UV lamps widely used in water treatment applications, which are low-pressure and medium/high-pressure lamps. A typical UV lamp is similar in construction to the fluorescent lights we see in the offices and homes everyday. In this case, the glass tube contains mercury; while electricity is applied, the tube emits light.

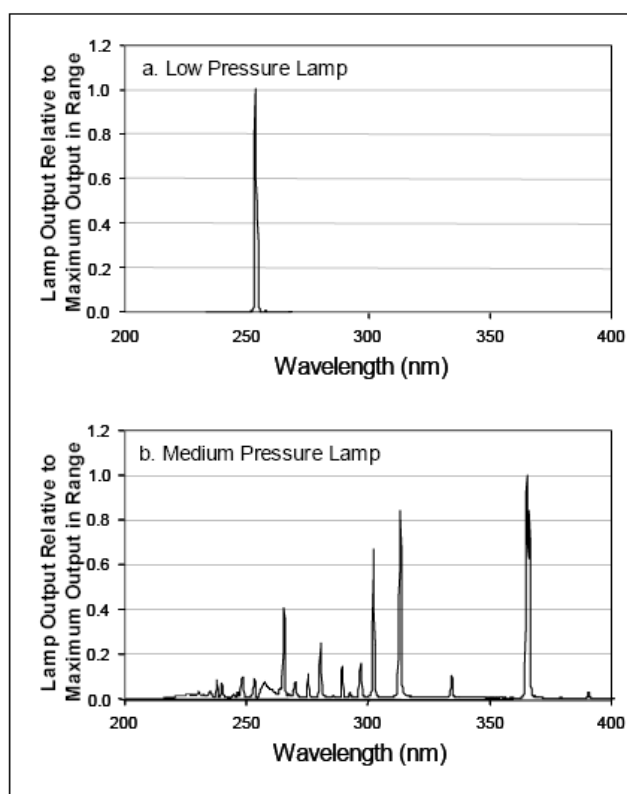


Figure 2-3 UV output of LP (a) and MP (b) Mercury Vapor Lamps [Sharpless and Linden , 2001]

Low pressure lamps produce almost all of their UV output at a wavelength of 253.7nm (85%-90%) and about 7-10% at 184.9nm. However, for the radiation from 184.9nm wavelength the water itself is the main absorber and this wavelength is filtered out by ordinary quartz. So normally, for low pressure lamps, only 253.7nm wavelength is considered to be the interesting wavelength for UV photolysis applications. Since DNA and RNA are scrambled best at this wavelength, a low pressure lamp will inactivate microorganisms. These lamps generally convert up to 38% of their input watt into usable UV-C watts, which is much higher than other classes of lamps. Low pressure lamps typically run on low-input power about 0.5 to 10 W/cm at an optimal operation temperature around 40 °C–130 °C, and ordinary lamp lifetime is about 8,000 to 12,000 according to the operating current of the lamp.

Medium/high-pressure lamps generate polychromatic UV lights and the spectral distribution of the radiation emitted covers a wide wavelength range, from UVV to IR. And the lamp spectrum is characterized by multiple lines superimposed on a small continuum, which indicates that there is some radiation at all UV wave-lengths. The wide emission in the UV and visible spectral is from 200nm to 600nm and has a high germicidal UV output. These lamps generally convert only 10%-20% of input watts into UV light. The remaining is converted into heat and visible light. The input electrical power is 50-250 W/cm, and operating temperature varies from 600-900 °C. Ordinary life time for a lamp is from 1,500 to 10,000 hours [USPEA, 2003].

For all kinds of lamps, lamp aging will happen, and lamp aging can be affected by the following factors:

Ballast operation, including power setting, frequency, and harmonic distortion of the voltage and current driving the lamp

Water temperature and heat transfer from lamps

Vibration of the lamp sleeves caused by water flowing through the reactor

The frequency of on-off cycles

2.1.6 UV Reactor

The goal in designing a UV reactor for drinking water treatment is to distribute the UV light efficiently and uniformly through the reactor, and approach plug-flow behavior of the water as it flows through the reactor. Thus an uniform exposure to the radiation field will be achieved in the whole treatment volume, in other words, a uniform UV dose distribution.

Reactors are designed to optimize dose delivery, and the reactor hydrodynamics plays an important role in design. Lamp placement, inlet and outlet conditions, and baffles all affect mixing within a reactor. Improvements to the hydraulic behavior of a reactor are always interesting to researchers.

An example UV reactor is shown in figure 2-4, which has a similar design as the reactor used in Chapter 6 of this study. This is a typically closed channel UV reactor which is used in drinking water applications. The commercial UV reactors consist of closed channel vessels containing UV lamps, lamp sleeves (made by quartz most of the time). UV intensity sensors, lamp sleeves wipers, and temperature sensors. UV lamps are located within the lamps sleeves, which protect and insulate the lamps from the water. UV intensity sensors, flow meters are used to monitor dose delivery over the reactor.

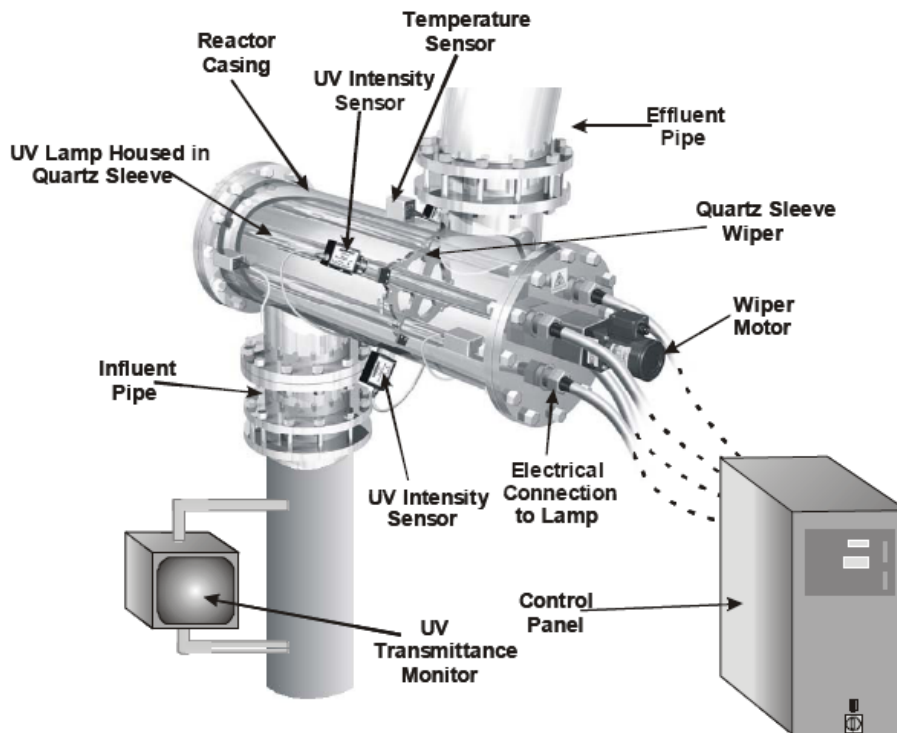


Figure 2-4 UV reactor schematic

2.2 Advanced Oxidation Processes

2.2.1 Introduction

Glaze and Kang (1990) defined advanced oxidation processes (AOPs) as ambient temperature processes that involve the generation of highly reactive radical intermediates, particularly the hydroxyl radical. The aim of AOPs is to mineralize the pollutants in water by oxidation, which can convert the constituents of an organic pollutant into simple, relatively harmless and inorganic molecules. The study of AOPs application in the Netherlands started in the early nineties in the last century. At that time, bromate, which is formed by parallel oxidation of bromide by ozone, was found to be a suspected carcinogen. From that time, studies on ozonation of pre-treated water for degradation of a wide range of organic substances for drinking water have switched to AOPs [IJpelaar, 2002]. The commonly used AOPs include UV/H₂O₂ process, UV/Ozone Process, UV/Titanium Dioxide and Fenton's Reagent.

2.2.2 Transition State Theory

Transition State Theory tells that there is an activation energy barrier in elementary reaction, and the colliding molecules must have sufficient energy to overcome this energy barrier to react. This theory indicates that the rate of a reaction is not a matter of energy alone, but also requires a preferred configuration by a change of entropy. Decreasing the enthalpy of the reaction could speed up the reaction itself. This is the fundamental theory under lining the speed of the AOPs reaction, which provides guidance for the search of the most efficient AOPs.

In terms of thermodynamics, normal oxidants such as oxygen, ozone and hydrogen peroxide will form activated complexes with organic pollutants with large enthalpy. This reaction is thermodynamically less favorable than reactions between hydroxyl radicals and organic compounds, during which the enthalpy change are really several orders smaller. Therefore, converting these ordinary oxidants to hydroxyl radicals first could increase reaction rates significantly.

Thus AOPs could be found by any combination of oxidants such as oxygen, ozone, and hydrogen peroxide with catalysts such as UV photons, transition metals and ultrasound.

2.2.3 Chemical Kinemics

Chemical kinetics of AOPs focuses on the rate of a reaction through studying the concentration profile with time. The chemical reaction itself can be classified as zero, first, or second order based on the number of reactants involved. The simplified mathematic descriptions of the chemical kinetics of the various orders are given below:

2.2.2.1 Zero-Oder Reactions

The rate law for a zero order reaction can be expressed as

$$-\frac{dA}{dt} = k[A_0]^0 = k \quad (2.3)$$

Where A is the concentration of reactant, and t is the time for reaction, k is the reaction rate constant.

The above equation 2.3 can be integrated as 2.4:

$$\int_{A_0}^A dA = -k \int_0^t dt \quad (2.4)$$

Therefore, the time required to reduce half of the concentration of reactant A is:

$$t_{1/2} = \frac{1/2A_0}{k} = A_0/2k \quad (2.5)$$

The rate constant could be expressed as:

$$k = \frac{A_0}{2t_{1/2}} \quad (2.6)$$

The rate of zero-order reaction is independent of the concentration of the reactant and the unit of the rate constant of zero-order reaction is $(\text{time})^{-1}(\text{concentration})^{-1}$.

2.2.2.2 First-Order Reactions

The rate law for the first-order reaction is:

$$\frac{dA}{dt} = -k[A] \quad (2.7)$$

Therefore, the time dependence of concentration A is:

$$-\ln[A] = -kt + \text{constant} \quad (2.8)$$

The concentration profile of reactant A is:

$$\frac{[A]_t}{[A]_0} = -kt \quad (2.9)$$

Therefore, the rate constant k is

$$k = \frac{\ln 2}{t_{1/2}} \quad (2.10)$$

Where the unit of k is $(\text{time})^{-1}$

For each AOP, the degradation rate is investigated to search for the most efficient process.

2.2.2.3 Second-Order Reactions

The rate law for the second-order reaction can be expressed as:

$$\frac{dA}{dt} = -k[A][B] \quad (2.11)$$

Where, A and B are the concentration of reactants, t is the reaction time and k is the reaction rate constant.

Assume the x moles of reactants A and B have been reacted and x moles of C have been produced, then the production rate of C should be:

$$\frac{dx}{dt} = k(A_0 - x)^1(B_0 - x)^1 \quad (2.12)$$

After integration of this equation,

$$\int_0^x \frac{dx}{k(A_0 - x)(B_0 - x)} = \int_0^t dt$$

$$kt = \frac{1}{B_0 - A_0} \ln \frac{A_0(B_0 - x)}{B_0(A_0 - x)}$$

$$k = \frac{1}{t_{1/2} A_0} \quad (2.13)$$

where the unit of rate constant k should be (time)⁻¹(concentration)⁻¹.

2.2.4 UV/H₂O₂ Process

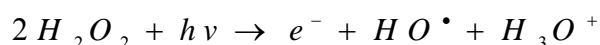
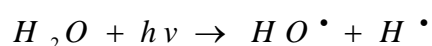
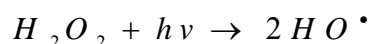
2.2.4.1 Background

The UV/H₂O₂ process may degrade organic contaminants either directly by photolysis or indirectly by hydroxyl radicals. It has been applied to remove a wide range of toxic hazardous substance from ground water, drinking water and wastewaters [AOP handbooks, 1997,1998; Watts et al., 1990, 1991]. The first commercial application of UV/H₂O₂ process emerged in 1977 after Koubek (1975) at the U.S. Naval Academy was awarded a patent for his work on ‘oxidation of refractory organics in aqueous waste streams by hydrogen peroxide and ultraviolet light’. During the last decade’s full-scale application of this technology has become commercially available. UV/H₂O₂ process could also cause significant pesticide degradation and the formation of harmful by-products proved to be insignificant [Kruithof, 2002].

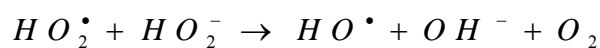
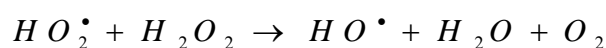
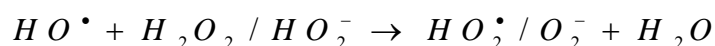
2.2.4.2 Theory of UV/H₂O₂ process

During UV/H₂O₂ process, hydroxyl radicals initiate oxidation reactions when the photo wavelength is greater than 254nm, otherwise, the direct photolysis takes the major responsibility. Those reactions generate organic radicals which could continuous react with OH^\bullet and produce final products from organic contaminants. The enhanced oxidizing ability of H₂O₂ is due to production of hydroxyl radicals (HO^\bullet), pre-hydroxyl radicals (HO_2^\bullet), and super-oxide anion (O_2^-) under the irradiation of UV light. The molar extinction coefficient of H₂O₂ at 254nm is 19.6M⁻¹s⁻¹ [Lay, 1989], which is very low. Comparatively, the molar extinction coefficients of ozone, naphthalene and pentachlorophenol (at pH7) are 3300, 3300

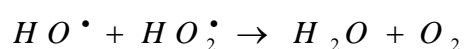
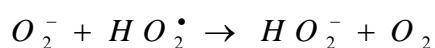
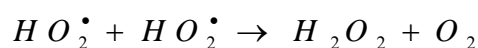
and $10,000 \text{ M}^{-1}\text{cm}^{-1}$ respectively. This means that the concentration of H_2O_2 has to be rather high in order to generate a sufficiently high level of OH radicals in a solution which contains strong photon absorbers. For the most commonly applied low-pressure mercury vapor lamps with a 254nm peak emission, the most absorbance of H_2O_2 occurs at about 220nm. Because of low-absorption coefficient when applying low pressure lamps, a high concentration of H_2O_2 is needed to generate enough hydroxyl radicals. However, the high concentration of H_2O_2 scavenges the radicals, and the reactions mentioned terminates explains what will happen. During the process, the possible reactions are showed in the followings:



Propagation



Termination



2.2.4.3 UV Photolysis in UV/ H_2O_2 process

In an advanced oxidation process, degradation of the organic compound can happen either by direct or indirect photolysis. In order to undergo photochemical transformation, light energy should be adsorbed by the molecule to produce an electronically excited state molecule and chemical transformations of the excited state should be competitive with deactivation processes.

The rate of direct photolysis of a chemical compound at a concentration [C] is:

$$-\frac{d[C]}{dt} = I_0 \phi_c f_c (1 - \exp(-A_t)) \quad (2.14)$$

Where ϕ_c is the quantum yield of C, which is the fraction of adsorbed radiation that results in photolysis, and I_0 is the incident flux of radiation (254nm in this case). The factor f_c is the ratio of light absorbed by C to that absorbed by other components of the solution and A_t is the total absorbance of the solution times a factor of 2.3.

When concentration of absorbers is very large, $\exp(-A_t)$ is approximately zero, and the equation above could be simplified to:

$$-\frac{d[C]}{dt} = I_0 \phi_c f_c \quad (2.15)$$

When C is a minor absorber, its rate of decay will be first order and when C is the principle absorber, its rate will be zero order. When the concentration of absorbers is small, $[1-\exp(-A_t)]$ could be expanded in a Taylor series to yield the familiar first order expression [Leifer, 1988]:

$$-\frac{d[C]}{dt} = 2.3 I_0 \phi_c \varepsilon_c [C], \quad (2.16)$$

where $\varepsilon_c [C]$ is the absorbed radiation.

2.2.4.4 Mechanism of UV/H₂O₂ process

The elimination rate of organic compounds has at least two contributions: direct photolysis and hydroxyl-radical attack. The mechanism for the process is usually described as follows:

$$-\frac{d[C]}{dt} = I_0 \phi_c f_c (1 - \exp(-A_t)) + k_{OH,C} [OH][C] \quad (2.17)$$

The first part of the equation shows the effect of direct photolysis and the second part is the result from hydroxyl-radicals. $k_{OH,C}$ is the second-order reaction rate constant of hydroxyl radical with compound C. When the concentration of hydroxyl radical is assumed to be constant over the range of reaction, pseudo-first-order rate can be applied

$$-\ln \frac{C}{C_0} = k't \quad (2.18)$$

Where k' is the pseudo-first-order constant, s^{-1} .

However, because H₂O₂ itself is a hydroxyl radical scavenger [Christensen et al., 1982], there is a limit beneficial effects of added peroxide ($K_{OH,H_2O_2} = 2.7 \times 10^7 M^{-1} s^{-1}$).

2.2.4.5 UV/H₂O₂ Process in Drinking Water Applications

The treatment of natural humic water with UV (254nm) and H₂O₂ was studied by Backlund (1992). Both dissolved organic carbon contents and UV absorbance of the water decreased substantially during the treatment. The decreases were dependent on the time of irradiation as well as on the H₂O₂ dose applied. The humic molecules had been degraded to smaller fragments during the irradiation. Oxalic acid, acetic acid, malonic acid and n-butanoic acid are the main degradation products detected.

Parkinson et al. (2001) studied the removal of natural organic matter (NOM) in two Australian waters by UVA, UVB, UVC and UV/H₂O₂. The toxicity of the water was examined by Vibrio Fisheri-based Microtox test, Daphna carinata acute immobilization test and African green monkey kidney cell test. No significant toxicity was monitored in any of the tests for all the irradiated samples. This result is different from the report from Frimmel (1998). Frimmel indicated that both UVA and UVB irradiated aqueous NOM samples contains significant toxicity to Daphnia magna.

The degradation of NOM was also studied by Wang et al. (2000) by solar and high pressure mercury vapor lamp and H₂O₂. In their research, the optimum dose of H₂O₂ was found to be 0.01% and the NOM oxidation and H₂O₂ degradation followed first-order and zero-order reaction kinetics respectively.

Degradation and by product formation of diazinon in water during UV and UV/H₂O₂ treatment by Shemer and Linden (2006) studied used both LP and MP lamps UV sources in a quasi-collimated beam apparatus. Hydrogen peroxide assisted degradation of diazinon was found more efficient as compared to direct photolysis. The high reactivity of diazinon with the hydroxyl radical was reflected in its high rate constant (k_{OH}) value of $(9.0 \pm 0.4)E-9 \text{ M}^{-1}\text{s}^{-1}$. The trace byproduct diazoxon was detected during the reaction, but this byproduct can be further degraded.

2.2.3 Fenton's Reagent

In 1881, Fenton published a brief description of powerful oxidizing properties of a mixture of hydrogen peroxide and ferrous salts. This mixture was the well-known Fenton's reagent, the reaction became known as the Fenton's reaction. In 1934, Haber and Weiss studied Fenton's reaction and concluded that this reaction can be expressed as a series of chain reactions with reaction pathways dependent on the concentration of the reactants. In the late 1980s, Fenton's reagent was applied to the field of environmental science. Various contaminants were studied in the laboratory to determine the optimum circumstances. Practical application has also been found by pilot-plant and continuous treatment systems in wastewater.

2.2.4 Ultraviolet/Ozone

The UV/Ozone process is largely used for decomposition of toxic organic compounds often found in surface water as well as ground water. Photolysis, ozonation and reactions of hydroxyl radicals are three dominant reactions to degrade organic pollutants during UV/Ozone treatment processes. Physical parameters such as temperature, pH, UV intensity, initial compound and ozone concentrations, and ozone partial pressure will affect the reaction rate and removal efficiency of compound. However, the generation of hydroxyl radicals is still essential in this process.

UV irradiation, pH and the presence of free-radical scavengers could influence the decomposition rate of ozone. There are four major factors affect the oxidation rate of organic pollutants: pH, relative concentration of oxidants, photon flux in the UV/O₃ system and radical scavenger concentration. However, this reaction has a disadvantage that a by-product bromate could be found after the treatment of bromide-containing waters.

2.2.5 UV/Titanium Dioxide

Titanium Dioxide (TiO₂) is an excellent catalyst for semiconductor photo-catalysis due to its good environmental engineering applications. It is also the most widely used catalyst in photo-catalytic degradation of organic pollutants because of its suitable band-gap energy of 3.05eV over a wide range of pH.

Photo-catalytic oxidation is a surface-catalyzed reaction and the chemical must first be adsorbed onto the TiO₂ surface before it can undergo photo-catalytic oxidation. The fundamental theory for UV/TiO₂ reaction involves photo-excitation and hydroxyl radical formation.

2.3 Byproducts of Direct UV Irradiation and AOPs

For UV disinfection, byproducts arise either directly through photochemical reactions or indirectly through reactions with products of photochemical reactions. Photochemical reactions will only take place if a chemical species absorbs UV light, and the resulting excited state reacts to form new species. This resulting concentration of new species will depend on the concentration of the reactants and the UV dose.

In drinking water applications, research has focused on the impact of UV light on the formation of disinfection byproducts after subsequent chlorination and the transformation of organic material to more degradable components. Over years, direct

reactions with UV irradiation had been thought not to produce by-products of any kind [Wolf, 1990]. For ground water and filtered drinking water, UV disinfection at typical dose has been shown no impact on the formation of trihalomethanes or haloacetic acids, two categories of disinfection byproducts currently regulated by the United States Environmental Protection Agency [Malley et al., 1995; Kashinkunti et al., 2003]. The conversion of nitrate to nitrite is possible with MP lamps that emit at low wavelengths [Von Sonntag and Schuchaman, 1992]. But due to the low conversion rate [about 1 percent; Sharpless and Linden, 2001], this is of minimal concern in drinking water applications. However in the presence of nitrates or nitrites, studies show that elevated levels of mutagenic substances are formed from various amino acids on irradiation of water under neutral conditions [Mole, 1999].

By-products are also found in the AOPs, mainly from the degradations of organic contaminants in water. In addition, some of them are found to be present long after the contaminants have been oxidized. In 1999, Richardson and her colleagues identified 3-methyl-2,4-hexanedione as a by product of UV/TiO₂ treatment. Later, Chang and Young (2000) found the use of AOP in treating water contaminated with MTBE (methyl-tert-butyl ether) was successfully oxidized, but a by-product tert-butyl formate (TBE) was left. And a significant amount of TBF was also formed and it persisted after the MTBE had been degraded. In 2005, research by Adedapo [Adedapo, R. Y., 2005] found that when UV/H₂O₂ processes are applied to drinking water treated with chlorine, fewer post-UV chlorination disinfection by-products (PCDBPs) than UV photolysis. Besides these, bromate is a famous disinfection byproduct (DBP) of the ozonation of bromide-containing water.

2.4 Parameters Impacting AOPs Efficiency

Reactor design Different reactors even those using the same lamp type can have significantly different efficiency for a particular water and contaminant due to reactor characteristics, such as lamp spacing, lamp configuration (horizontal, vertical, parallel, perpendicular and angled), place of inlet and outlet piping relevant to lamps, numbers of pipe diameter upstream and downstream of the reactor, baffles and other interior mixing devices.

Water quality Absorption of UV by water itself is quite important in AOPs application. Produced electrical energy per order is influenced by water transmittance over the spectral UV range of interest. Some common constituents that affect water transmittance are dissolved NOM, nitrate and ferrous/ ferric ions. Therefore, the implementation of upstream water treatment processes can have a positive effect on the performance of UV treatment system.

Lamp type In general, MP pressure lamps are applied for AOPs treatment because higher power output comparing with LP lamps. But people are keeping using LP lamps for the longer lamp life and relatively higher energy converge rate.

Lamp age Lamp power output will decrease as a lamp ages, that is, more power is required at the end of lamp life than at the beginning in order to achieve the same performance.

Design flow rate Water flow rates in the reactor is important because the longer retention time the water in the reactor, more UV dose the same water face will get. The efficiency of AOPs under same lamp conditions decreases as the flow rate increases.

Contaminant characteristics Treatment efficiency also depends on the molar absorption coefficients of the target contaminant over the spectral range emitted by the lamp, and on the quantum yield of UV photolysis.

CHAPTER 3

DEGRADATION OF 4TBP BY UV/H₂O₂ TREATMENT

3.1 Background

3.1.1 Organic Contaminants in Natural Water Environment

Recently, the increasing occurrence of organic contaminants in the natural water environment has attracted a lot of concern from the society. This problem was first identified in the last seventies, and throughout the last three decades, there have been increasing number of reports of presence of these chemical compounds in natural water systems [Sch, 1970, Sow,1980].

The contaminants concentration discovered range from the order of a few nanograms per liter in surface waters to a few micrograms per liter in waste water effluents. For most substances, such concentrations do not pose a direct threat to human health and do not cause immediate environmental problems but are rather alarming because their effects and fates in the environment during long time period of existing are not clearly understand.

3.1.2 Endocrine Disrupting Substances

A very disturbing type of contaminants measured in natural waters is Endocrine Disrupting Chemicals (EDCs). EDCs are natural or manmade chemicals, which can interfere with the endocrine system. A more broad definition of EDCs is that they are exogenous chemical agents that interfere with the synthesis, secretion, transport, binding, action, metabolism, or elimination of natural hormones. They are a group of chemicals with diverse structures [USEPA, 1997]. There is concern, and some evidence from aquatic populations, that EDCs can give rise to changes that could lead to disruption of wild populations. For instance, male fish can change to female when exposed to a mixture of persistent EDCs [GWRC, 2003].

In many cases, it is not yet clear how EDCs affect human health. However, EDCs are suspected of causing various types of human cancer, including breast cancer, prostate cancer, and testicular cancer. Over the past 50 years, the incidence of prostate cancer in some countries has doubled. It has similarly been shown that since 1940 the

incidence of female breast cancer has risen in Western Europe and the US. A number of studies have shown the presence of residues of DDT and other organochlorine pesticides in human breast milk and adipose tissue. Exposure to these pesticides has been implicated in breast cancer risk [Yu, 2004]. At this moment there is no firm evidence that environmental endocrine disrupting chemicals cause health problems at low levels of exposure. Since compounds have been detected in animal with hormonal functions and structures related to those in humans, it is possible that man will eventually be affected by the huge concentration of oestrogen-mimicking compounds which are spreading throughout the environment [Sha, 1998]. The fact that high levels of chemicals can impair human healthy leads to raising concerns about the possible harmful effects of EDCs even at low background levels[Barlow et al.,1999].

Phenols and their tert-butyl derivatives are important contaminants belonging to the group of EDCs. Recently, 4-tert-butylphenol (4TBP) has come on the blacklist of EDCs contaminants by U.S. Environmental Protection Agency. 4TBP is used to make alkylphenol polyethoxylate (APE) surfactants and plasticizers. It has an immediate toxicity on human, which can cause serious allergy on skin, and extremely toxic to human membranes, which may lead to death. It also disturbs human endocrine system [Haavisto and Adamsson, 2003].4TBP has been discovered in surface waters worldwide; reports show its concentration in Japan surface water is 6.9~47.5 ng/L [Ruruichi, 2004], and the maximal concentration of 4TBP measured from Spain river water is 21.9µg/L [Ce'spedes, 2005].

3.1.3 Application of AOPs

There has been a study of 4TBP transformation by the influence of UV and combination of microwave and UV [Cirkva et al., 2005]. Advanced Oxidation Processes (AOPs) have been investigated for removal of EDCs in the water, and there are studies that show good results for degradation of EDCs [Sun, 2007]. In this chapter, UV/H₂O₂ technology was applied to 4TBP contaminated Shanghai water, the kinetics of this reaction was studied.

3.2 Materials and Methods

3.2.1 Water

The water used in this study was taken from Taihe Water Plant, which is located in the northeast of Shanghai Municipality and uses Yangtze River water as raw water intake source. The treatment process scheme of Taihe water plant is: raw water,

chlorination, flocculation, sedimentation, filtration, secondary chlorination and effluent. The water after filtration and before the secondary chlorination was used. This studied water had nearly the same water quality as the effluent of Taihe Water Plant except the values of bacteria, including E. Coli, and was almost free of residual Chlorine. The water was kept in the refrigerator with constant temperature at 4°C. The pH was 7.4, and measured turbidity was 0.33NTU, higher than that of the 2003 yearly average Taihe Water Plant Effluent Water [Water Quality of Taihe Water Plant, 2006].



Figure 3-1 Filters and Water Sample at Intake, Taihe Water plant

3.2.2 Reagent

The reagent chosen for this study is 4-tert-butylphenol (4TBP), a white crystalline powder, which was brought from ALDRICH, the purity is 99+%. All solutions were prepared with the product water from Taihe Water Plant.

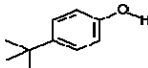
CAS NO	Molecule weight (g/mol)	Molecular formula	Melting point (°C)	Water Solubility mg/L	Structural formula	Log K _{ow}
98-54-4	150	C ₁₀ H ₁₄ O	96 ~ 100	>600(25°C)		3.04-3.31

Table 3-1 Physical and Chemical Properties of 4TBP

3.2.3 Photolysis Equipment-Collimated Beam

The experiment used a bench-scale device which is called collimated beam apparatus. The apparatus delivers UV light usually to a microbial suspension contained within a completely mixed batch reactor. The UV light enters the suspension with a near zero degree angle of incidence and is relatively homogenous across the surface area. UV dose delivered to the suspension is calculated using measurements of incident UV

intensity, exposure time, suspension depth and the absorption coefficient of the suspension. All the experiments were carried out by the collimated beam apparatus at Tongji University, Shanghai, People's Republic of China.

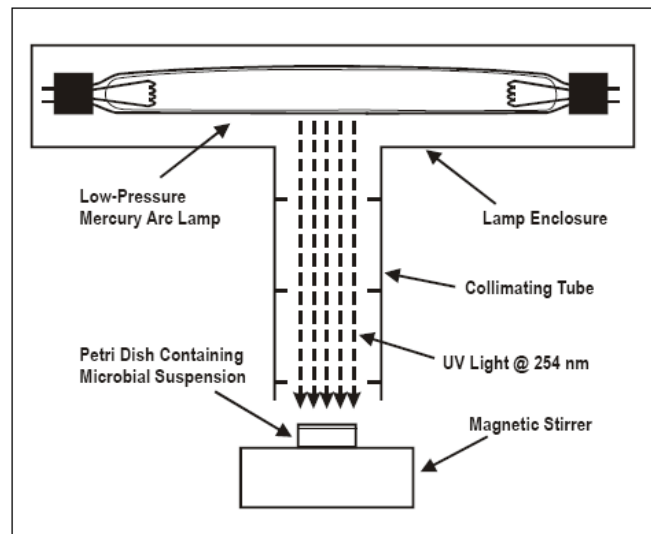


Figure 3-2 Collimated Beam Principle (top) and Used Collimated Beam Apparatus in the Study (bottom)

The collimated beam apparatus available at Tongji University can be equipped with different types of UV lamps. Water samples of 40 mL were irradiated in a Petri dish, which can be located at a flexible distance from the UV lamp. The intensity of the UV lamp was measured with UV-B illuminometer, from Beijing Shifan University, Beijing, People's Republic of China.

In this study, a low pressure mercury UV lamp was applied (GPH287T5L/4p) and the main irradiation spectrum was 253.7nm. The irradiation times were determined by a well-known method [Bolton, 2002]. Calculating the irradiation times no corrections were applied. The radiometer reading at the center of Petri Dish was $141\mu\text{w}/\text{cm}^2$, and the average Germicidal Irradiance throughout the water volume was $82\mu\text{w}/\text{cm}^2$. The detailed calculation sheet is given in Appendix 1. No loss of 4-TBP due to volatilization or/and hydrolysis was observed in unexposed stirred samples.

3.2.4 Analysis Apparatus-Liquid Chromatograph

Quantification of 4TBP was performed on a Liquid Chromatograph (Daojin LC-2010AHT) with Shim-pack VP-ODS chromatograph pole (150mm×4.6mm). The mobile phase was de-mineralized water, methanol and acetonitrile (Fish USA). All the samples were tested after 72 hours after end of the experiment.



Figure 3-3 Liquid Chromatograph Used in the Experiment at Tongji University

3.3 Advanced Oxidation Experimental Procedure

4TBP solution (392.8 μ g/L) was prepared with Taihe Water at room temperature (around 20°C). Different initial H₂O₂ concentration water samples were prepared by adding H₂O₂ into the 4TBP solutions. 40mL of mixture water sample was put into a 9cm Petri dish under the beam from the UV lamp for a range of time from 1 minute to more than 2 hours according to the calculation results from irradiation time table. This calculation was based on the relation between UV Dose and irradiation time. During the experiments, stirring was applied to ensure good mixture of the water sample.

UV Dose (mJ/cm ²)	Irradiation Time Applied (s)
0	0
10	122
25	304
50	609
100	1217
200	2434
300	3651
600	7303

Table 3-2 UV Dose and Irradiation Time Applied

3.4 Results and Discussions

3.4.1 Degradation of 4TBP with H₂O₂ Only

There was a study in the past that showed initial concentration of H₂O₂ does not have significant effect on 4TBP degradation after adding H₂O₂ within 90 minutes [Li, 2006]. But the performance at longer residence time was not mentioned in the old literature.

In this study, in order to get more ideas of H₂O₂ performance, a certain amount of H₂O₂ was added to prepared 4TBP solution. After 72 hours, the concentration of 4TBP was measured and compared to the original value.

Table 3-3 gives the measurement results for this experiment. A clear decreasing trend of 4TBP concentration was found with increasing concentration of H₂O₂. When the H₂O₂ concentration was 10mg/L in the mixed sample, the 4TBP degradation was already more than 20%. With increasing initial H₂O₂ concentrations, the value of C/C₀ decreased. However, the decreasing trend was not evident from 20mg/L to 60mg/L of H₂O₂ concentration, while the value of H₂O₂ concentration trebled, the addition

achieved 4TBP decomposition was only 2%. However, when adding H₂O₂ concentration to 100mg/L, the degradation reaction was speed up again, which was indicated by a steeper slope at the right end of figure 3-4. The results show that H₂O₂ alone does have a degradation effect on 4TBP after 72 hours. In the tables and figures mentioned below, C represents the measured concentration of 4TBP, while C₀ is the initial concentration value.

H ₂ O ₂ (mg/L)	C(μg/L)	C ₀ (μg/L)	C/C ₀
0	308.078	309.038	0.996894
10	309.038	392.528	0.787302
20	295.605	392.528	0.75308
40	290.203	392.528	0.739318
60	287.939	392.528	0.73355
100	257.156	392.528	0.655128

Table 3-3 4TBT Concentration Change after 72 Hours with Different Initial H₂O₂ concentration

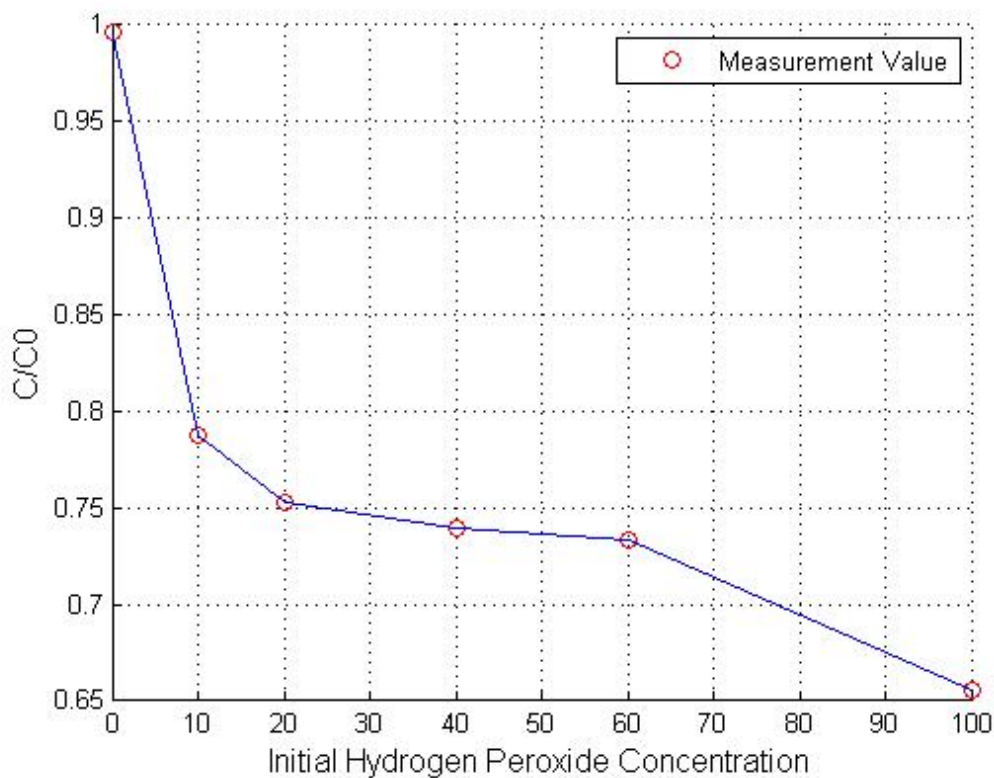


Figure 3-4 Degradation of 4TBP with Different Initial H₂O₂ Concentrations

3.4.2 Degradation of 4TBP with UV/H₂O₂ Process

UV degradation of 4TBP experiments were performed at 10,20,40,60,100 mg/L H₂O₂ concentrations to examine the kinetics of 4TBP destruction with increased UV dose and hydrogen peroxide concentration.

3.4.2.1 Influence of UV Dose

Eight UV doses were applied in the experiments, and the UV irradiation time was calculated from the calculation table [Bolton, 2002]. From the control of irradiation time, UV dose was applied to the water sample. Two of the results from the experiments are given below:

UV Dose	C(μ g/L)	C ₀ (μ g/L)	C/C ₀	Ln(C/C ₀)	Time(s)
0 mJ/cm ²	309.038	392.528	0.7873018	-0.2391436	12.171
10 mJ/cm ²	275.851	392.528	0.702755	-0.352747	121.7
25 mJ/cm ²	269.307	392.528	0.6860835	-0.3767559	304.3
50 mJ/cm ²	208.062	392.528	0.5300565	-0.6347718	608.6
100 mJ/cm ²	172.66	392.528	0.4398667	-0.8212835	1217.1
200 mJ/cm ²	100.753	392.528	0.2566772	-1.3599359	2434.2
300 mJ/cm ²	90.604	392.528	0.2308218	-1.4661095	3651.4
600 mJ/cm ²	98.567	392.528	0.2511082	-1.3818714	7302.7

Table 3-4 4TBP degradation results of UV dose with H₂O₂ initial concentration=10mg/L

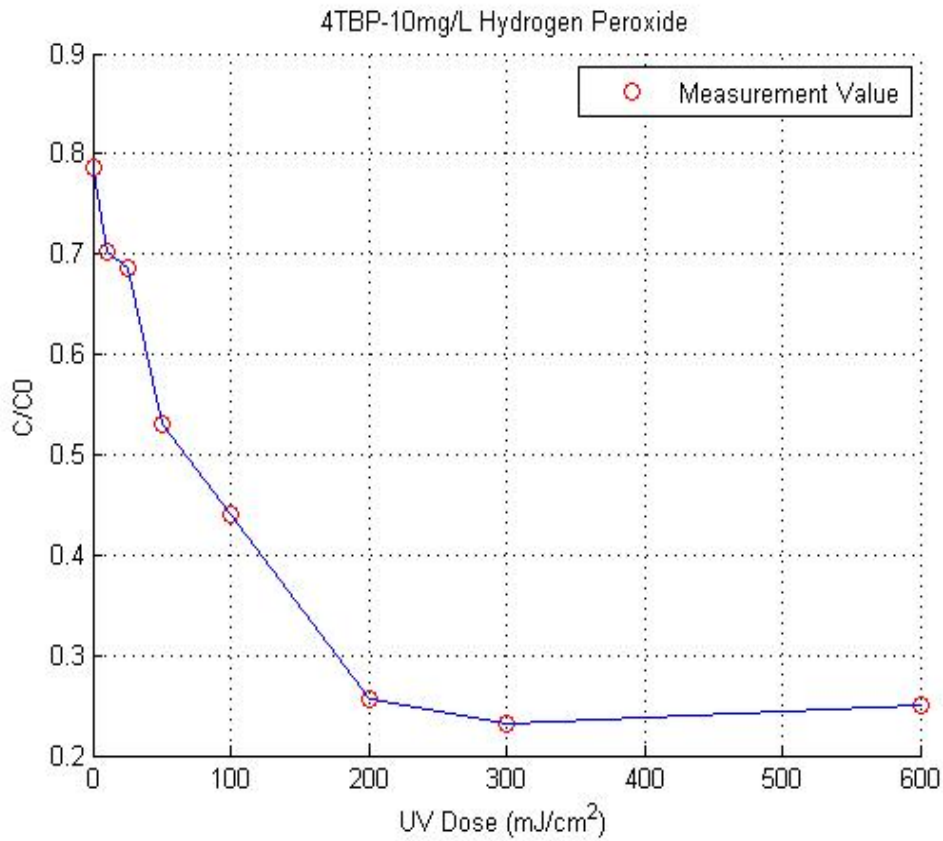


Figure 3-5 Degradation of 4TBP with 10mg/L H₂O₂ concentration

UV Dose	C(μg/L)	C ₀ (μg/L)	C/C ₀	Ln(C/C ₀)	Time(s)
0 mJ/cm ²	257.156	392.528	0.6551278	-0.422925	12.171
10 mJ/cm ²	223.008	392.528	0.5681327	-0.5654002	121.7
25 mJ/cm ²	126.891	392.528	0.3232661	-1.1292794	304.3
50 mJ/cm ²	128.013	392.528	0.3261245	-1.1204761	608.6
100 mJ/cm ²	46.041	392.528	0.1172935	-2.1430756	1217.1
200 mJ/cm ²	17.021	392.528	0.0433625	-3.13816	2434.2
300 mJ/cm ²	14.663	392.528	0.0373553	-3.2872806	3651.4
600 mJ/cm ²	14.586	392.528	0.0371591	-3.2925457	7302.7

Table 3-5 4TBP degradation results of UV dose with H₂O₂ initial concentration=100mg/l

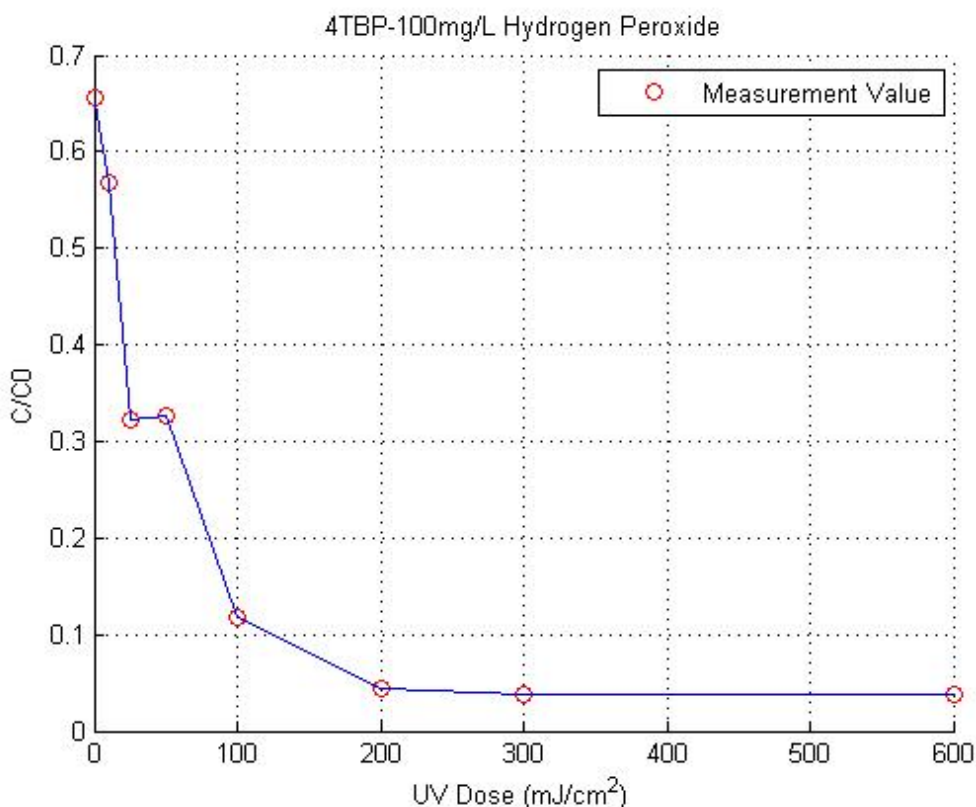


Figure 3-6 Degradation of 4TBP with 100mg/L H₂O₂ Concentration

From Figure 3-5 and Figure 3-6 it can be seen that UV/H₂O₂ process can effectively degrade 4TBP in the water sample. When 10mg/L of H₂O₂ concentration was applied, at the beginning, before irradiated by UV, the concentration decrease was only about 20%, but when UV dose increased up to 600mJ/cm², the degradation degree went up to around 75%. The reduction degree keeps increasing until the 200 mJ/cm² UV dose. In Table 3.5 it can also find that even with 100 mg/L H₂O₂ concentration and 600mJ/cm² UV dose, there was still residual 4TBP in the sample, 3.7% 4TBP was left.

With other H₂O₂ concentrations, the results were also following the same trend: degradation degree of 4TBP was increasing with increased amount of UV dose and stopped increase at around 200 mJ/cm² of UV dose. This indicated no hydroxyl radical generation from UV dose of 200~600 mJ/cm² in the experiments. Other tables and figures can be found in Appendix 2.

3.4.2.2 Influence of Initial H₂O₂ Concentration

Results from the section above for UV dose show the degradation of 4TBP only happened until 200mJ/cm² UV dose in the reaction. The same UV dose was applied to

water samples with different H₂O₂ concentration. The results got from the experiment are given below:

H ₂ O ₂ Concentration	10mg/L	20mg/L	40mg/L	60mg/L	100mg/L
UV Dose(mJ/cm ²)	ln([4TBP]/[4TBP ₀])				
0	-0.2391436	-0.28358	-0.30203	-0.30986	-0.422925
10	-0.352747	-0.315	-0.56184	-0.56096	-0.5654002
25	-0.3767559	-0.66423	-0.60575	-0.91857	-1.1292794
50	-0.6347718	-0.80257	-1.13525	-1.03097	-1.1204761
100	-0.8212835	-1.06508	-1.62828	-1.8377	-2.1430756
200	-1.3599359	-1.45289	-1.7042	-3.22131	-3.13816

Table 3-6 Degradation of 4TBP with Same UV Intensity and Different H₂O₂ Concentrations

Plotting ln([4TBP]/[4TBP₀]) versus UV dose (Figure 3-7) results in a linear relationship indicating pseudo first order degradation kinetics. The slope of Figure 3-7 gives the pseudo first order rate constant *k*. Addition of hydrogen peroxide concentration from 0 to 60mg/L led to an increase in removal rates of 4TBP at the same UV dose, which is as expected. It is because that photolysis of hydrogen peroxide led to the formation of very strong oxidizing species, hydroxyl radical. Hence, oxidation by free radicals can be determined as the dominant degradation mechanism of 4TBP in the UV/H₂O₂ system, as compared to its direct photolysis:



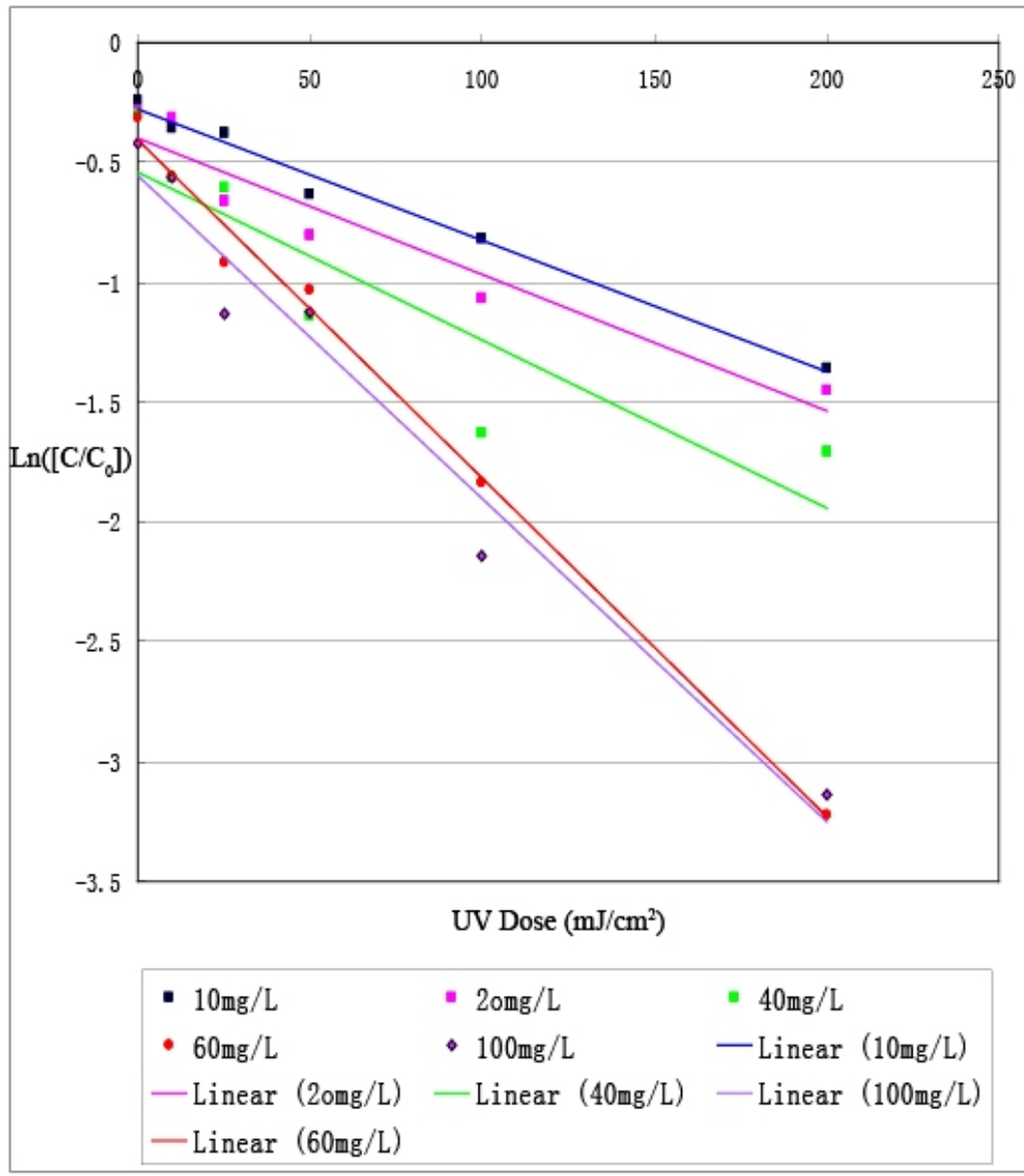


Figure 3-7 Influence of initial H₂O₂ concentration on 4TBP degradation

Formula (2.7), which can be rewritten as

$$\frac{d[4TBP]}{dt} = -k[4TBP], \quad (3-2)$$

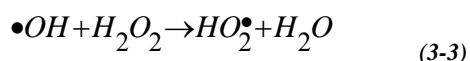
Where *k* is the pseudo first order constant.

The calculated *k* is listed on the table below:

H ₂ O ₂ (mg/L)	k(cm ² mJ ⁻¹)
10	0.0055
20	0.0057
40	0.0070
60	0.0141
100	0.0135

Table 3-7 Pseudo first order constant with Initial H₂O₂ Concentration

As also seen in Figure 3-7 and Table 3-7, when the initial concentration was very high (100mg/L in this case), the degradation rate does not increase anymore. The results got from experiments suggest that hydrogen peroxide concentration greater than 60mg/L may scavenge the generated hydroxyl radicals, forming the less reactive HO₂[•], thus making the UV/H₂O₂ process maybe even less effective at high hydrogen peroxide concentrations. This can be explained by the formula below:



3.5 Conclusions and Recommendations

Hydrogen Peroxide alone is able to degrade 4TBP within 72 hours. With 100mg/L of Hydrogen Peroxide initial concentration, the 4TBP degradation degree could reach 35%.

This study shows that UV/H₂O₂ process can more effectively decrease 4TBP concentration than hydrogen peroxide alone. The main degradation reaction happened with UV dose from 0 to 200mJ/cm², and suggested good free oxidation radical production within this UV dose range by a low pressure mercury lamp. The removal percentage of 4TBP can reach 96% at 200 mJ/cm² UV dose, 100mg/L H₂O₂ concentration.

When same initial H₂O₂ concentration was applied, 4TBP degradation degree increased with increasing UV dose.

The 4TBP degradation process fits with pseudo first order equation for UV-dose and H₂O₂-dose. However, at very high H₂O₂-doses (100mg/L), the scavenging of hydroxyl-radicals needs to be taken into account.

CHAPTER 4

THEORY OF CFD MODELLING AND VALIDATION

4.1 Introduction

This chapter aims at giving a brief idea of applications of numerical modeling on UV based water treatment processes, in which, Computational Fluid Dynamics (CFD) takes a leading position lately. The concepts and components of CFD are discussed in the following paragraphs, and the importance for CFD validation is also mentioned.

4.2 Introduction of CFD

4.2.1 What is CFD?

Computational Fluid Dynamics or CFD is the analysis of systems involving fluid flow, heat transfer and associated phenomena such as chemical reactions by means of computer-based simulation. From the 1960s CFD techniques has been integrated into aerospace industry for the design, R&D and manufacture of aircraft and jet engines. The use of computational dynamic to predict internal and external flows has risen dramatically in the 1980s [Versteeg and Malalasekera, 1995]. Until the 1980's, the study of computational fluid dynamics as means of solution for fluid flow problems, was the filed of post doctor gradates and academic researches [Sande, 2006]. CFD codes are more commercial now because the widespread availability of engineering workstations together with efficient solution algorithms and sophisticated pre- and post- processing facilities. This technique is very powerful and spans a great range of industrial as well as non-industrial application areas in 1990s. Some of the application examples are:

aerodynamics of aircraft and vehicles: lift and drag

hydrodynamics of ships

power plant: combustion in IC engines and gas turbines

turbomachinery: flows inside rotating passages, diffusers etc.

electrical and electronic engineering: cooling of equipment including microcircuits

chemical process engineering: mixing and separation, polymer moulding

external and internal environmental of building: wind loading and heating/ventilation

hydrology and oceanography: flow in rivers, estuaries, oceans
meteorology: weather prediction
biomedical engineering: blood flows through arteries and veins
water treatment: decomposition of organic compounds in UV reactors

4.2.2 Elements of CFD

All commercial CFD programs contain three main elements: Pre-processor, Solver and Post-Processor.

- Pre-processor

Pre-processing in CFD application means the input of a flow problem to a CFD program by means of a user friendly interface and the subsequent transformation of input into a form suitable for use by the solver. This is the basic and starting step for every CFD model, which includes about five steps.

- 1 Model Definition: Selection of the physical and chemical phenomena that need to be modeled by CFD program.
- 2 Fluid Definition: Definition of fluid properties.
- 3 Geometry Definition: The definition of region of interest which is called computation domain in the CFD program.
- 4 Boundary Condition Definition: Specification of appropriate boundary conditions at cells which coincide with or touch the domain boundary.
- 5 Grid Generation: Divide the domain into a number of smaller, non-overlapping subdomains. Which are called grid (meshes) or cells (or control volumes or elements).

The flow conditions are described by a set of particle diffusion equations. The solution of a flow problem is defined at nodes inside each cell and the accuracy of the CFD solution is highly depended on the number of cells in the grid. In general, the larger the number of cells, the better the accuracy of solutions will be. Also, the fitness of grid decides the accuracy of a solution, its cost in terms of necessary computer hardware and calculation time. In most cases, optimal meshes are non-uniform. Over 50% of time spent in industry on a CFD model is for definition of the domain geometry and grid generations. And a general rule for applying different meshes is: finer at the area where large gradients occur from point to point and coarser at the area where little change happens [Versteeg and Malalasekera ,1995].

- Solver

The solver is the part where the CFD calculation will take place, which includes the following steps: approximation of the unknown flow variables by means of simple functions; discretization by substitution of approximation into the governing flow equations and subsequent mathematical manipulations; solution of the algebraic

equations. There are three numerical methods available to solve the equations that describe the motion of a fluid: finite difference method, the finite element method and the spectral method. The difference between these three lies in the numerical technique used to integrate the basic model equations (differential equations expressing the conservation of mass and momentum). Comsol V3.3a used in this study applies the finite element method to solve the fluid equations.

- Post-processor

The post processing is that part in which the output is visualized. Often this user-friendly interface generates graphs and diagrams of the computational results. Recently more and more work has been put on post processing. The leading CFD packages are now equipped with versatile data visualization tools, which include: domain geometry and grid display; vector plots; line and shaded contour plots; 2D and 3D surface plots; particle tracking; View manipulation (translation, rotation, scaling etc.); color postscript output.

4.2.3 Problem solving with CFD

Before using CFD to solve a fluid flow problem, there is a stage of identification and formulation of the flow problem in terms of the physical and chemical phenomena that needs to be considered. Typical decisions that might be needed are whether to model a problem in two or three dimensions. In the study of Chapter 5, a 2-D flow model was made for instance. To make every good choice needs good modeling skills, because in all but the simplest problems people need to make assumptions. The user needs to continually aware of all the assumptions that they has made.

A good understanding of the numerical solution algorithm is also crucial. One of the most important and problematic one is convergence. Convergence is the property of a numerical method to produce a solution which approaches the exact solution as the grid spacing, control volume size or element size is reduced to zero. It is usually very difficult to establish in practice. Then different solvers can be applied for solving the problem.

4.3 Modeling for UV based water treatment processes

UV technology, which is used for both drinking water and waste water treatment, has been used more and more in recent years. And a lot of concerns have been put on the studies for the effects of treatment designs for the performance. The design of treatment operations, for example UV disinfection systems, has been relied on empirical guidelines, therefore it is very difficult to optimize. Since more understanding about the progress dynamics as well as development of more powerful

numerical models, the process optimization has become one of the top issues on researchers' lists.

A good designed UV reactor itself is one of the most important parts which ensured the first step in a successful treatment performance. For the design goal, a uniform UV distribution is preferred although it is never homogeneous in the real applications. And UV reactor simulation can be achieved by linking the rate of reaction with non-homogeneous UV-radiation power through the local volumetric rate of energy absorption. [Sozzi and Taghipour, 2006]. There have been many published studies using numerical model tools to study the UV related water treatment process.

In 1983, Romero published a paper setting up the fundamental balances which are needed for solve the mass, momentum, energy and chemical reaction rate equation for annular UV reactors, using axial symmetry and simple equation for two dimensional geometries [Romero et al., 1983]. Cassano studied different geometries and reaction kinetics lately using those methods because of the lack of computer ability at that time [Cassano et al., 1995]. Chiu and his colleagues studied effect of UV system modification on disinfection performances for example [Chiu, et al., 1999]. In Chiu's researches, they found that there are critical paths through which particles moved and experience low UV doses. And in vertical UV systems, those paths are revealed near the channel walls with characteristics of high velocity and low turbulence intensity, which may also experience low UV intensity. Models have also been developed to study the performance of comparison of low and medium pressure Hg lamps for both direct and H₂O₂ assisted UV photo-degradation for N-Nitrosodimethylamine in drinking water treatment [Sharpless and Linden, 2003], and predicated that H₂O₂ may enhance NDMA removal by UV. In addition, because the process of UV radiation through energy absorption in the reactor is spatial dependent, with a good combination of reactor hydrodynamics and local radiation intensity, the good result of reaction rate can be achieved [Pareek et al., 2003].

Computational fluid dynamics (CFD) is becoming an affordable engineering tool to simulate and optimize reactor designed with the increased performance of computational resources and the fast development of simulation software. CFD is widely used and shows great viability for the design and optimization of chemical reactors [Marchisio and Barresi, 2003]. It is an easy use and fast tool for simulation of UV related water treatment reaction. CFD has been applied to the simulation of UV-reactor Hydrodynamics as well as UV reactor performance based on integrated models. CFD modeling has been used study the reactor hydrodynamics for on waste water disinfection [Janex et al., 1998]. Kaminura integrated reactor hydrodynamics, radiation distribution and UV reaction kinetics to simulate UV reactor performance [Kamimura et al., 2002].

4.4 CFD Validation

CFD computation involves the creation of a set of numbers that constitutes a realistic approximation of a real-life system. One of the advantages of CFD is that the users could almost choose infinite details and conditions for the solution. With CFD simulation there are countless small details, which need to be worked out in order to get the most reliable model, and thus the solution closest to the real case. However, how to decide the appropriate solution and have the right calculation earns a lot of attentions.

It is quite important and necessary to make sure that the main outcome of any CFD models should improve understanding of behavior of the interested system, but since there are no guarantees regarding the accuracy of simulation, the validation of CFD model becomes a rising issue for researcher and normal users.

The performance of ultraviolet reactors used for water treatment is greatly influenced by the hydrodynamics due to the non-homogeneity of the radiation field. Reliable modeling of the reactor flow structures is therefore crucial for the design process, which also gives a great challenge for CFD users because of the complicated water flow. Validation of the outcome of CFD for the flow is discussed in this work because of its leading importance in the UV related reactions. A common way to conduct CFD validation is to use experimental data to compare with CFD simulation result. In water treatment field, this method has been applied to study process of dissolved air flotation. Researchers from Thames Water Group Research built up a small laboratory model to measure the generic flow patterns in dissolved air flotation, they compared those measured data with preliminary single-phase CFD models, and decided κ - ϵ model of turbulence gave a close agreement [Hague et al., 2001].

CHAPTER 5

THE CFD MODEL FOR UV DOSE CALCULATION

5.1 Introduction

The CFD model applied for this study is a 2-D model developed using the software package Comsol, V3.3a. The final UV dose model is a combination of a flow model and a UV radiation model. The theory and method for building up the model and the results calculated from the model are described in this chapter.

5.2 Problem Geometry and Formulation

A 2-D definition sketch of the problem geometry studied in the present work is given below. The inflow water passes through a 6 meter length, 0.125 meter width pipe and enters into the UV reactor. The water flows through this single 0.3m diameter round reactor module (from left to right in figure 5-1), containing 4 vertical cylindrical UV lamps tubes, each of diameter 47.8mm, including a 1.9 mm thick quartz layer.

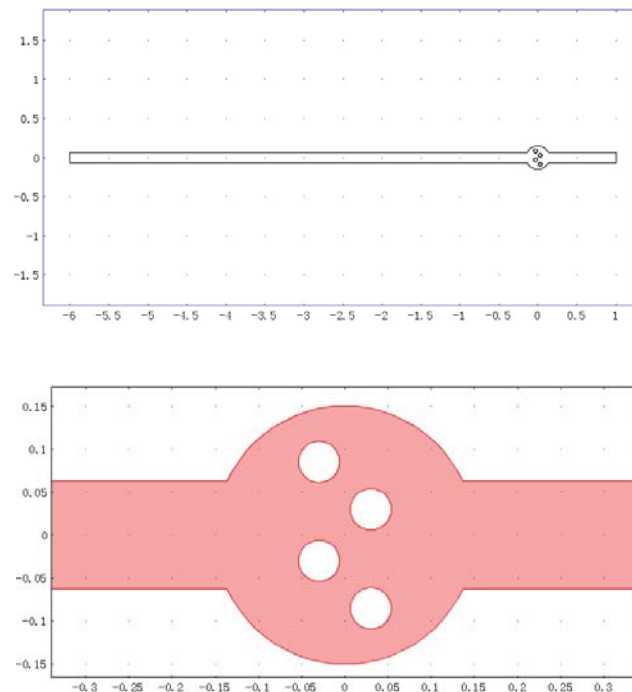


Figure 5-1 The geometry of the model (total, top) and reactor (bottom)

The numerical model assumed flow to be steady and two-dimensional, thereby neglecting variations and motions over the depth and time. Gravitational effects were also neglected. The temperature effects of lamps heating up the water which will cause water viscosity changing were not considered as well. Variations over the depth in the UV intensity are assumed negligible because of the typical large length-to-diameter ratio of UV lamps.

5.3 Mesh of the Model

The interested area of the study is the UV reactor, and the meshes of the reactor and pipe are shown below. Around the quartz tubes and near the boundary of walls the meshes are finer. Within the feed pipe, mapped meshes were applied in order to save solving memory during calculation. At the beginning, a shorter feed pipe was applied, but it was found out soon that turbulent kinetic energy at the inlet of the reactor was not developed symmetrically yet, which indicated a poor mixing and turbulence of the feed water. It was found that the feed pipe should be rather long (with 20 times of pipe diameter) with finer meshes near the pipe walls in order to achieving a well developed turbulence flow at the beginning of the reactor [Wright and Reddy, 2003].

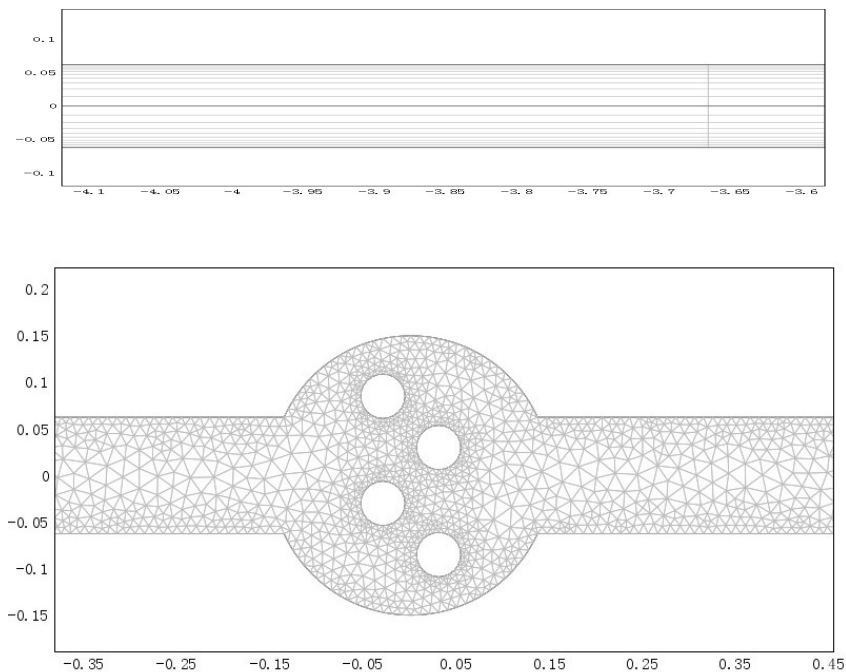


Figure 5-2 The meshes for the straight inlet pipe (top) and the reactor (bottom)

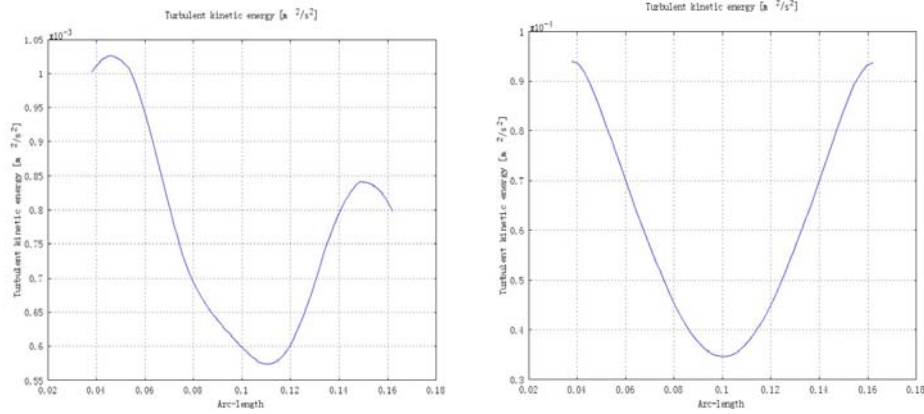


Figure 5-3 Poorly developed turbulent flow with unsymmetrical turbulent kinetic energy with 1 meter length feed pipe (left); Well developed turbulent flow with symmetric turbulent kinetic energy with 6 meters length feed pipe (right)

5.4 Building up of Flow Model

5.4.1 Reynolds Averaged Navier-Stokes Equations

In the model of this study, turbulent flow model is applied because the flow in the UV reactors is considered to be at turbulence regime [Sozzi and Taphipour, 2006]. Turbulence can be considered as a characteristic state of the flow that can only be described in a statistical manner. In this statistical representation of turbulent flow, the mean quantities are of main interest. However, fluctuations in different field quantities also play an important role.

It is important that the nature of the fluctuations around the mean flow is accounted for. This is included in the Reynolds Averaged Navier-Stokes (RANS) equations [Comsol V3.3 a, Chemical Engineering Module, User Guide,2006],

$$\rho \frac{\partial \mathbf{U}}{\partial t} - \eta \nabla \cdot \nabla \mathbf{U} + \rho \mathbf{U} \cdot \nabla \mathbf{U} + \nabla P + \nabla (\overline{\rho \mathbf{u}' \otimes \mathbf{u}'}) = \mathbf{F} \quad (5.1)$$

$$\nabla \cdot \mathbf{U} = 0 \quad (5.2)$$

,where η denotes the dynamic viscosity ($M L^{-1} T^{-1}$), \mathbf{u} the velocity vector ($L T^{-1}$), ρ the density of the fluid ($M L^{-3}$), P the pressure ($M L^{-1} T^{-2}$), \mathbf{U} is the averaged velocity field ($L T^{-1}$), $\mathbf{u}' \otimes \mathbf{u}'$ is the velocity fluctuation metrics ,and \mathbf{F} is the volumetric force vector ($M^{-2} L T^{-2}$).

The last term on the left of formula 5.1 represents fluctuations around a mean flow and is called the Reynolds stress tensor which explains the correlation between fluctuations in different directions due to the random turbulent fluctuations in fluid momentum.

5.4.2 k-ε model

The flow model in this study is k-ε mode, which is a widely used turbulence model. In this model, two extra transport equations are solved for two introduced variables; the turbulent kinetic energy, k, and the dissipation rate of turbulent energy, ε. Turbulence transport of momentum is:

$$\rho \overline{(u' \otimes u')} - \frac{\rho}{3} \text{trace}(\overline{u' \otimes u'}) \mathbf{I} = -\eta_T (\nabla U + (\nabla U)^T) \quad (5.3)$$

$$\eta_T = \rho C_\mu \frac{k^2}{\varepsilon} \quad (5.4)$$

Where η_T is the turbulent viscosity ($M L^{-1} T^{-1}$), defined above, and C_μ is a model constant; empirical to the system the equations describe.

Turbulent viscosity in Formula 5.4 is more common to be written as turbulent kinetic viscosity, which is:

$$\nu_T = \frac{\eta_T}{\rho} = C_\mu \frac{k^2}{\varepsilon} \quad (5.5)$$

This gives closure to the system and results in the following equations for the conservation of momentum and continuity:

$$\rho \frac{\partial U}{\partial t} - \nabla \cdot [(\eta + \rho C_\mu \frac{k^2}{\varepsilon}) \cdot (\nabla U + (\nabla U)^T)] + \rho U \cdot \nabla U + \nabla P = F \quad (5.6)$$

$$\nabla \cdot U = 0 \quad (5.7)$$

where ρ denotes the density of the fluid ($M L^{-3}$), U represents the averaged velocity ($L T^{-1}$), η the dynamic viscosity ($M L^{-1} T^{-1}$), P pressure ($M L^{-1} T^{-2}$), k the turbulent kinetic energy ($M^2 T^{-2}$), F a body force term ($M L T^{-2}$), ε is the dissipation rate of turbulence kinetic energy ($L^2 T^{-3}$), ν is the turbulent kinetic viscosity, and $u' \otimes u'$ is the velocity fluctuation metrics. The transport equation for k can be derived by taking the trace of the equations for the Reynolds stresses:

$$\rho \frac{\partial k}{\partial t} - \nabla \cdot \left[\left(\eta + \rho \frac{C_\mu}{\sigma_k} \frac{k^2}{\varepsilon} \right) \nabla k \right] + \rho \mathbf{U} \cdot \nabla k = \rho C_\mu \frac{k^2}{2\varepsilon} (\nabla \mathbf{U} + (\nabla \mathbf{U})^T)^2 - \rho \varepsilon \quad (5.8)$$

For ε :

$$\rho \frac{\partial \varepsilon}{\partial t} - \nabla \cdot \left[\left(\eta + \rho \frac{C_\mu}{\sigma_\varepsilon} \frac{k^2}{\varepsilon} \right) \nabla \varepsilon \right] + \rho \mathbf{U} \cdot \nabla \varepsilon = \rho C_{\varepsilon 1} \frac{k^2}{2} (\nabla \mathbf{U} + (\nabla \mathbf{U})^T)^2 - \rho C_{\varepsilon 2} \frac{\varepsilon^2}{k} \quad (5.9)$$

The model constants in the above equations are determined from experimental data and are summarized by Wilcox [Wilcox, 1998]. Constant values are:

Constant	Value
C_μ	0.09
$C_{\varepsilon 1}$	1.44
$C_{\varepsilon 2}$	1.92
σ_k	0.9
σ_ε	1.3

Table 5-1 Values of constants used in k- ε equations [Comsol V3.3 a, Chemical Engineering Module, User Guide, 2006]

5.4.3 Boundary condition settings

Feed flow rates are 2.1m³/h and 5m³/h, these two values were got from Kiwa Water Research to reach the ask for sufficient water residence time in the reactor. The numerical simulations are based on the solutions of continuity equation together with the steady two-dimensional Reynolds-averaged Navier-Stokes equations.

The assumed isotropic turbulence viscosity ν_t is related to turbulent kinetic energy k , and the rate of dissipation of turbulent energy ε by the model equation.

The flow equation is complemented by boundary conditions. At the inlet, a uniform unidirectional approach velocity ((u, v)=($U, 0$)) is applied. At the outlet, the pressure of the boundary was set to zero. The outlet was set sufficiently away from the reactor region, such that the precise outflow boundary conditions should not have any significant effect on the flow within the lamp module.

Comsol 3.3a. chooses logarithm wall function for all the solid walls in the model, which implies an empirical relation between the value of velocity and the wall friction near the wall :

$$k = \frac{u_{\tau}^2}{\sqrt{C_{\mu}}} \quad (5.10)$$

$$\varepsilon = \frac{u_{\tau}^3}{\kappa y} \quad (5.11)$$

$$\tau_w = \frac{\rho C_{\mu} k^2}{\varepsilon} \frac{\partial U}{\partial n} \quad (5.12)$$

Where k is the turbulent kinetic energy, ε is the dissipation rate of turbulent kinetic energy, C_{μ} is a model constant (0.09), κ is the Karman's constant (about 0.42), y is the coordinate perpendicular to the wall, u_{τ} is the velocity scale, τ_w is the wall shear stress, ρ is the density of fluid, U is the velocity parallel to the wall and n is the unit vector normal to the wall.

For the model, a 6 meters length straight inflow pipe was used, but because the interesting area is within the reactor, the flow simulation result of the pipe is not given below (see Appendix III). The initial values for turbulent kinetic energy and dissipation of turbulent kinetic energy are set in order to obtain good converge. The constants used for boundary condition and sub-domains are listed below:

Constant	Value
Temperature	293(K)
k_0	0.02(m ² /s ²)
ε_0	0.03(m ² /s ²)
Feed flow rate	2.1/5 (m ³ /h)
Material	Liquid, Water

Table 5-2 Values of constants used in boundary condition settings [Comsol V3.3 a, Chemical Engineering Module, User Guide, 2006]

5.4.4 Flow model predictions

The flow direction in the model is from left to right, and two different feed flow rates were applied at the inlet, which are 2.1m³/h and 5m³/h separately. The figures below give the model predictions of velocity field and turbulent kinetic energy in both cases. Symmetric turbulence flow is well developed before entering the reactor. The difference in velocity value can be read from the colorful scale bars. The model predicted areas where have very low velocities; those areas are at the top and bottom of the reactor as well as behind the quartz tubes. The turbulence of high inflow

velocity is higher than that of low velocity, and the differences of the highest values of turbulent kinetic energy for the high inflow are ten times of the lower one, which is logical because turbulent kinetic energy has a linear relationship with the square of velocity(The scale for the figure 5-4 is different).

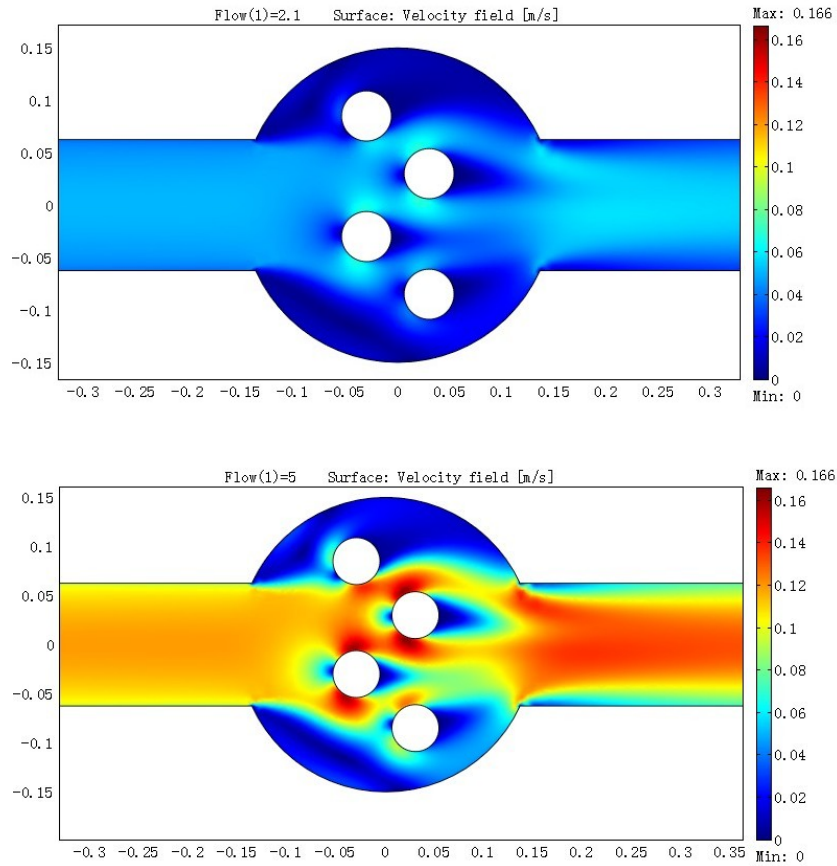
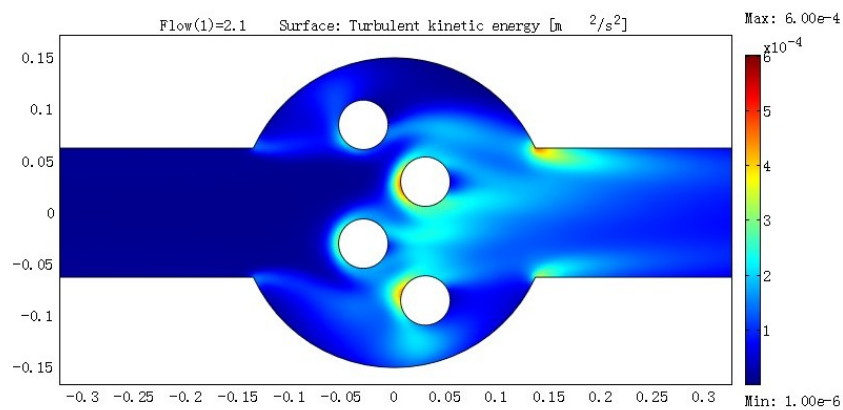


Figure 5-4 Velocity field with flow of 2.1 m³/h (top) and 5m³/h (bottom)



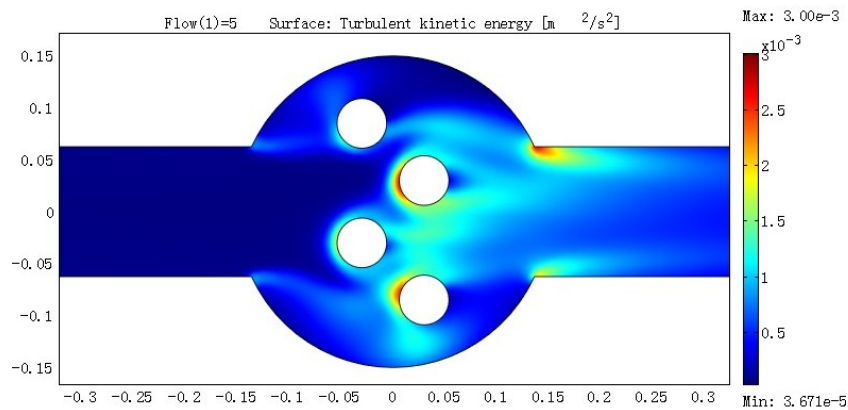


Figure5-5 Turbulence kinetic energy with flow of 2.1 m³/h (top) and 5m³/h (bottom)

With both predictions, there are small areas with negative x velocity behind the tubes, which predicts water recirculation in those areas. Also there are bigger areas with recirculation at the top and bottom of the entrance of reactor when the water surface is just becoming wider, which is clearly showed in the streamlines figure.

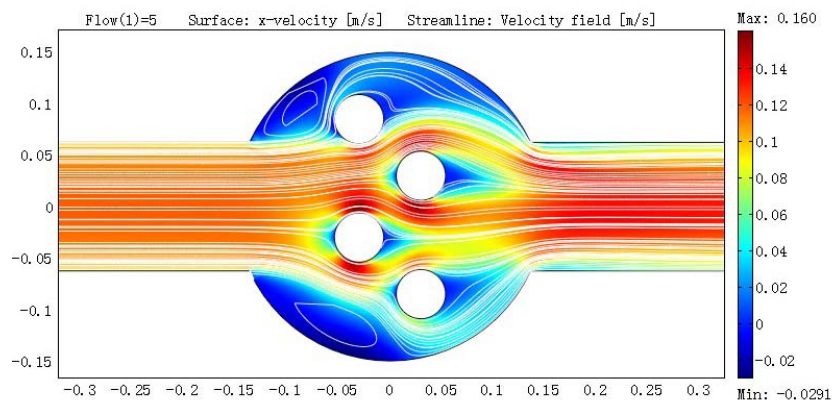


Figure5-6 Velocity field with stream lines of 5 m³/h flow

5.5 Building up of UV irradiation model

5.5.1 UV intensity without reflection and refraction

In the model, Φ is the radiant power emitted in all directions by a radiant energy source, and radiant intensity (I) is the power emitted from a point source into a small solid angle $d\Omega$ spherical about a given direction from the source. This solid angle Ω is defined as the surface area of a section of a sphere divided by the power of the sphere

radius. And the SI units of I are $W sr^{-1}$. From the point source, $\Phi=4\pi I$, and distance was not diminished in a non-absorbing medium. The element of radiant power is $d\Phi=Id\Omega=I\sin\theta d\theta d\phi$, where θ is measured from z-axis.

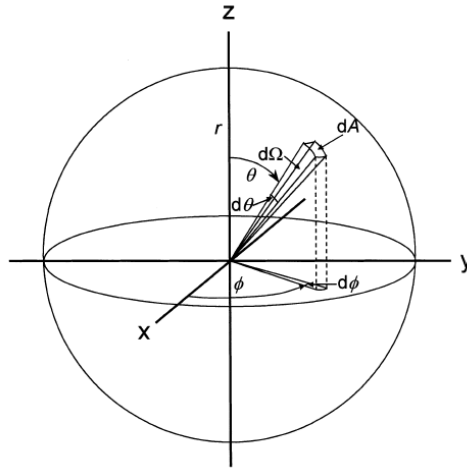


Figure 5-7 Solid angle in spherical polar coordinates

The water and quartz sleeves have absorption of the UV intensity. The beam intensity is diminished by the factor $(1-R)$ as it passes through the quartz sleeve into water. And the absorption factor of water is also considered.

The total UV lamp is considered as a lot of sections of point sources, using the theory of multiple point sources summation (MPSS) approximation [Jacob and Dranoff, 1970; Scheible et al., 1985; Suidan and Severin, 1986, Bolton, 1999]. The basic assumption is that a lamp can be represented by a finite series of co-line point sources. The emission of a linear lamp is defined equivalent to that of n point sources spaced equally along the long axis of the lamp. The power output for each of the point source is the total Φ , which is the total UV power output of the linear lamp in the wavelength band of interest, divided by the number of the points, n .

In the model used in this study, the n is set to be 100. A model for I_i incorporating with the effect of adsorption by the quartz sleeves and water was obtained using the point-source-summation technique mentioned above [Blatchley, 1997]

$$I(R) = \frac{S}{4\pi R^2} \exp[-\alpha_w (R - r \cdot f)] \exp(-\alpha_q t_q f) \quad (5.13)$$

Where S is the power available from the point source (mW); R is the distance between the point source and the received point (cm); r is the diameter of the lamp (cm); f is the ratio of $R/(R^2 - z^2)^{0.5}$; z is the distance between the point source and

received point in the direction of centerline of the lamp(cm); α_w is the absorbance coefficient of water (cm^{-1}); α_q is the absorbance coefficient of quartz sleeves (cm^{-1}); and t_q is the thickness of the quartz sleeves. The effects of reflection and refraction were assumed to be negligible.

In this calculation, the UV intensity at a certain position of the reactor is the function of its location. The overall value of a given property is then the sum of the values of that property calculated for each of the n point sources. The spatial distribution of $I(x,y)$ is determined as the sum at a point of the intensity contribution from all UV lamps in the system.

$$I(x,y) = \sum_{i=1}^N I(x,y,x_i,y_i) \quad (5.14)$$

In this calculation through out the reactor, an intensity filed of the whole reactor can be built for a given combination of lamp orientation, lamp output power, and system optical characteristics.

In this study, the shadow effect, in which the UV lamps intercept the radiation of other lamps, is not included as a simplification. Shadowing and reflections by reactor wall are also neglected.

5.5.2 Refraction and Snell's Law

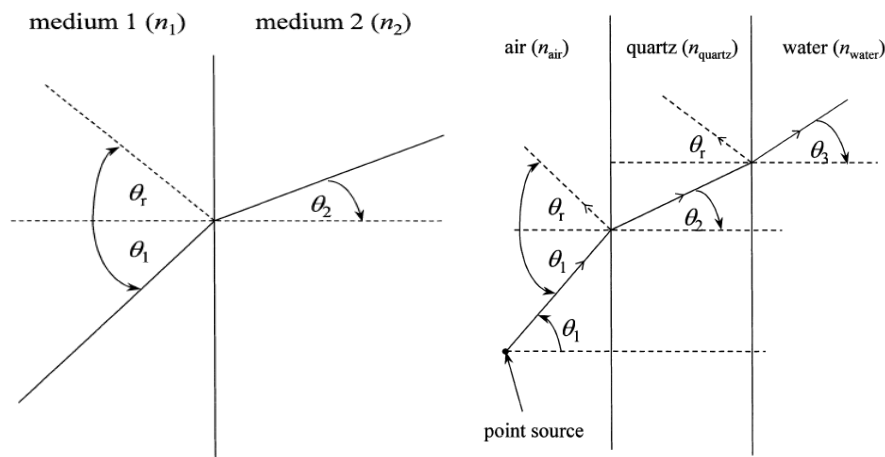


Figure 5-8 Reflection and refraction between a medium of refraction index n_1 and another medium of refractive index n_2 (left); the air, quartz, and water interface (right)

The radiant energy has refraction when it transmitted through a certain surface, Snell' law explained this refraction property (Figure 5-9), which can be written as:

$$n_1 \sin \theta_1 = n_2 \sin \theta_2 \quad (5.15)$$

where n_1 and n_2 are the refractive indices of the two media. If $n_2 > n_1$, the angle of refraction θ_2 is less than the angle of incidence θ_1 .

5.5.3 Reflection and the Fresnel laws

A certain amount of radiant energy is reflected at the angle $\theta_r = \theta_1$ (Figure 5-9) when the radiant energy passes through surface of two medias; the rest passes through the interface into the second media and undergoes refraction. According to Fresnel Laws [Meyer-Arendt, 1984],

$$r_{\text{perpendicular}} = \frac{n_1 \cos \theta_1 - n_2 \cos \theta_2}{n_1 \cos \theta_1 + n_2 \cos \theta_2} \quad r_{\text{parallel}} = \frac{n_1 \cos \theta_1 + n_2 \cos \theta_2}{n_1 \cos \theta_1 - n_2 \cos \theta_2} \quad (5.16)$$

r is the amplitude of polarized radiant energy, and perpendicular and parallel is the relevant radiant energy direction to the plane of incidence. Reflectance R for unpolarized radiant energy is described below,

$$R = \frac{1}{2} [r_{\text{perpendicular}}^2 + r_{\text{parallel}}^2] \quad (5.17)$$

R is also varies with angle for an air/quartz interface.

5.5.4 Factor setting for the UV intensity model

The length of UV lamp is 0.15m, and the number of points in radiation direction, n , was set to be 100. In total four lamps were used. The diameter of the lamp r is 22mm (which is diameter of the quartz tubes minus the thickness of the quartz layer). Refraction and reflection are considered. Refraction factor of water is 1.33, and the value of quartz and water are 1.54 and 1.0 separately. When applied with low pressure lamp, UV wave length is 254nm, with output power of 150W/m, UV transmittance of water is 0.79, and of quartz is 0.96.

5.5.5 UV intensity model prediction

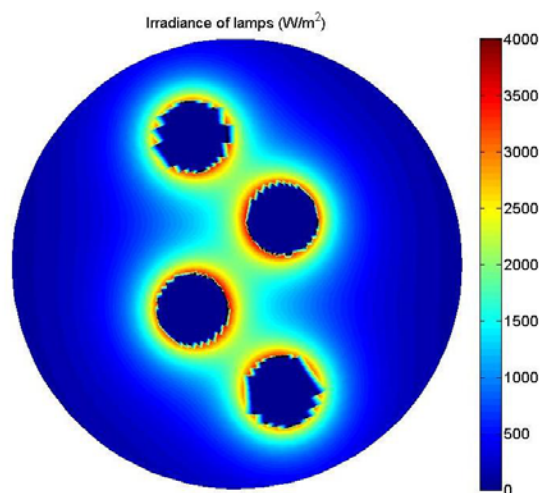


Figure5-9 Model simulation of UV irradiation (UV 254nm)

The lamp position in Figure5-9 is used in flow measurement experiments later discussed in the study. The dark blue circles indicated the position of the UV lamps. From the intensity prediction above, areas around the quartz tubes received strong irradiation, while the zones between the lamps have strongest UV intensity output, while with an increase of distance between water and center of the lamps, the UV irradiation decreases quickly. And there are positions with zero irradiation, which are the entrance and exit of the reactor.

5.6 UV dose model

5.6.1 Random-walk theory

The UV dose calculation is based on a lagrangian particle tracking model which is called the random-walk model. The random motions of each individual microorganism form an appropriate basis for the determination of a dose-distribution function. Random-walk models are related closely to diffusion phenomena [Bailey, 1964] and have been discussed in the context of mixing in surface waters [Fischer et al.,1979] as well as transport in ground water systems [Kinzelbach,1986]. It also used in UV disinfection model by Chiu [Chiu, et al., 1999]. The model has two ground assumptions. First, this model assumes a steady two-dimensional flow, which is characterized by mean velocity field(u, v) in the (x, y) directions, and departures from the mean are attributed to random turbulent fluctuations, characterized by the standard deviations of the instantaneous velocity distributions(S_x, S_y). Second, the model

assumes particles moving with the fluid. The basic equation for position of a particle at time or age $t+\Delta t$ is related to the position at the step before t by

$$\begin{aligned}x_p(t + \Delta t) &= x_p(t) + [\overline{u(x_p(t), y_p(t))}] \Delta t \\y_p(t + \Delta t) &= y_p(t) + [\overline{v(x_p(t), y_p(t))}] \Delta t\end{aligned}\quad (5.18)$$

The quantities (\bar{u}, \bar{v}) were taken from the flow model calculated before. The residence time distribution of the model is determined by adding a tracer at the inflow boundary. The spreading of the tracer is modeled with an advection-diffusion equation. The advection follows from the mean velocities of the flow model and the diffusion is derived from the turbulent kinetic energy (k) and turbulent dissipation (ε) of the turbulence model. The turbulent diffusion is equal to:

$$D = C_\mu \frac{k^2}{\varepsilon} \quad (5.19)$$

where the standard value of 0.09 is used for C_μ .

In addition, a lagrangian technique is applied. Individual trajectories are calculated for a large number of particles. These may represent bacteria, viruses or contaminants, which are assumed to be small enough to move passively, so no drag, lift or gravity forces are taken into account. A drift correction proportional to the gradient of the diffusion is added to prevent particles from accumulating at places with low diffusions. Every time step a particle has a displacement, which consists of an advection, turbulence diffusion as well as a drift part. The values of these contributions follow from the finite element flow model with k - ε turbulence modeling.

Using 5.18, the displaced positions of particle are then,

$$x_p(t + \Delta t) = x_p(t) + [\overline{u(x_p(t), y_p(t))}] \Delta t + R \sqrt{6D(x_p(t))} \Delta t + 3R^2 \frac{\partial D}{\partial x} \Delta t \quad (5.20)$$

$$y_p(t + \Delta t) = y_p(t) + [\overline{v(x_p(t), y_p(t))}] \Delta t + R \sqrt{6D(y_p(t))} \Delta t + 3R^2 \frac{\partial D}{\partial y} \Delta t \quad (5.21)$$

R is a random displacement taken from a uniform distribution between -1 and 1, independent in x , y , or z -direction, The diffusion induced displacement is consistent with diffusion coefficient D at the particle position in accordance with equation 5.19. For small time steps, the particle method must be consistent with the advection diffusion equation. As the particle method uses the same velocity field and turbulence viscosity, it must converge to the Eulerian solution. In the model, 2000 time steps were applied and each time step is 0.5s, this time step is chosen according to the

previous study of Bas Wols [Wols, 2007]. At the inlet, a total number of 5000 particles were released randomly in a uniform distribution.

5.6.2 Calculation of UV dose

The UV received by an individual particle in traversing the irradiated zone was calculated by integrating intensity along the path traveled by the particle by:

$$D_{\text{dose}}(t) = \int_0^t I dt \quad (5.22)$$

where D_{dose} is the total dose, t is the time.

The UV intensity for each step was calculated from the UV intensity model described before as the average of the intensity at the beginning and end positions of each step. The velocity field of every point in the reactor with a certain inlet flow was calculated from the flow model mentioned before.

5.6.3 UV dose model prediction

5.6.3.1 Different flow conditions

Two different flow rates at the inlet and low pressure lamps are applied with model calculation, and the dose prediction gives results in Figure5-10,11. The x axis is the value of UV dose, and y axis is the number of particle which received certain dose.

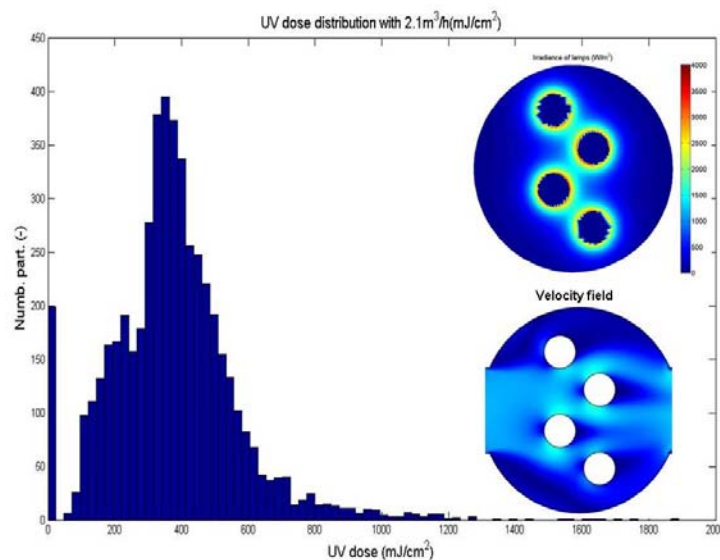


Figure5-10 UV dose distribution with flows =2.1m³/h , UV 254nm

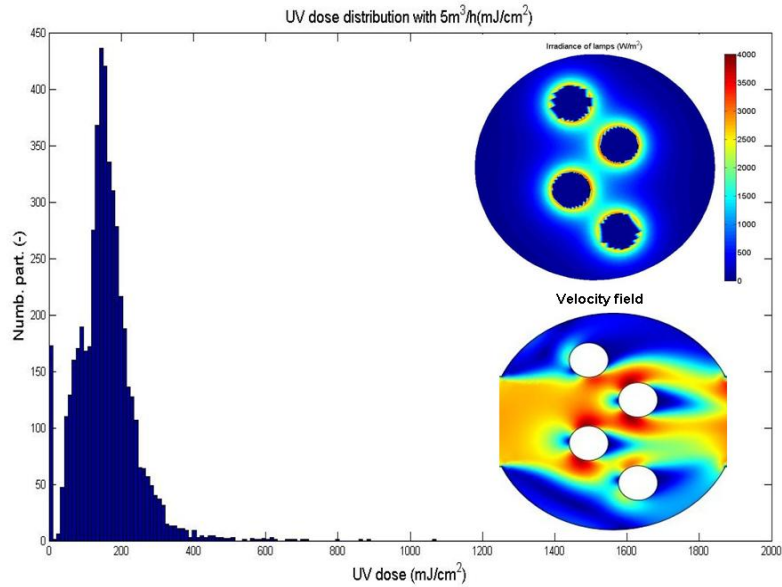


Figure5-11 UV dose distribution with flows = 5m³/h; UV 254nm

The results indicate that with lower flow rate the particles in the reactor received higher UV dose as well as a wider dose distribution than the high flow rate, with the same lamp configuration. There is one column with zero in both figures because of the flow model calculates flow diffusion in the boundary of the reactor. While a particle is very close to the boundary, with the random walk model, those particles can “walk” out of the reactor wall because of position replacement is out of the reactor region. While the model only count particle dose which are coming out at the end of the reactor, those particles which are randomly walked out the reactor wall were not counted, and are not attributed to the final dose calculation. The number of particles that were not counted in is around 3%~4% of the total particle number depending on the flow conditions.

The peak dose for the low flow rate is significantly higher than the higher flow rate. For 2.1 m³/h flow, the average value of UV dose is 393mJ/cm², and the value is only 163mJ/cm² for 5m³/h flow, the ratio of average dose value is 2.4, which is also the ratio between the two flow rates. This is because when the water velocity is lower, particles retention time in the reactor is longer even with the same path, which means that the total irradiation time is longer. The model predicted well about the time difference caused by velocity difference. When same UV intensity field applied, flow velocity is important for deciding the UV dose. Comparing with two flows, 5m³/h is preferred with a narrow dose distribution pattern which means better hydraulic performance. In order to achieve 200mJ/cm² average dose for 4TBP degradation, 4.1m³/h is suggested.

5.6.3.2 Different UV lamp configurations

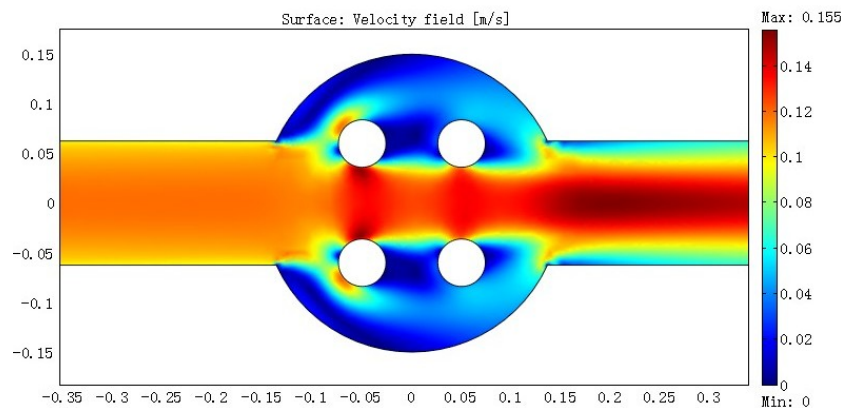
In total three different UV lamp configurations with four lamps in the same UV reactor are discussed in this study, the parameter of the positions are given in the table below, in which position 0 is the same as tested reactor discussing in next chapter:

Combinations	Center position coordinates of the lamp in the reactor(m)			
	Lamp1	Lamp2	Lamp3	Lamp4
Position 0	(-0.03,0.085)	(-0.03,-0.03)	(0.03,0.03)	(-0.03,-0.085)
Position 1	(-0.05,0.06)	(-0.05,-0.06)	(0.05,0.06)	(0.05,-0.06)
Position 2	(-0.05,0.04)	(-0.05,-0.04)	(0.05,0.08)	(0.05,-0.08)

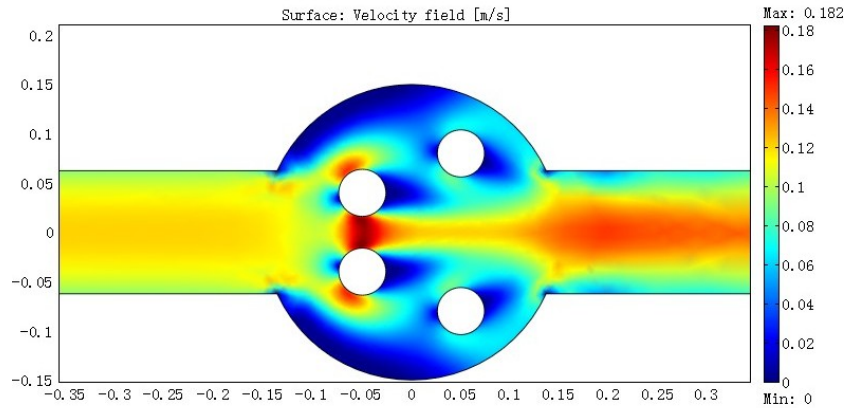
Table5-2 Coordinates of lamps in the reactor

Same boundary conditions and constants as before are used, and the velocity field predictions with $5\text{m}^3/\text{h}$ feed flow are given below. The result for position 0 is already discussed in the section above.

With the position 2, higher velocity was achieved comparing with position 1, which is because the narrower distance between the tubes which are close to the inlet. Combine those model predictions, it can be conclude that the flow model can predict well developed turbulence flow at the inlet and show the concentrated velocity field between the tubes. Behind the tubes there are small circulations, and big circulations are locating at the top and bottom near the inlet of reactor.



(a)



(b)

Figure5-12 Velocity field of different lamp positions with $5\text{m}^3/\text{h}$ flow (position 1, a, position 2, b)

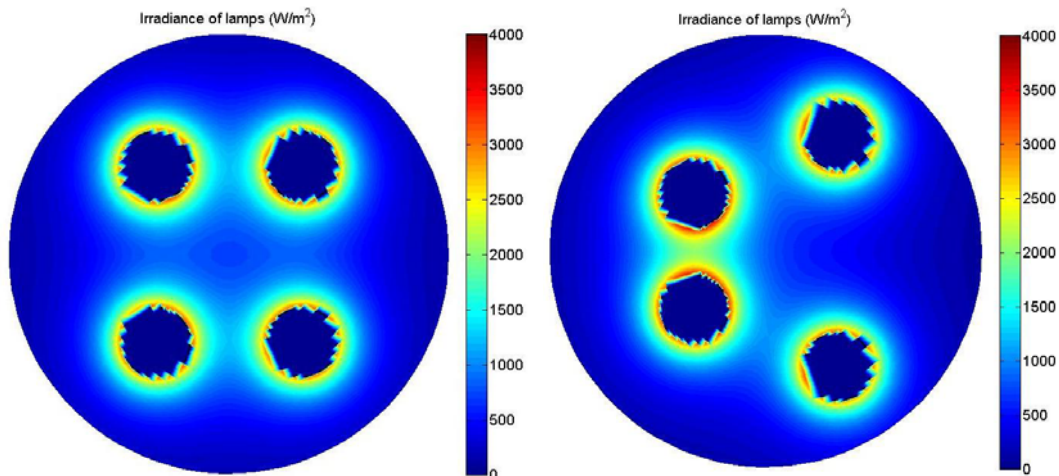


Figure5-13 UV irradiance prediction by the model with different lamp positions (UV 254nm; position 1, left; position 2, right)

When the same UV intensity and wavelength applied, use same number of UV lamps, with different lamp configurations, different UV irradiances can be calculated by the model, figure 5-13. The dark blue circles indicated the position of the UV lamps. As discussed before, UV irradiance just around the lamp has highest value, while with the increased distance between the lamp and received water, the value of irradiance decreases. There are areas in the reactor which receive zero irradiance as well. With these two different lamps combination, the fields which received around $1000\text{W}/\text{m}^2$ UV irradiance increased than position 0 because the lamps are more far away from each other comparing with the original design.

As discussed earlier in this chapter, UV dose for three UV lamp configurations with low pressure lamps are calculated, the results are as follows:

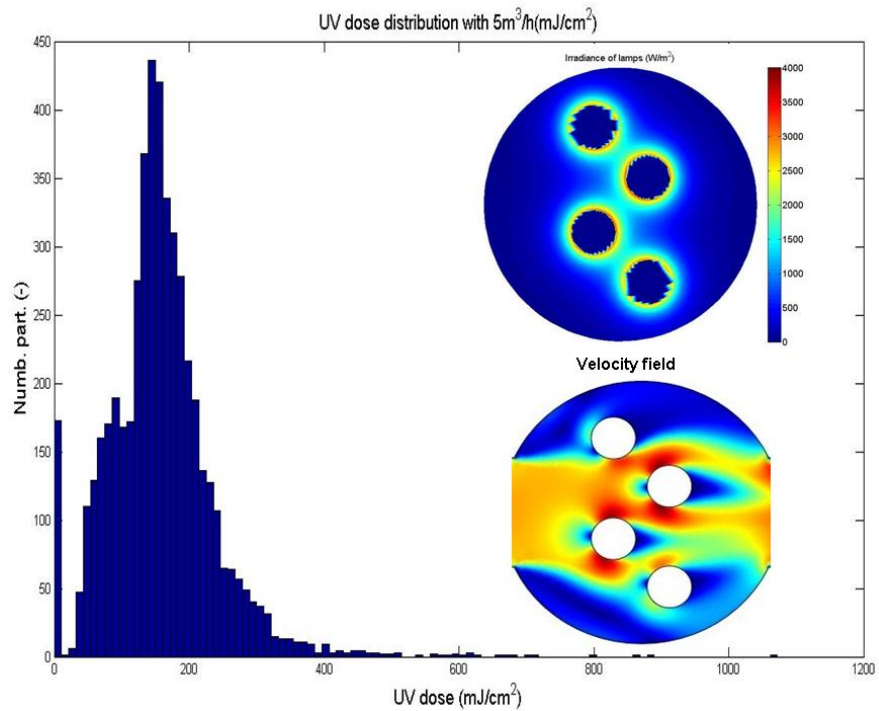


Figure5-14 UV dose distribution with position 0, UV 254nm, 5m³/h flow

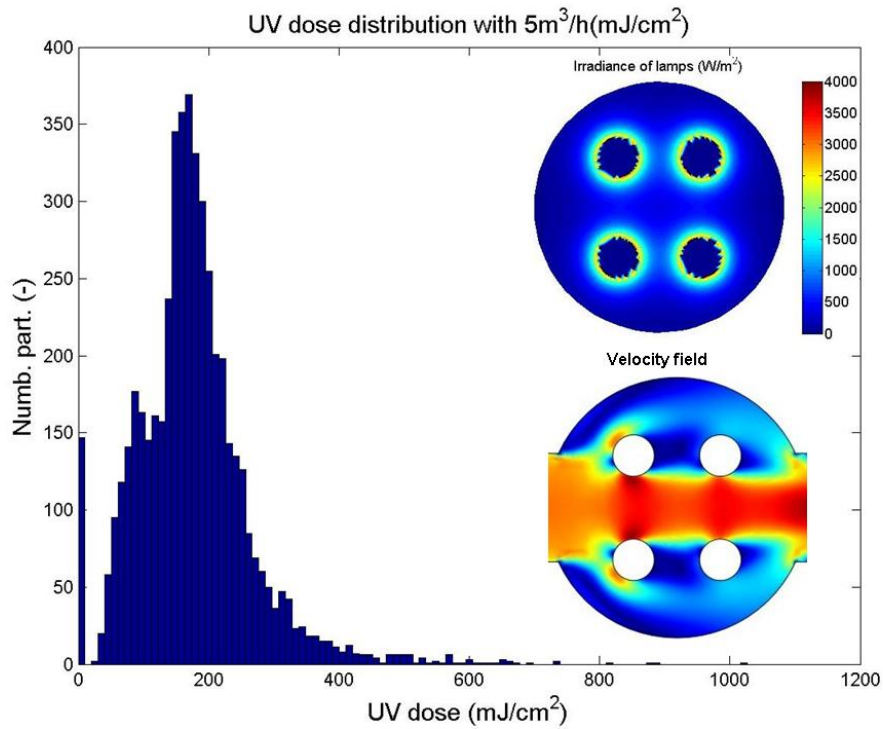


Figure5-15 UV dose distribution with position 1, UV 254nm, 5m³/h flow

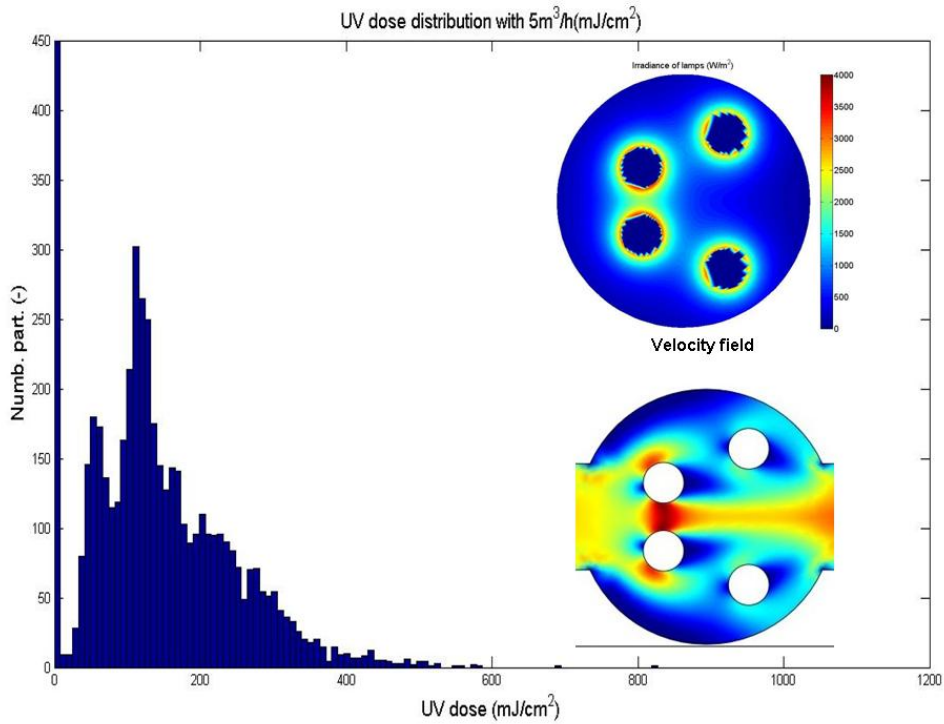


Figure 5-16 UV dose distribution with position 2, UV 254nm, 5m³/h flow

With position 2, the number of particles received zero dose is significantly higher than other positions (more than 2 times higher), which predicted this design failed to give an overall well distributed dose. This much more zero dose occurrence cannot be only explained by the particles that walked out of the reactor without counting at the end of calculation. It indicated that with position 2, there are areas in the reactor where has zero UV intensity irradiation.

In order to compare the three different lamp configurations, UV n% is introduced in this study. UV n% is defined as the value of UV dose that n% of the total particle got through the model calculation. Here, UV 5%, UV 50% and UV 95% are used.

Lamp Configuration	UV 5%(mJ/cm ²)	UV 50%(mJ/cm ²)	UV 95%(mJ/cm ²)
Position 0	40	162	280
Position 1	35	145	320
Position 2	32	145	380

Table 5-3 UV distribution with different lamp configurations

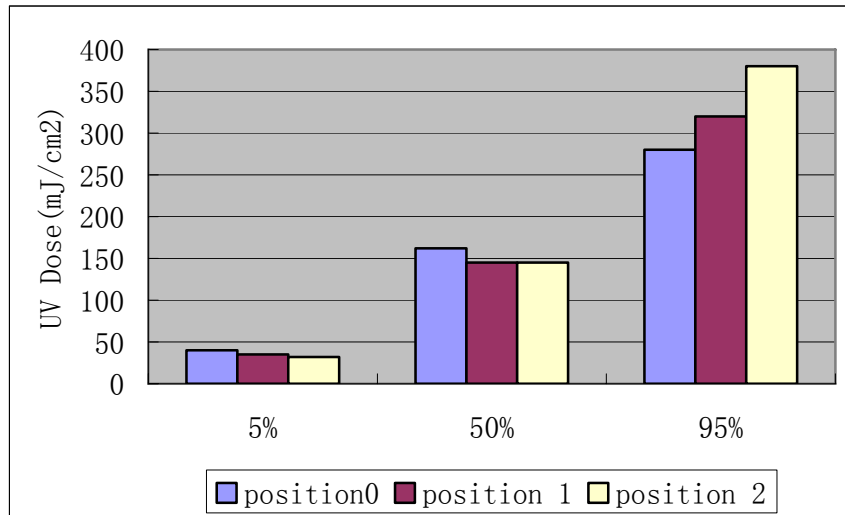


Figure 5-17 UV distribution with different lamp configurations

The average dose of position 0 is higher than other positions, that is because that with other positions, the flow is more concentrated in the center and flow rate between the vertical lamps are higher, which means a lot particles leave reactor quicker.

While discussed about the dose distribution of a UV reactor, narrow distribution indicates better hydraulic performance which means UV 5% and UV 95% should be as close as possible. From table 5-3 and figure 5-17, we can conclude that for the three UV lamp configurations listed above, position 0 is the best design of the three. It has the narrowest distribution pattern as well as the highest average dose among the three, explained by a well combination of velocity field and UV intensity field.

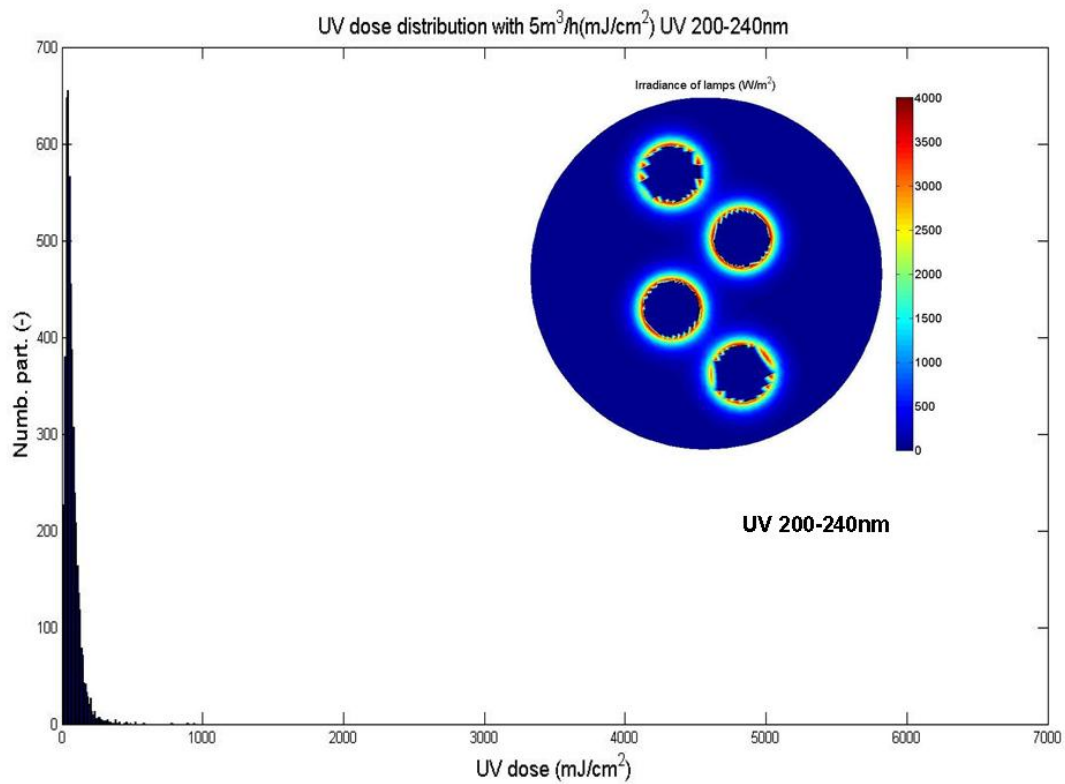
5.6.3.3 Calculation of medium pressure lamps

For low pressure lamp, 254 nm is the only wavelength that contributes to the power output, and the calculation already discussed before.

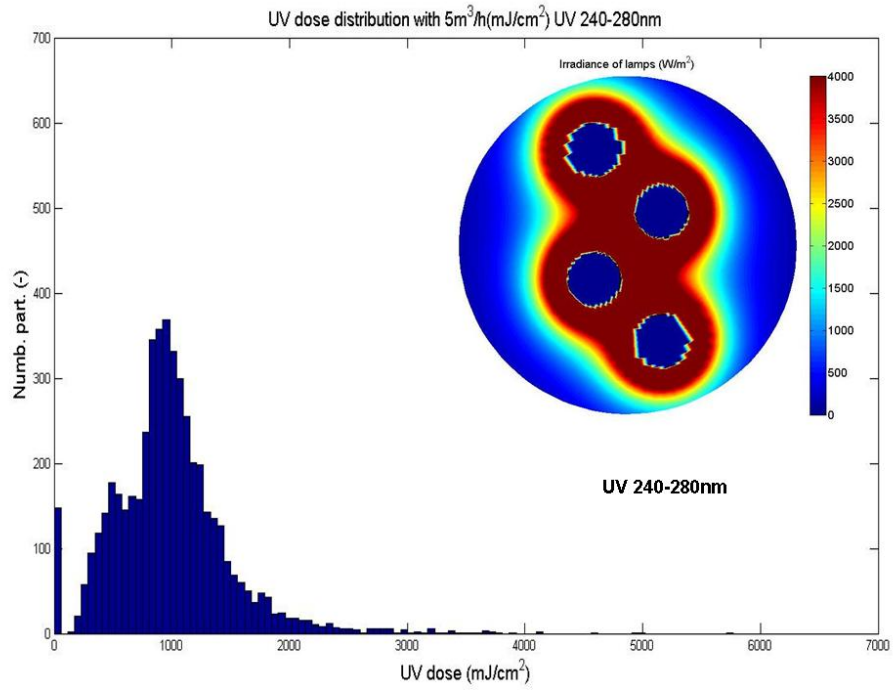
For medium pressure lamps, there is a spectrum of wavelengths that contributes to the total power output, which makes it is rather difficult for calculation of dose. To give an estimation of the effective intensity, the spectrum is split up in three parts. Part one is from 200-240nm, and represents 10% of the total spectrum. Part two and three are from 240-280nm, 280-315nm, and represent 45% of total effective emitted intensity each. The transmittance in quartz was assumed to be the same for the good quality of the quartz. For different range of UV length, the transmittance in water is different, and the values are got from DZH water at pumping station Bergambacht. Position 0 is applied with a feed flow rate of 5m³/h. The parameters of low pressure lamp and medium pressure lamp used for calculation are mentioned in the table 5-4 :

Type of Lamp	Total Power output	Chosen UV wave length	Account percentage of total power output	Specified wavelength	Transmittance in the water	Transmittance in quartz
Low Pressure	150W/m	254nm	100%	150W/m	79%	96%
Medium Pressure	2000W/m	200-240nm	10%	200W/m	35%	96%
		240-280nm	45%	900W/m	80%	96%
		280-315nm	45%	900W/m	90%	96%

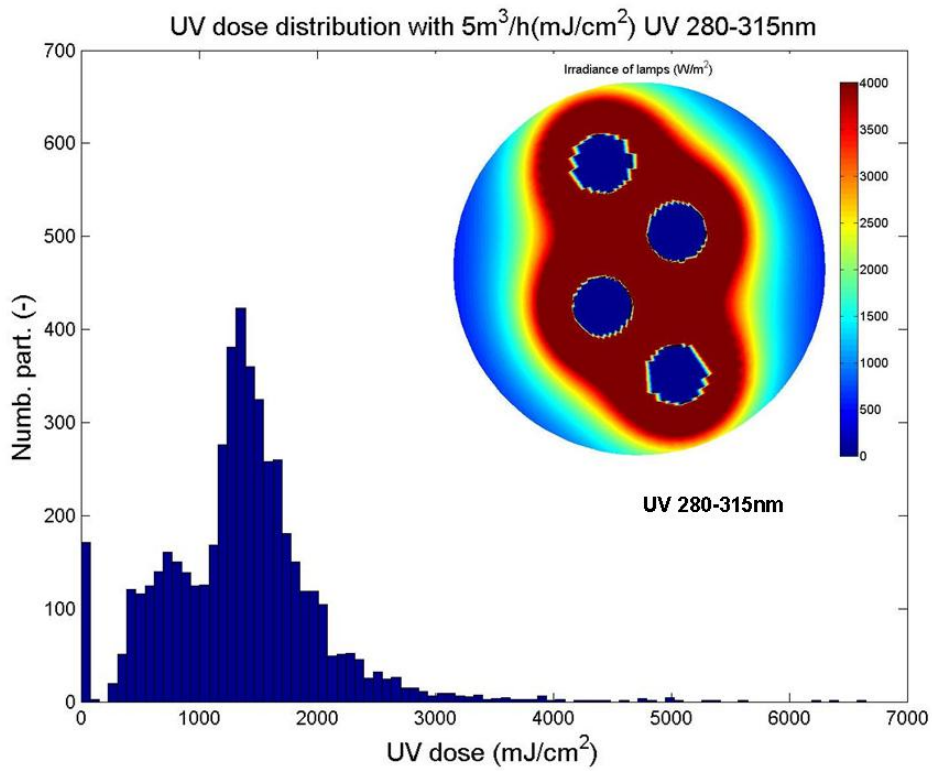
Table5-4 Parameters of different UV lamps used for calculation



(a)



(b)



(c)

Figure5-18 UV dose distribution with position 0, $5\text{m}^3/\text{h}$ flow, for medium pressure lamps, UV 200-240nm (a), UV 240-280nm (b), UV 280-315nm(c)

The same flow condition (5m³/h, position0) was applied. For estimating the average UV dose of medium pressure lamps, the average dose of three parts were added together, which results in 2369mJ/cm². The calculated average UV dose with same flow condition is only 163mJ/cm² for low pressure lamps.

Type of Lamp	Lamp number	Total Power output	Average UV Dose	Ratio (poweroutput/UV Dose)[(W/m)/mJ/cm ²]
Low pressure	4	150W/m	163mJ/cm ²	0.92
Medium pressure	4	2000W/m	2369mJ/cm ²	0.84

Table 5-5 Comparison of low pressure lamps and medium pressure lamps

The ratio of lamp output power and resulted UV dose for low pressure lamps and medium pressure lamps are compared in table 5-5. With the same lamp power output, low pressure lamps can provided about 8% more UV dose than medium pressure lamps, which indicated better dose efficiency. However, medium pressure lamps do result much higher average UV dose with the same number of lamps, so that they can be implied to situations that ask for high UV dose.

5.7 Conclusions

The UV dose model in this study combined three parts, a flow model, a UV intensity model and a random walk model. Long feed pipe for the UV reactor was applied with finer mesh near the pipe walls.

With the same conditions of lamps, the flow rate in the reactor is the crucial factor for the dose distribution pattern. Smaller flow rate gives longer resident time for water in the reactor and results in higher average dose. The higher feed flow gives a narrower UV dose distribution which is preferred in the study.

While same number and types of lamp applied, different lamp configurations can change the flow as well as UV dose. For the three lamp configurations in this study, position 0 showed the best dose prediction due to a well-distributed flow pattern.

Medium pressure lamps can significantly increase the average dose than the low pressure lamps. However, according to the model calculation, low pressure lamps have about 8% more power output to UV dose efficiency.

CHAPTER 6

FLOW MODEL VALIDATION

6.1 Introduction

This chapter describes the experimental study for the UV reactor hydrodynamics, aiming at providing experimental data for comparing with CFD model prediction and validation of the CFD flow model used in Chapter 5 and for reactor design study. Laser Doppler Flow Meter was used for flow velocity measurements in the reactor; conductivity meter measurement with salt dose and dye were used for mixing and retention time study for the reactor.

6.2 Experiment Apparatus and Materials

- Water pump

The main water pump has a capacity of 8m³/h

- Salt dosing pump

The pump for salt dosing has a capacity of 60L/h

- Conductivity Meter

Conductivity Meters got from Waternet, The Netherlands, were used for measuring the salty water conductivity.

- UV Reactor

The UV reactor was achieved from Kiwa Water Research, The Netherlands. This reactor was designed for UV/H₂O₂ advanced oxidation applications. The surface of the reactor is round with a diameter of 30 cm, four quartz tubes placed perpendicularity to the surface, and each of the tube diameters is 48.9mm including the quartz layer. Those tubes were used for putting in UV lamps for the advanced oxidation treatment process, but in this experiment, no UV lamps were installed in those tubes. The surface of UV reactor was made by metal at the beginning. For the experiment, plastic transparent flanges were used to replace the metal flanges in order to allow laser beam to go through the reactor. The water flows in and out the reactor with pipes which have a diameter of 125mm. The picture below shows how the reactor looks like in this study.



Figure 6-1 Picture of the UV reactor with transparent flanges (inflow water direction: left to right)

- Laser Doppler Flow Meter

Laser Doppler Flow Meter is used to be a precision instrument for flow measurement and analysis in this experiment. Velocity range of the system is 0.001-0.75m/second, bi-directional in two dimensions. The velocity is sensed in an ellipsoidal volume of approximately 0.1mm^3 .

- The water used in the study is normal tap water.

6.3 Flow Velocity Measurements

6.3.1 Theory

- Doppler Effect

The Doppler Effect, named after Christian Doppler, is the change in frequency and wavelength of a wave as perceived by an observer moving relative to the source of the waves. The theory of Doppler Shift tells that light from moving objects will appear to have different wavelengths depending on the relative motion of the source and

observer. Observers looking at an object that is moving away from them see light that has a longer wavelength than it had when it was emitted(a red shift), while observers looking at an approaching source see light that is shifted to shorter wavelength(a blue shift).

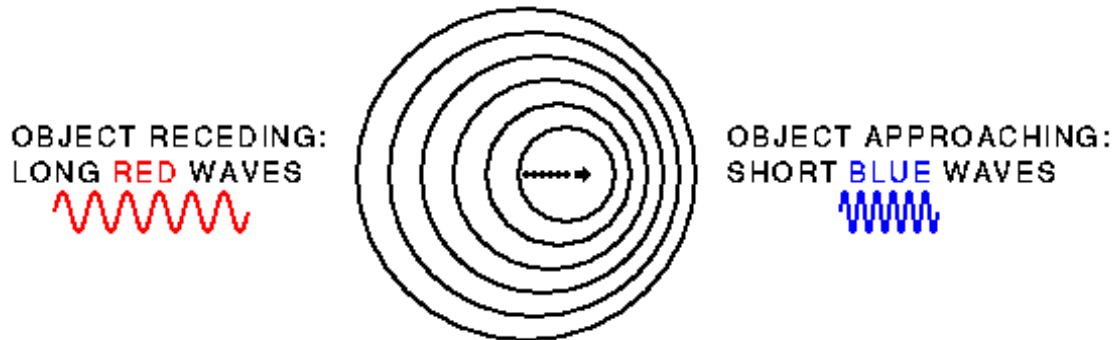


Figure 6-2 Red Shift and Blue Shift

- The theory of Laser Doppler Measurement

Commonly all fluids contain very small particles, for example dust, with a diameter in the order of one micrometer. If a beam of light is projected into a fluid containing particles, part of the light incident on these particles will be scattered in all directions and most of it will be in a forward direction. And this scattered light can be observed with a detector.

If the particles are moving relatively to the light source and the detector, the frequency (f_s) of the scattered light in a certain direction will undergo a small shift relative to the frequency (f_i) of the incident light. This frequency shift is called the Doppler Shift or Doppler frequency.

The values of this Doppler frequency (f_d) is proportional, among other things, to the velocity of the particle and depends on the direction of the light beams. However, the relationship between the Doppler frequency and the velocity depends only on the velocity and frequency of the light and some geometrical data, which means that no direct calibration is necessary.

The velocity of the fluid is determined from the measurement of the Doppler frequency with which it has a linear relationship. The existence of small particles in the fluid is essential for the measurement and fortunately the normal water contains enough of those particles. The magnitude of the Doppler shift is relatively very small. For a particle velocity of 1 cm/s the Doppler shift is only in the order of 10^3 HZ in contrast to the frequency of light which is of the order of 10^{14} HZ. In order to measure such a small frequency shift, the only way is to measure the Doppler frequency (f_d).

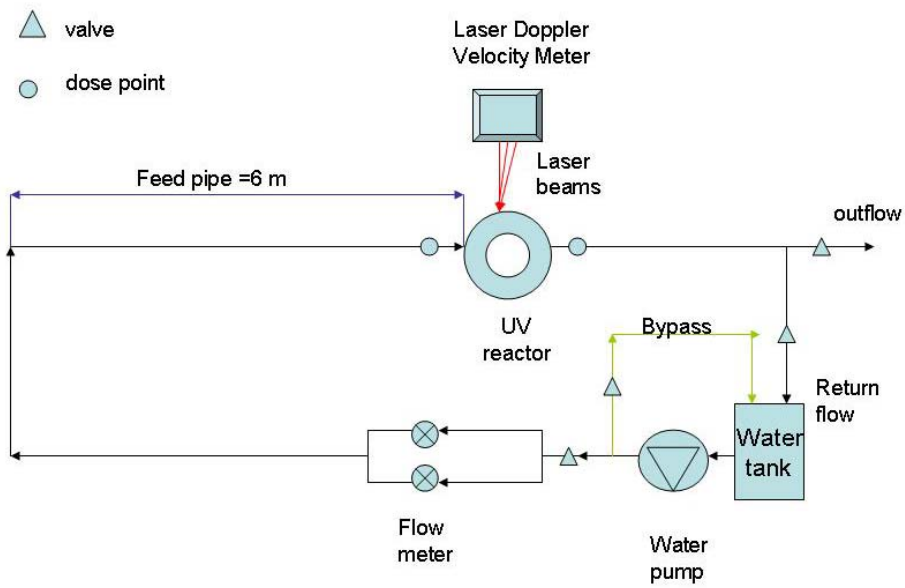
By comparing the frequency of the scattered light with that of the incident beam and not to measure the light frequency itself directly, this frequency shift could be decided. One way of doing this is by mixing the scattered light from a certain direction with light from the same direction which has not undergone this shift, on the surface of a photo detector. The reference beam can be much weaker than that of the incident main beam and the output signal of the detector contains amongst other things the Doppler shift (f_d) between the two frequencies [LDFM technical manual, delft hydraulic laboratory].

For this measurement it is essential that the scattered light beam and the reference beam are optically coherent, this means that the two beams must be obtained from one and the same coherent light source, a laser, using a beamsplitter.

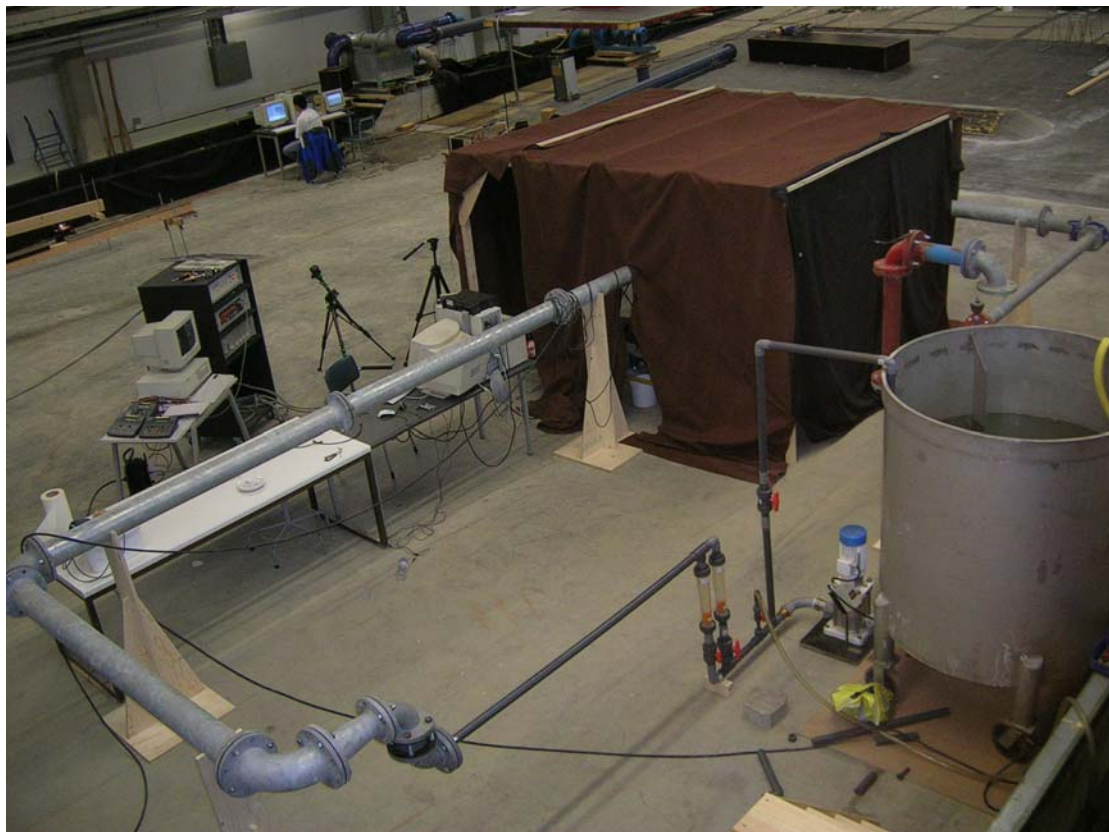
6.3.2 Experimental set-up

The experimental set-up for the fluid velocity measurements was based on the attempt to have a constant, well developed turbulent flow in front of the reactor. In order to achieve this goal, in front of the reactor, 20 diameter length of straight inflow pipe was used. A 200 m³ water tank filling with tap water was used to provide water for the pump. The pump was connected with two flow meters, the capacities of the flow meters are 3m³/h each. A by pass pipe was also connected in order to prevent too much flow in the system. 6 meters straight inflow pipe was connected in front of the UV reactor which surface was placed perpendicular to the ground, and the outflow water was collected by another pipe which flowed back to the water tank. In this way, the water is constant re-circulated in the system.

In front of the reactor stood the Laser Doppler Flow Meter, which emits three beams of laser. The Laser Doppler Flow Meter was put on a computational controlled, moveable shelf in order to change the positions for the measurements, the measured ellipsoidal water volume is approximately 0.1mm³, and the actuality of the positioning is ± 0.0001 m. The flow meter and shelf were covered by dark cloth because the laser can cause problems to human eyes with direct radiation. The data from the reading of the Laser Doppler Flow Meter was sent to another computer for analysis.



(a)



(b)

Figure 6-3 Experiment setup for fluid velocity measurement inside UV reactor, drawing (a), picture(b)

6.3.3 Experiment Procedures

Two experimental flow rates were applied in this study, $2.1\text{m}^3/\text{h}$ and $5\text{m}^3/\text{h}$. Coordinates for some points at the edge of the reactor were defined first according to the measurement range of the velocity meter. By changing the coordinates of the shelf with the computer, the laser beam aiming positions were changed. Each measurement for a certain position was conducted during 3 minutes in order to get a more reliable velocity reading. The velocity reading was set to be 1000 times per second, and the output data of water velocity is the average value of every 10, which means the reading output was 100 per second. The direction of X is defined as the direction parallel to the inflow, and the direction Y is defined as the direction vertical to the ground, and the direction Z is parallel to the quartz tube. Only the velocities of directions X and Y can be measured. And the velocity vectors measured by the Laser Doppler Velocity Meter has a negative angle of 45 degree to the velocity vectors X and Y, with a simple calculation, the X and Y velocity of the flow in the reactor can be obtained.

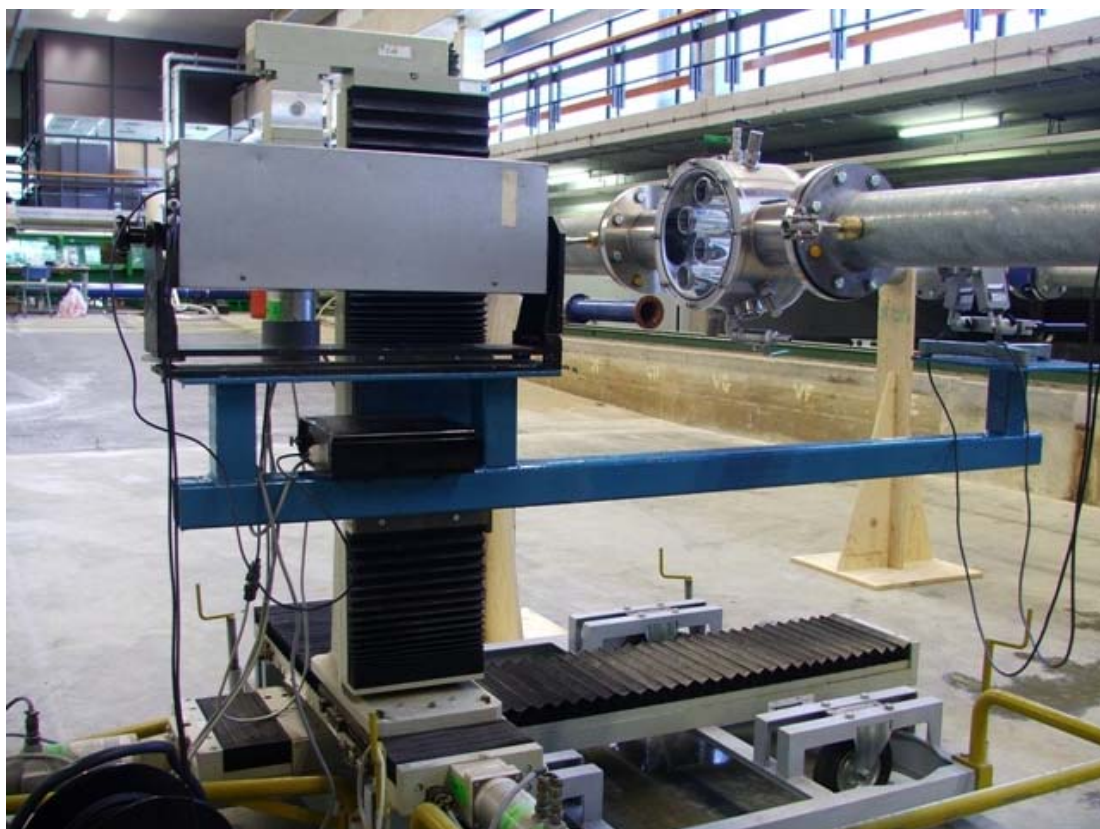


Figure 6-4 Laser Doppler Velocity Meter with Computer Controlled shelf in front of the UV reactor

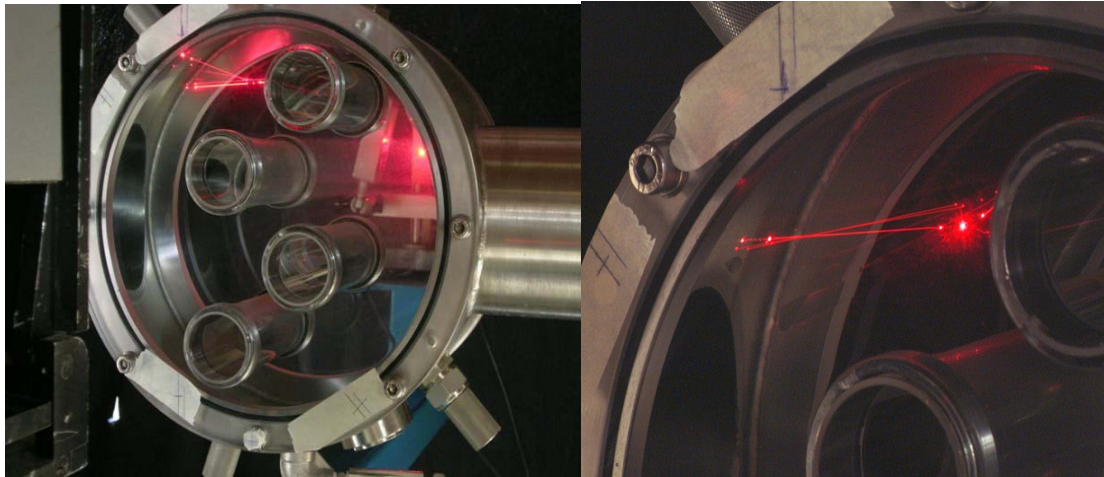


Figure 6-5 Laser beams crossed inside the UV reactor (whole, left; part, right), the red light beams are the laser beams

6.4 Flow Velocity Measurements

6.4.1 Measurement cross sections

Because it is too difficult to measure the water velocity at all the positions inside the reactor, in this study, several cross sections were chosen for the measurements. The cross sections were chosen widely spread in the whole reactor in order to provide more information for understanding of the hydrodynamics characteristic of this UV reactor.

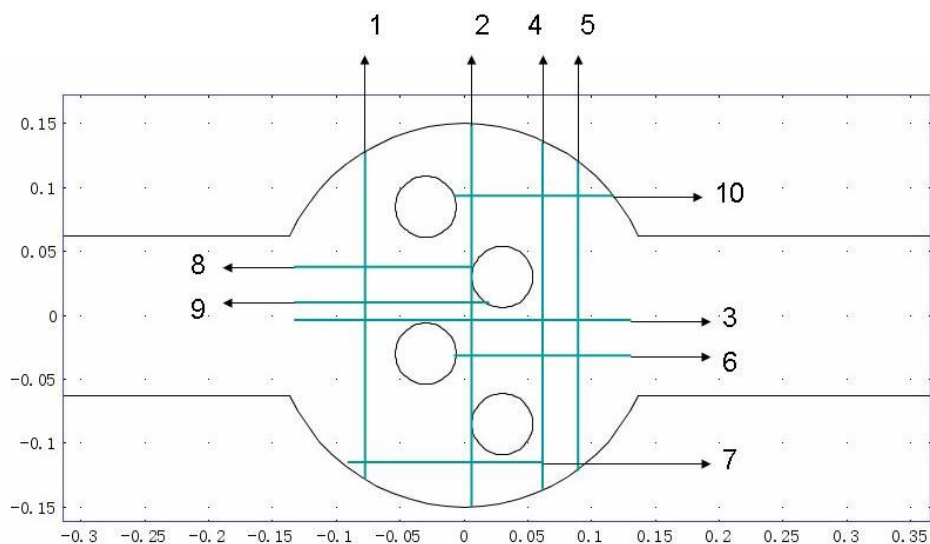
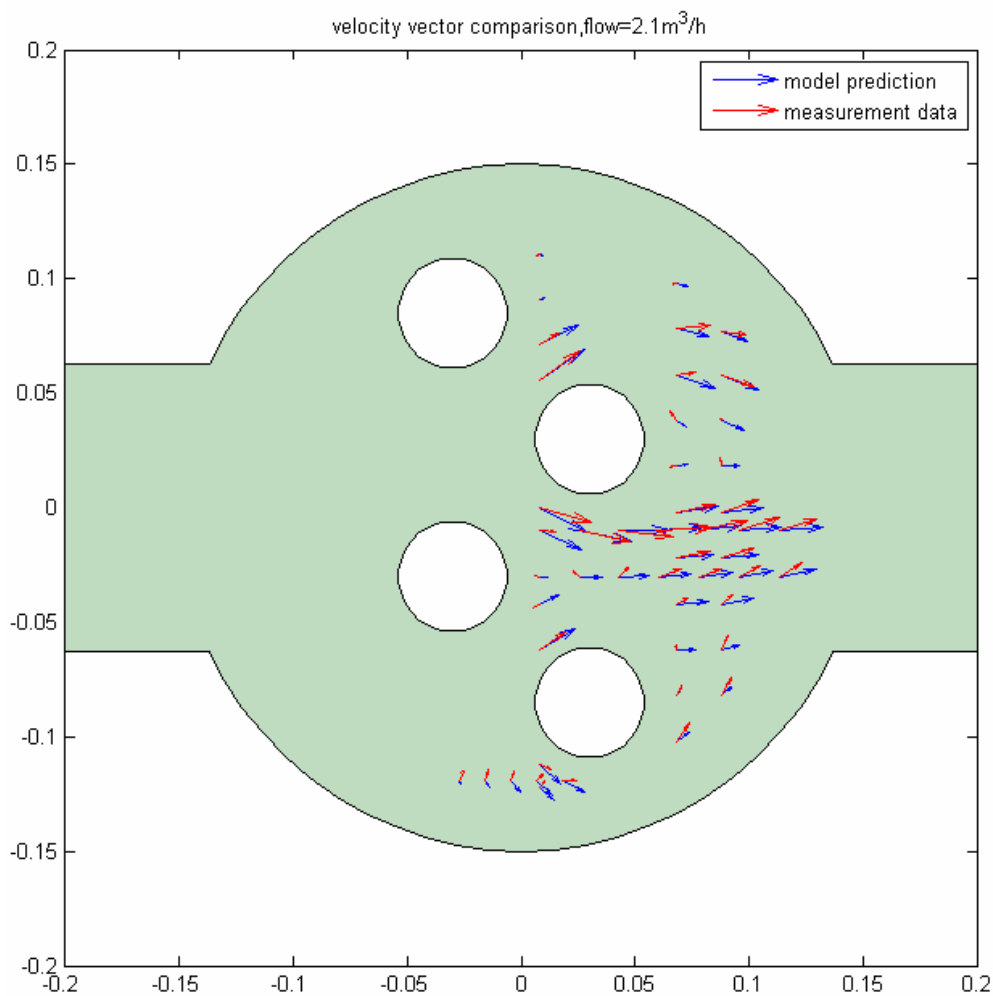


Figure 6-6 Position and number of measured cross sections

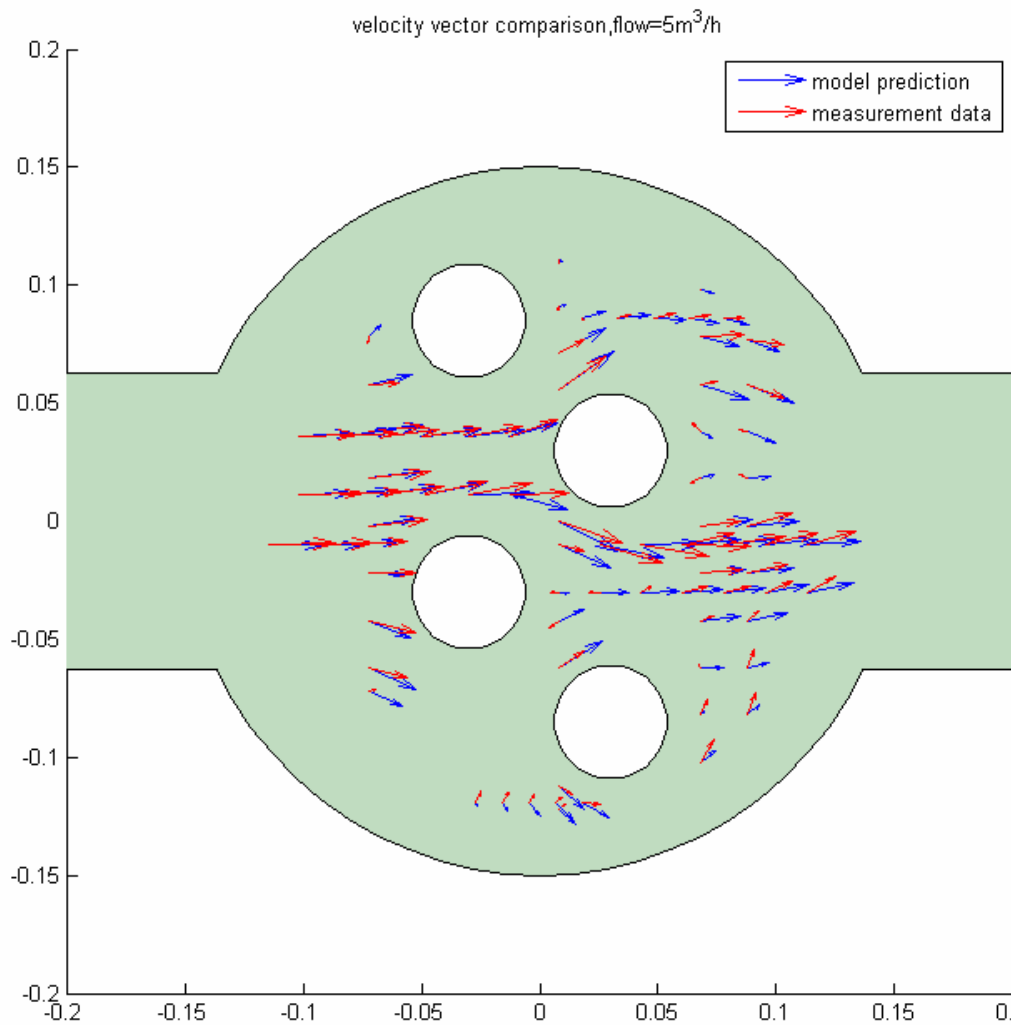
For this study, the central profile of the reactor is most interesting for comparing with the 2-D CFD hydrodynamics model. For a flow of 2,1 m³/h, for the central profile, 6 cross sections were chosen, and for flow of 5m³/h, in total 10 cross sections were chosen. For other profiles in Z direction, velocities of water for some other cross sections were also measured to give more idea of 3-D water flow. The figure below shows the cross sections measured in the study, and green lines indicate the position for the chosen cross sections. A list of the coordinates of cross sections corresponding to the reactor can be found in the Appendix.

6.4.2 Velocity vectors comparisons

For the mentioned cross sections, X and Y mean velocity along the experiment conducted time were measured, with the inflow velocity set at 2.1m³/h and 5m³/h separately. The velocity vectors measured and predicted by the CFD flow model are compared in the figure below. The blue arrows are the velocity vectors predicted by the model and the red ones are measurements (water flows from left to right).



(a)
- 68 -



(b)

Figure 6-7 Velocity Vectors comparison with inflow velocity=2.1(a) and 5m³/h(b)

In general, patterns of the velocity vectors from the model and measurements for both flows show good qualitative agreement. Best direction and value agreement is for the area before the quartz tubes, although the values have smaller differences. Areas behind the quartz tubes also shows good agreement in values, but the flow directions in the measurement are more upwards than the model simulation.

The measurement and model results for cross section which is very close to the lowest lamp position gave totally different directions. The model predicted water flowing downwards, while the measurement tells that the flow direction is actually upwards. This difference means the model failed to give good prediction of eddies and circulations behind the quartz tubes. And the flow is more centered and condensed

than the model predicted. The comparison also demonstrated that around the quartz tubes, the differences are bigger than other locations.

6.4.3 Well predicted area

For the area before the tubes, the model and measurement results give good agreement, in cross section 1 for instance, for x velocity, y velocity and turbulence kinetic energy. In the figures below, arc-length is the length of reactor at the cross section along the direction of arrow besides it. The blue curve is the model prediction along the arc-length, and green stars are the model prediction results at the measurement points, while the red dots are the measured velocity value at those points.

It is not hard to conclude that because those areas are just before the tubes, the flow is not disturbed by suddenly changing of the shapes in the reactor, which also says that the flow model is working well in those areas. However, the measured flow is more concentrated in the center of the reactor than the model simulation.

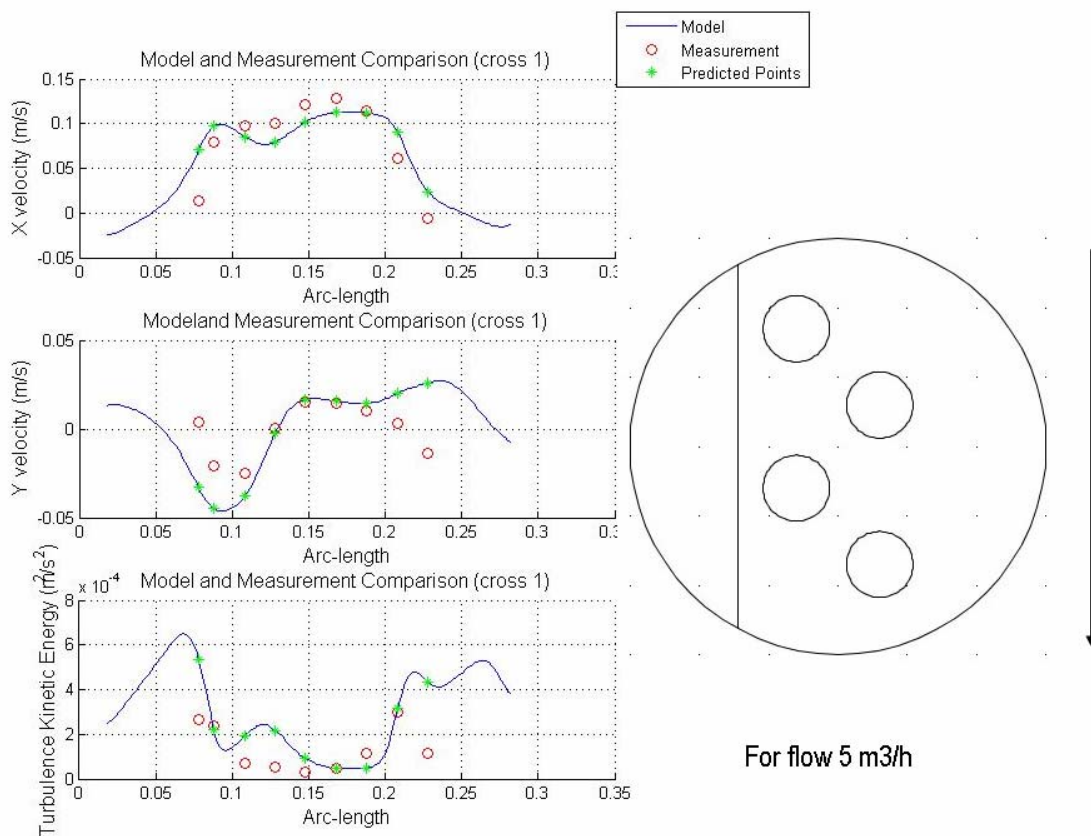


Figure 6-8 Model and measurement comparison with cross section 1

6.4.4 Poorly predicted area

Cross 7 located just in front of the lowest lamp, in this area, as can be told from the velocity vector figures, the predictions of Y velocity directions are quite opposite. The Y velocities are negative in the model prediction, with means the flow direction is downwards in the model; while the measurement Y velocities are almost all positive except the last point, which shows the water was tending to flow upwards at this area in the reaction. The k, turbulence kinetic energy also has lower values than the model predicted, which means the water retaining in this area longer than the flow model expected because of less turbulence.

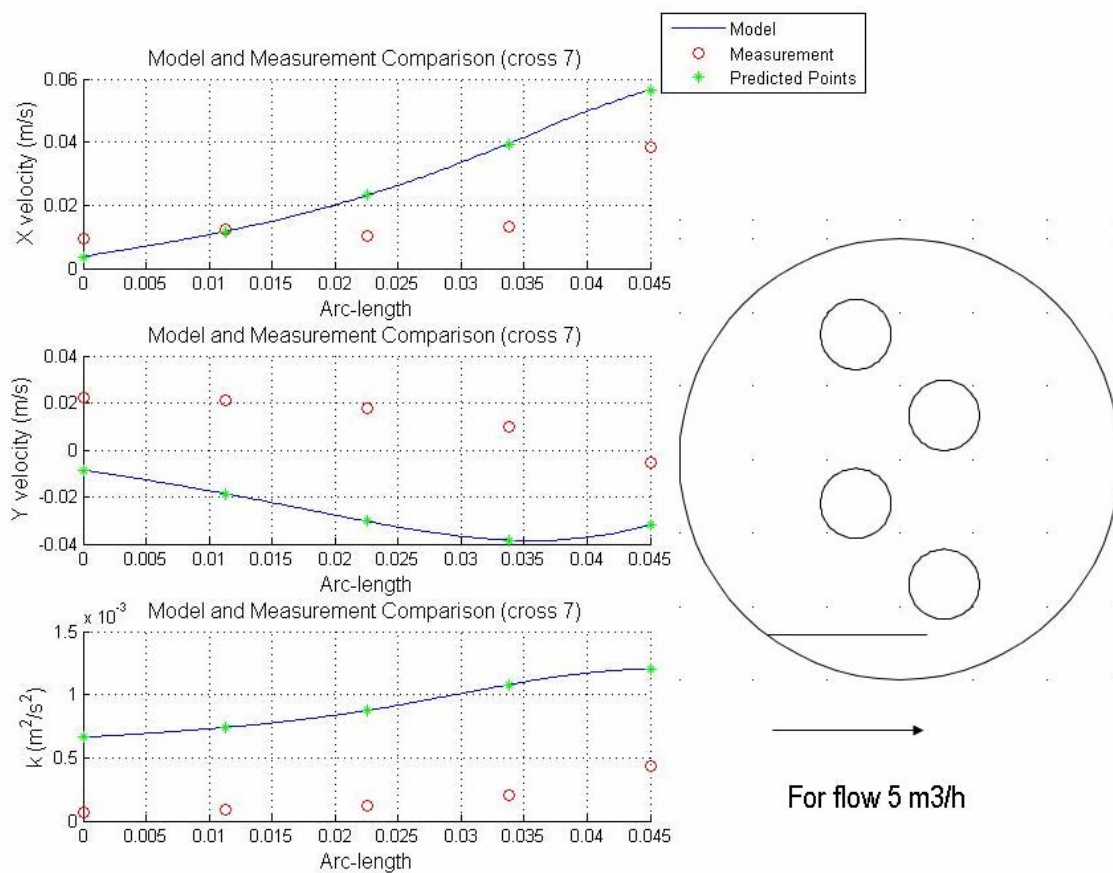


Figure 6-9 Model and measurement comparison with cross section 7

6.4.5 Failed prediction of circulation behind the quartz tubes

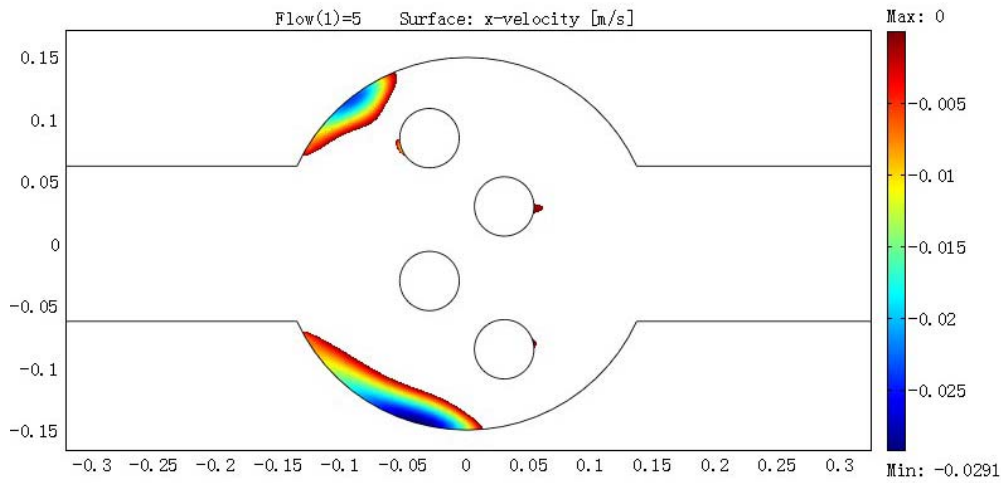
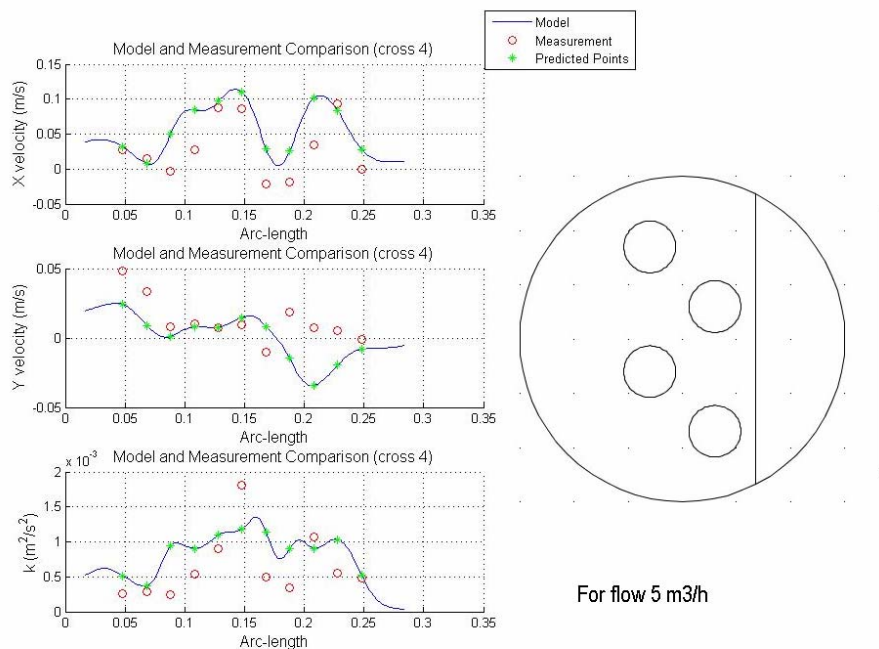
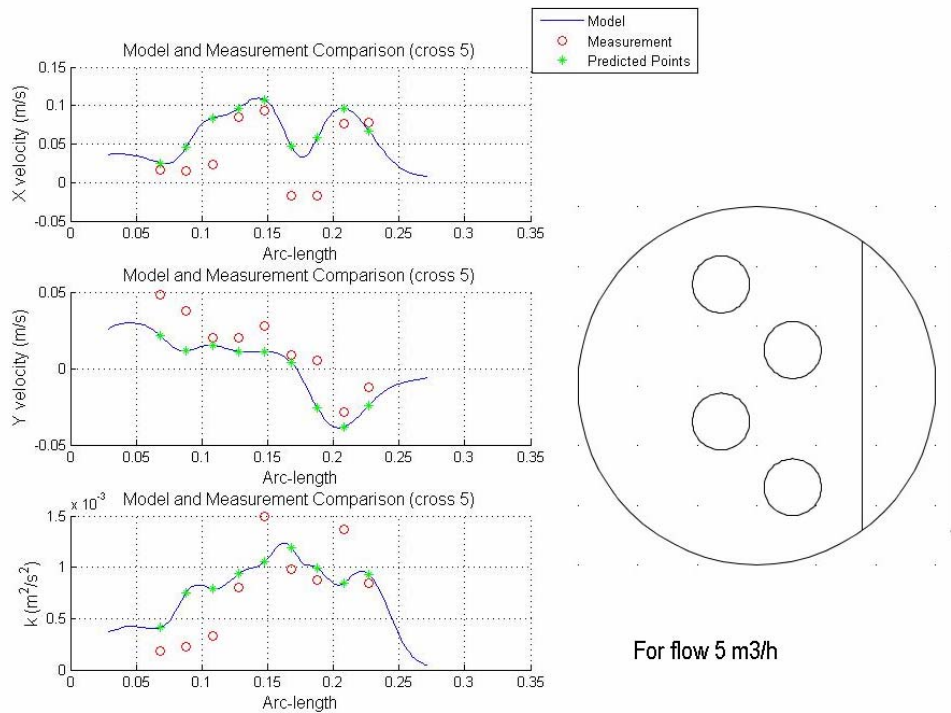


Figure 6-10 The model prediction of negative x velocity, flow= $5\text{m}^3/\text{h}$

Figure 6-10 is the model prediction result for negative x velocity in the reactor. The interesting area is the small red points just behind the right column of quartz tubes, which indicated water recirculation behind the tubes. From the model calculation, the recirculation zones are rather small and only located behind the right column of the quartz tubes, and a little bit before the top-left tube. Cross section 4 and 5 are chosen to study the area behind the right column tubes.



(a)



(b)

Figure 6-11 Model and measurement comparison with cross section 4 (a) and 5(b)

For the areas behind the right column of quartz tubes, all the measurements reveal certain circulation in those areas, where the x velocities give negative values. While in the model, x velocities keep positive values in these two cross sections where measurement values are negative. Also, the turbulent kinetic energy for the areas behind the quartz tubes is 3 times higher than the model prediction in cross section 4, which confirms the recirculation and eddies behind the tubes. Cross section 2 is behind the left column of quartz tubes, and in the measurement, negative x velocity values can also be found (see Appendix). The comparison indicates that the flow model fails to predict the accurate size of recirculation of water behind the tubes.

6.4.6 2-D model with 3-D flow measurements

The flow model built up in Chapter 5 is only 2-Dimensional while in the measurement the water is flowing in a 3-Dimensional reactor. Although for the comparison the central profile for the reactor was chosen, there are still reasonable influences from the differences of dimensions.

The central profile in the reactor towards z direction was set to zero, in total five profiles with different z values are chosen. Because cross section 1 is the well predicted in the model, X mean velocity measured in cross 1 with different z profiles

is given in figure 6-12, while axis x value is the position of measurements along x direction, axis y value is the measured x mean velocity. From the measurement it is not difficult to discover the velocity in reactor is not perfectly symmetric even without disturb by the quartz tubes. The central profile has highest velocity value in both flow cases (only $5\text{m}^3/\text{h}$ condition is listed below). The shapes of all velocity profiles are not symmetric to the center 0 may be because there are a bent before the 6 meters of straight inflow water pipe.

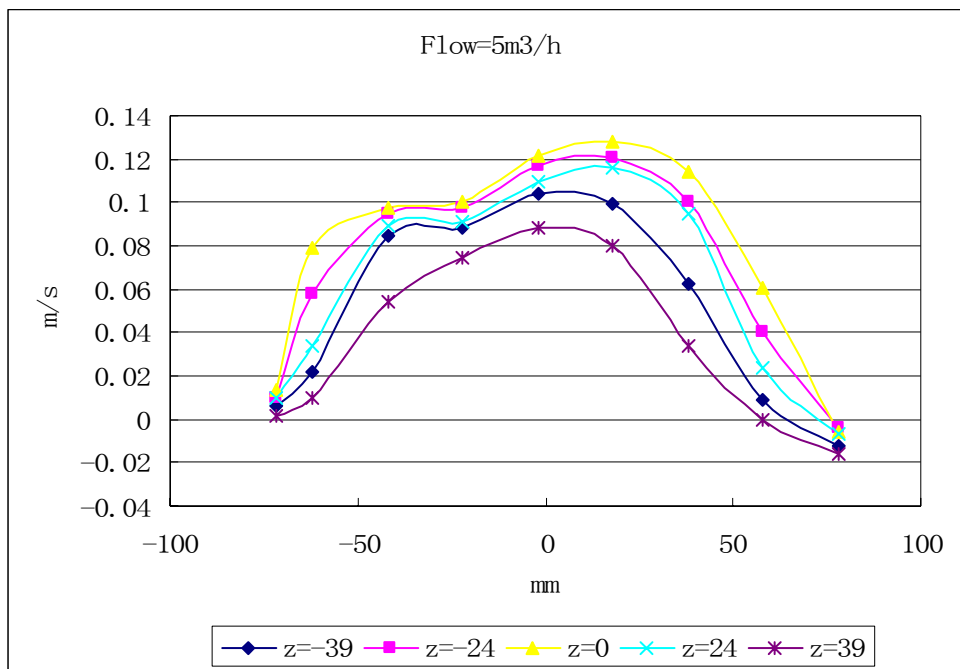


Figure 6-12 X-mean velocity with different z profiles in cross 1, flow= $5\text{m}^3/\text{h}$

6.4.7 Possible influences on the UV dose prediction

As discussed in section 6.3, there are differences of the flow in the reactor in reality with the model prediction. Behind the quartz tubes, there are water recirculation zones which are underestimated by the flow model simulation, and for the profiles away from the reactor center, deviations of velocities are also observed. Because the flow determines the dose pattern, poor accuracy of flow prediction can result in poor UV dose prediction. From the validation of flow model, it can be concluded that the flow prediction is good in general. For the poor predicted areas (at the top and bottom of reactor near the inlet), since the UV intensity is pretty low there (near zero), the UV dose in those areas is very small, and the effect can be neglected. Possible influences caused by the difference of model prediction and measurements are discussed here:

Overestimated dose because of recirculation zones:

Behind the quartz tubes, the recirculation zone occupied about one fourth of the total tube perimeter. As already mentioned in chapter 5, the area around the UV lamps has highest UV intensity. While there is recirculation in these areas, only a small amount of water stays there and receives great amount of UV dose caused by longer retention time with high UV irradiation, most of water just flows way from this part of lamp. In other words, one fourth of the lamp perimeter is not fully used. This results in dose model prediction higher than the reality. As a rough estimation, the overestimated dose is about one fourth more.

Underestimated dose because of 2D model:

The central profile in the reaction has highest feed velocity which is showed in figure 6-12. The model in Chapter 5 is based on the calculation of central profile with higher velocity, which underestimates the real retention time of water inside the reactor, and results in underestimating the final dose prediction because the dose is depended on the calculation retention time. From figure 6-12, when the velocity at position (0,0), the central velocity is about 0.12m/s, and the average velocity is 0.10m/s over five profiles. Based on the fact that velocity differences causes retention time different, which reflects on the final dose prediction. The dose prediction of the model is about 20% less than the reality because of the 3-D and 2-D difference.

6.5 Salt dosing experiment

6.5.1 Theory

- Mass balance

The mass balance (also called a material balance) is an accounting of material entering and leaving a system. Fundamental to the balance is the conservation of mass principle, i.e. that matter cannot disappear or be created. Mass balances are used to design chemical reactors for instance. The basic principle can be described as,

$$IN=OUT+ACC$$

,when IN is the material entering the system, OUT is the material leaving the system, and ACC is the material accumulating in the system.

- Effect of the reactor shape

For a certain amount of salt dosing in the inflow of the reactor, when measuring the salt concentration of the outflow of the reactor, the accumulated amount of salt in the

outflow should be the same with that in the inflow. However, because of non-uniform reactor shape, a certain amount of water containing salt will stay longer in the reactor. The different salt concentration distribution between that in the inflow and outflow gives information of the reactor.

6.5.2 Experimental set-up and procedures

The set-up for salt dosing is based on the velocity measurements. A 60L vessel filled with salty water was prepared first with a certain salt concentration. One salt dosing pump with a capacity of 60L/h was connected in front of the two flow meters for pumping the salty water inside the system.

Two small pipes were inserted in the center of the inflow and outflow pipes just in front of and after the UV reactor. The length of two small pipes into the big pipes is half of the big pipes. These two pipes have holes which let water flow in the pipes and are connected with sensors of conductivity meter. The reading of conductivity meter was collected by computer.



Figure 6-13 Dosing vessel and dosing pump (top left); Insert pipe (top right); Salt dosing set-up (bottom left); conductivity meter reading (bottom right)

6.5.3 Results for salt dosing experiments

Because the reactor is not a straight pipe, a certain amount of water will be retained in the reactor longer. The figure below is the result from the salt measurements. The blue line is the salt concentration measurement results at the inlet of the UV reactor taken from just in front of reactor, and the green line is the salt concentration measurements for the water leaving the UV reactor. The peak concentration measured from the conductivity meter is set at value one. Time scale was set the same for the inlet and outlet, with zero cross when the concentration reading reached half of the peak concentration.

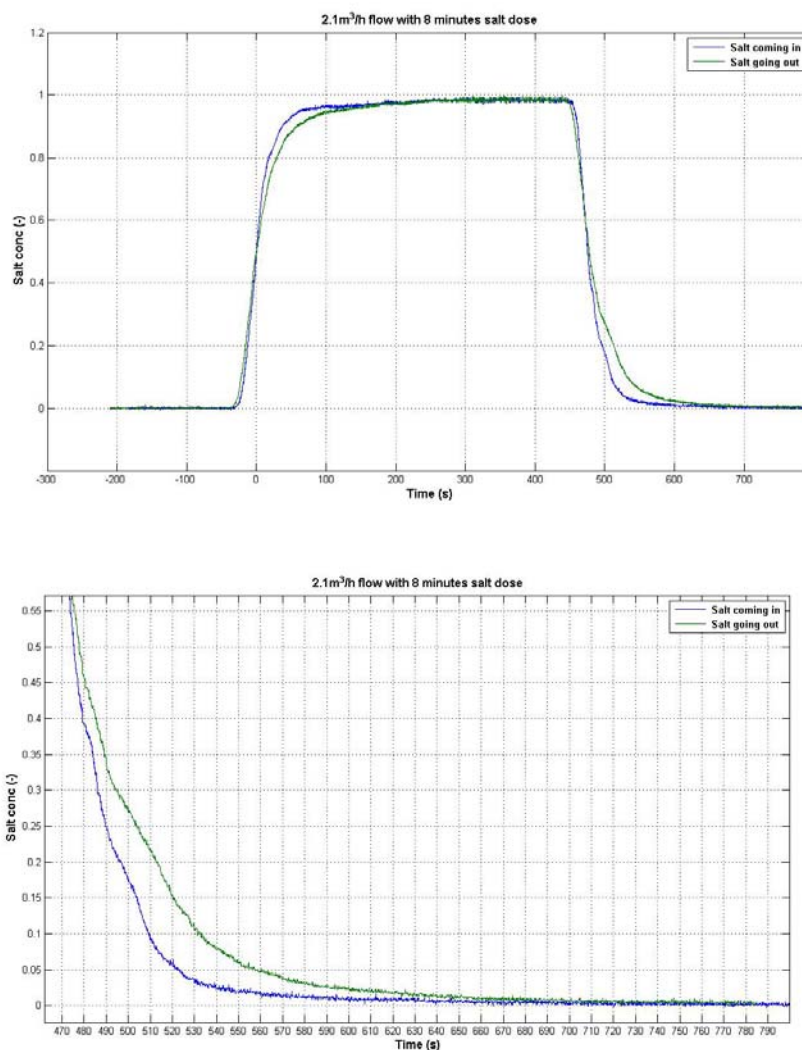


Figure 6-14 Concentration of salt with time, 2.1m³/h flow, 8 minutes of salt dose, whole (top), partly zoom in (bottom)

Figures of salt dose measurements can be used to determine the retention time expanded in the reactor. There is a clear difference between the two lines. From 50% until 100% of peak value, the salt concentration value measured after the reactor (green line) increased slower than that in the water from the inlet, which indicated that the reactor can smooth the peak. The value of the blue line reach zero earlier than the green line. The difference is caused by the effect of longer retention time for a certain amount of water in the reactor. The reactor retained salt about 50 seconds (from 610s to 660s in the figure 6-14), which is longer than a straight pipe with 2.1 m³/h flow. However, it is hard to determine how much of the amount actually is caused by the reactor because of the relevant pretty long response time for the sensor of the conductivity meters (4~5 seconds). Other dose times are also tried and the result is presented in the Appendix.

6.6 Dye experiment

6.6.1 Experimental set-up and procedures

KMnO₄ was dosed into the system just in front of the reactor and the same discharges as velocity measurements were set. Several videos were taken to visualize the dye in the reactor.

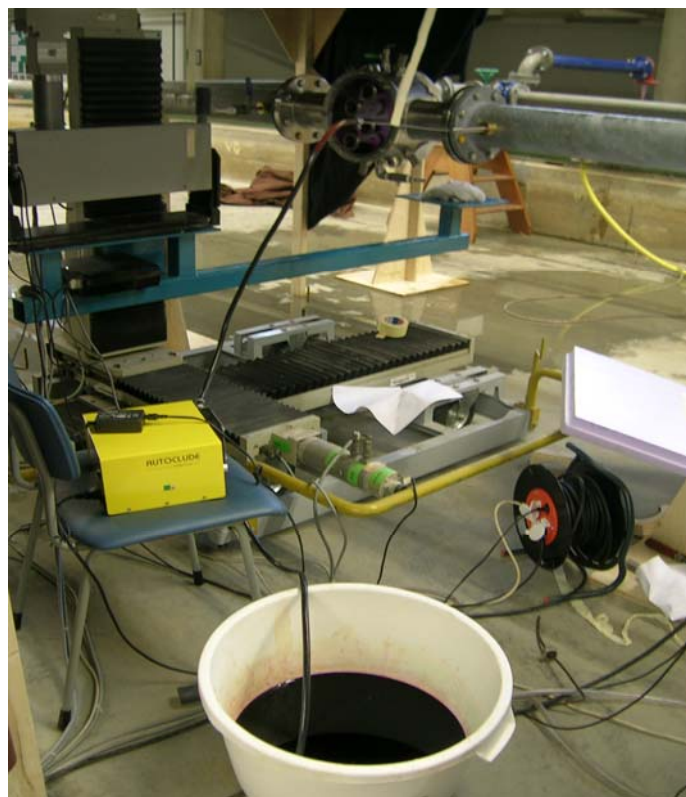


Figure 6-15 Dye Experiment Set-ups



Figure 6-16 Dye dosing pump (left) and dye used in the experiment (right)

6.6.2 Results and discussions of dye experiment

The dye experiment visualizes the dye with the flow inside the reactor, in the center of the reactor, the color of dye disappeared faster with both flow rates ($2.1\text{m}^3/\text{h}$ and $5\text{m}^3/\text{h}$) than other areas which is also proved by the flow model because the higher velocity between the lamps. During the experiment, a clear washed white zone appears just between the vertical lamps. On the top and bottom of the reactor, both near the inlet and out let, color of dye last longer and small eddies are also discovered, which is also fit well with the low velocity prediction and circle streamline in the flow model.

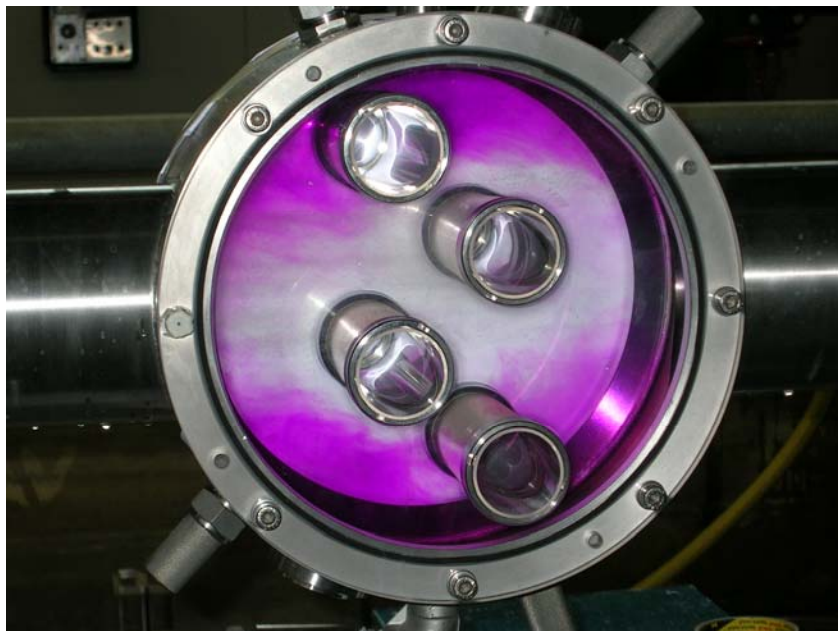


Figure 6-17 UV reactor with dye color in it, while the purple zone indicates the existing dye in the reactor, while zone is caused by dye washed away by clean water.

While the reactor is filled with dye color, the concentration of dye is defined as value 1, and when there is no dye in the reactor, the dye concentration is zero. Dye concentrations with time change at top half of the reactor (Y value from 0.0625m~0.15), bottom half of the reactor (Y value from -0.15~ -0.0625), were compared with that of the whole reactor (Y value from -0.15~0.15), the comparison figure is given in 6-18. In figure 6-18, axis x value is the measurement time divided by average retention time (feed flow rate/ total reactor volume), axis y value is the relative dye concentration.

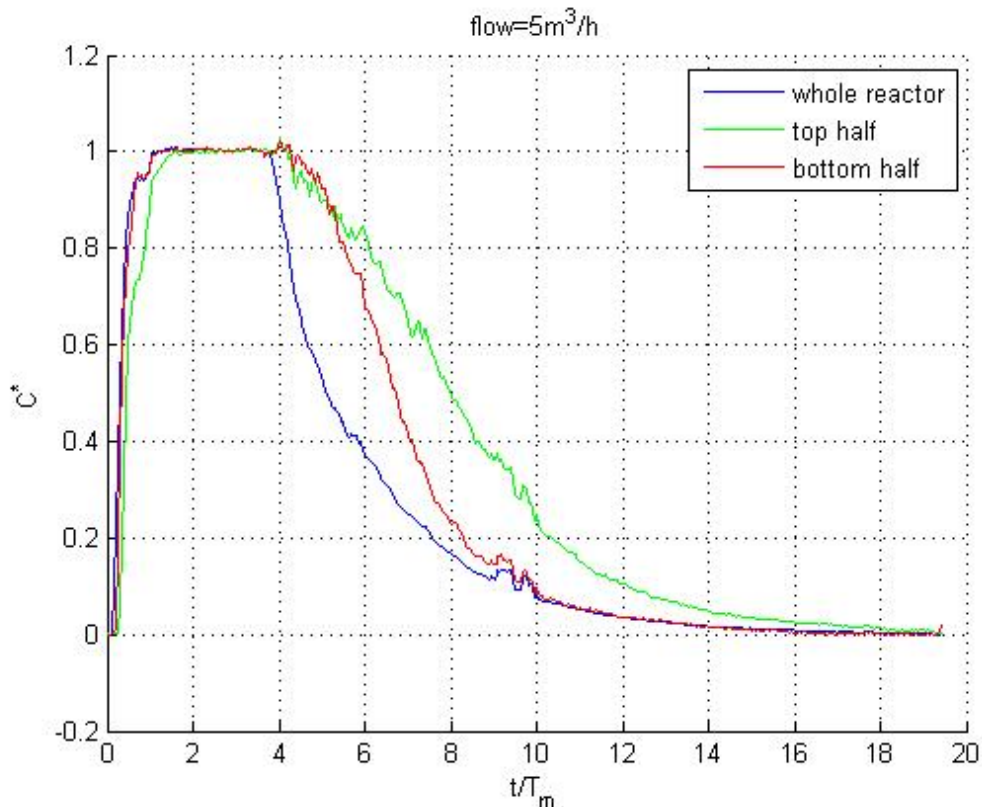


Figure 6-18 Dye concentration with relative time

Figure 6-18 gives clear view of dead zones in the reactor, which locate at the top and bottom of the reactor. Those parts have higher value of dye concentration than the average value of whole reactor at the same relative time after dye peak concentration value 1, which indicate longer retention time of water. And top part of the reactor has even longer retention time than the bottom.

6.7 Conclusions and Recommendations

6.7.1 Conclusions

Velocity measurements were conducted in several cross sections inside the reactor. The k- ϵ CFD flow model demonstrated generally good qualitative prediction of flow inside the reactor but failed to give correct prediction of recirculation zones behind the quartz tubes.

The best prediction areas are located at where the water just flows into the reactor, but the flow tends to be more concentrated to the center than the model prediction. The sudden shape change of water flow area, from straight pipe to bigger reactor, generated dead zones at the top and bottom near the inlet of the reactor which have very low velocities, and the bottom dead zone has longer retention time than the top zone. According to the measurements, bigger areas behind the quartz tubes that have water recirculation than the model predicted, which may result 25% of more UV dose prediction. There are differences caused by 2-D model and 3-D measurements, which may result about 20% less UV dose prediction.

The UV reactor design with position 0 and low pressure UV lamps can satisfied the demand for degradation of 4TBP in Shanghai (UV dose up to 200mJ/cm²) with advanced oxidation process. A flow rate around 4.1m³/h is suggested.

6.7.2 Recommendations

6.7.2.1 Improved mesh with improved prediction of circulation

In order to improve the recirculation prediction behind the quartz tubes, several methods were tried. The most effective one is to improve the mesh number and quality near the tube walls.

Position 1 was chosen because the tube position is symmetric. Considering the calculation memory, only half of the model was re-meshed. The recirculation prediction results before and after the re-mesh are given below.

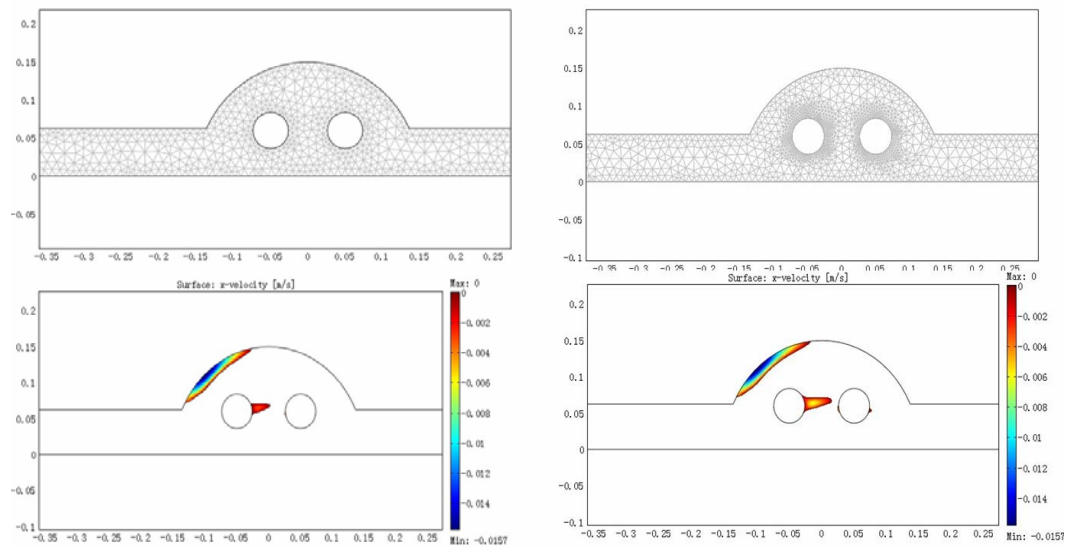


Figure 6-19 Mesh and recirculation prediction, original mesh and prediction (left), refined mesh and prediction (right)

In figure 6-19, original mesh and refined mesh near the tubes are listed. For the flow prediction, the colorful areas have negative x velocity, which indicates water recirculation there. With the old mesh, only the top left part of the reactor and behind the left tube there are recirculation zones. With the refined mesh, the recirculation zone also appears behind the right tube, and the size of recirculation area behind the left tube as well as on the top left reactor also becomes bigger. This explains the refined mesh around the tubes can improve flow prediction, although not very much.

6.7.2.2 Recommendations for further modeling

3-D model is suggested to be built for further study, as well as good defined meshes, especially for the areas near the quartz tubes. Temperature influence on the water viscosity needs to be included in the model. Further verification and development of the random walk model is necessary to prevent particle walking out of the reactor wall. Chemical reaction model is suggested to build up to give UV inactive predictions.

6.7.2.3 Recommendations for further experimental study

For the flow measurement, more positions are suggested to be used, as well as a longer feed pipe without bent at the beginning of the reactor set-up. For the salt dose experiment, more sensitive conductivity meters with shorter response time are suggested. In order to give a good validation of dose model, UV-sensitive dyed microsphere particle tracking experiment with dose indication is suggested.

6.7.2.4 Possible improvement of the current UV reactor design

To improve turbulence behind the quartz tubes, higher wall roughness quartz tubes can be used. Since there are big dead zones at the top and bottom of the reactor because of suddenly changed reactor shape from straight pipes, smaller ratios of reactor to feed pipe diameter are suggested. When use smaller reactors, continues reactor design can be applied with less lamps in each reactor and more reactors in series.

To distribute a more uniform flow, instead of the UV reactor discussed before, a Wedeco UV reactor can be applied, which can give very low head loss with a relative linear flow pattern. An example of Wedeco UV system is given below in figure 6-20.



Figure 6-20 Wedeco UV system K series

CHAPTER 7

CONCLUSIONS AND RECOMMENDATIONS

7.1 Introduction

For this thesis, two parts of research work were conducted. The first part is Chapter 2 and 3, for study the AOPs reaction kinetics using UV/H₂O₂ and hydrogen peroxide along to remove 4TBP in the contaminated Shanghai water.

The second part is Computational Fluid Dynamics modeling and validation of the UV reactor design in chapter 4,5 and 6. CFD models were used to predict UV dose and its distribution. There are three parts of this model, which are a flow model, a UV intensity model and a random walk model. Validation of the flow model was conducted by hydraulic measurements of the fluid inside the reactor.

7.2 Conclusions

Current UV reactor design at Kiwa Water Research, with position 0 and low pressure mercury lamps and a feed flow rate of 4.1m³/h can be used for advanced oxidation treatment of 4TBP in Shanghai. Higher roughness quartz tubes walls and relative smaller ratios of reactor to feed pipe diameter can be applied to improve reactor performance in the recirculation and dead zones with current design.

For the AOPs kinetics study, hydrogen Peroxide alone is able to degrade 4TBP within 72 hours up to 35%. UV/H₂O₂ process can more effectively decrease 4TBP concentration than hydrogen peroxide alone. Good free oxidation radical production within UV dose range 0 to 200mJ/cm² by a low pressure mercury lamp. The removal percentage of 4TBP can reach 96% at 200 mJ/cm² UV dose, 100mg/L H₂O₂ concentration. The 4TBP degradation process fits with pseudo first order equation for UV-dose and H₂O₂-dose. However, at very high H₂O₂-doses (100mg/L), the scavenging of hydroxyl-radicals needs to be taken into account.

For the CFD modeling and validation, a higher feed flow rate (5m³/h) is preferred, which contributes to a relative narrow UV dose distribution than the lower flow rate (2.1m³/h). With three lamp configurations, position 0 is the best among the three with the highest average UV dose as well as the narrowest dose distribution pattern. Model

also predicted low pressure lamps have about 8% higher power output to UV dose efficiency than medium pressure lamps.

The k- ϵ CFD flow model demonstrated generally good qualitative prediction of flow inside the reactor but failed to give correct prediction of recirculation zones behind the quartz tubes. The best prediction areas are located at where the water just flows into the reactor, but the flow tends to be more concentrated to the center than the model prediction. There are dead zones of water at the top and bottom near the inlet of the reactor which have very low velocities, and the bottom dead zone has longer retention time than the top one. Bigger areas behind the quartz tubes that have water recirculation than the model predicted, which may result 25% of more UV dose prediction by the model. There are differences caused by 2-D model and 3-D measurements, which may result about 20% less UV dose model prediction.

7.3 Recommendations

For the further study, the following recommendations are listed:

For the AOPs kinetics study, collimated beam experiment with UV photolysis alone is suggested to be conducted, which is not included in this study.

For CFD modeling, 3-D model with refined meshes around the quartz tubes are recommended to prevent the underestimation of UV dose caused by dimension differences and overestimation of UV dose by poorly predicted recirculation zones behind the quartz tubes. Further development and verification of the random walk model is necessary to prevent particles walking out of the reactor wall. Chemical reaction model is suggested to give UV inactivity predictions for learning the reaction performance of the UV reactor.

For CFD validation, UV-sensitive dyed microsphere particle tracking experiments are recommended for measuring the real UV dose and dose distribution.

REFERENCE

- Backlund,P.(1992), Degradation of Aquatic Humic Material by Ultraviolet Light. *Chemosphere* 25, pp.1869-1878
- Bukhari,Z., T.M Hargy, J.R. Bolton, B. Dussert, J.L.Clancy (1999), Medium-pressure UV for oocyst inactivation. *Journal AWWA* 91,pp 86-94.
- Buffle M.O., Chiu, K., Taghipour, F.(2000), Reactor Conceptualization and Performance Optimization with Computational Modeling, *Proceedings WEF Specialty Conference on Disinfection, New Orleans, LA*
- Cassano, A.E.,Martin, C.A.,Brandi, R.J., Alfano,O.M. (1995), Photo-reactor analysis and design: Fundamentals and applications. *Industrial &Engineering Chemistry Research*. Vol. 34,pp 2155-2201.
- Ce´spedes R.(2005), Distribution of endocrine disruptors in the Llobregat River basin (Catalonia, NE Spain), *Chemosphere*, vol. 61(11) 1710-1719
- Christensen, H. S., Sehested, H. And Corfitzan, H.(1982),Reactions of Hydroxyl Radicals with hydrogen peroxide at ambient and elevated temperatures. *Journal of Physical Chemistry* 86, pp.15-68
- Chijssen, R.T. and Hoogenboezem, W. (2000), Endocrine disrupting compounds in the Rhine and Meuse Basin, *Association of River Waterworks-RIWA*
- Chiu, K., Lyn.D.A. Savoye,P. BlatchleyIII E.R.(1999), Effect of UV system modification on disinfection performance, *Journal of Environmental Engineering*, Vol. 125. No.5,pp459-469.
- Debus, K., Berkoe, J. Rosendall, B. (2003) Computational Fluid Dynamics Model for Tacoma Narrows Bridge Upgrade Project, *Proceedings of FEDSM'03, 4th Asme.Jeme joint fluids engineering conference, July 6-11, 2003-Honolulu, Hawaii*
- Furuichi T. (2004), Contribution of known endocrine disruptingsubstances to the estrogenic activity in Tama River water samples from Japan using instrumental analysis and in vitro reporter gene assay, *Water Research* 38 (2004) 4491–4501
- Frimmet, F.H. (1998), Impact of light on the properties of aquatic natural organic matter, *Environment International*, vol 24, pp 559-571

GWRC (2003), Endocrine disrupting compounds, occurrence of EDC in water systems, global water research coalition, September 2003.

Handbook of Chemistry and Physics (1991), 72en edition , CRC Pressee, Boca-Raton, FL.

Haue,J., Ta,C.T. and Biggs, M.J.(2001).Small scale model for CFD validation in DAF application, Water Science and Technology, Vol 43, No8, pp167-173

IJplaar. G F. and Kruithof, J.(2002), UV photolysis and UV/H₂O₂ for the degradation of organic micropollutans, Workshop of UV in drinking water treatment, March 20-23,2002, Utrecht, the Netherlands

Janex, M.L., Savoye,P., Do-Quang, Z., Blatchley, E.R., Latine,J.M.(1998), Impact of water quality and reactor hydrodynamics on waste-water disinfection by UV, use of CFD modeling for performance optimization. Water Science and Technology, vol. 38, pp71-78.

Kaminura, M., Furukawa, S., Hirotsuji, J.(2002). Development of a simulator for ozone/UV reactor based on CFD analysis. Water Science and Technology, Vol.46, pp13-19.

Kashinkunti, R., Linden, K.G., Shin, G., D.H. Metz, M.D. Sobsey, M. Moran, and A. Samuelson.(2003), Achieving multi-barrier inactivation in Cincinnati: UV, byproducts, and biostability. JAWWA. Submitted January 9, 2003.

Keith, L.H.(1997). Environmental endocrine disruptors, a handbook of property data. John Wiley&Sons, Inc, New York, ISBN 0-471-19126-4.

Koller, L.R (1965), Ultraviolet Radiation, Ballard, S.S. (ed.), John wiley&Sons,Inc., New York, 1965, pp.1-312

Kruithof, J. C, PC Kamp and M Belosevic(2002) . "UV/H₂O₂-treatment: The ultimate solution for pesticide control and disinfection." Water Supply 2 (2002): 113-122

Kuklenyik, Z, John Ekong, Caroline D. Cutchins, Larry L. Needham, and Antonia M. Calafat(2003),Simultaneous Measurement of Urinary Bisphenol A and Alkylphenols by Automated Solid-PhaseExtractive Derivatization Gas Chromatography/Mass Spectrometry [J]. Analytical Chemistry,75 (24),6820-6825.

Lay, Y.S.(1989) Oxidation of 1,2-Dibromo-3pchloropropane in Ground Water Using Advanced Oxidation Processes, PhD Thesis, University of California at Los Angeles, USA.

LDFM, Laser Doppler flow meter technical manual, delft hydraulics laboratory

Leifer, A(1988), The kinetics of environmental photochemistry, Theory and Practice. ACS Professional Reference Book, York, PA, pp304

Lyn, D.A., Chiu, K., Blatchley, E.R.(1999), Numerical Modeling of Flow and Disinfection in UV Disinfection Channels, Journal Environmental Engineering. ASCE, 125(1), pp 17

Malley, J. P, Shaw, J.P and Ropp, J.R (1995). Evaluation of by-products produced by treatment of groundwaters with ultraviolet irradiation. Denver, Co.: AWWA Research Foundation

Marchisio, D.L., Barresl, A.A. (2003). CFD simulation of mixing and reaction: the relevance of the micromixing model. Chemical Engineering Science. vol. 58, pp 3579-3587.

Parsons, S. (2004), Advanced Oxidation Process for Water and Wastewater Treatment, ISBN: 1-84339-0175, IWA publishing

Parkinson, A., Barry, M.J., Roddick, F.A. and Hobday, M.D.(2001) Preliminary toxicity assessment of water after treatment with UV-irradiation and UV/H₂O₂. Water Research, pp 3656-3664

Pareek.V.K., Cox,S.J., Brungs. M.P., Young,B.,Adesina,A.A.(2003), Computational fluid dynamic (CFD) simulation of a pilot-scale annular bubble column photocatalytic reactor. Chemical Engineering Science, 58,pp859-865.

Philips, R.(1983), Sources and Application of Ultraviolet Radiation, Academic Press Inc., New York

Romero,R.L., Alfano,O.M., Marchetti,J.L., Cassano, A.E. (1983), Modeling and parametric sensitivity of an annular photoreactor with complex kinetics. Chemical Engineering Science,vol. 38,pp1593-1605.

Sharpless C.M., and K.G. Linden (2001). UV photolysis of nitrate: effects of natural organic matter and dissolved inorganic carbon, and implications for UV water disinfection. *Environmental Science and Technology* 35, no 1, pp2949-2955.

Sharpless C.M., Linden. K.G.(2003), Experimental and model comparisons of low-and medium-pressure Hg lamps for the direct and H₂O₂ assisted UV photodegradation of N-Nitrosodimethylamine in simulated drinking water, *Environmental Science and Technology*, vol. 37, 1933-1940.

Sander. M.B. van der.(2006), Computational modeling on the final closure gaps in the Saemangeum dam, South Korea, Master thesis.

Shemer, H. and Linden. K,G.(2006),Degradation and by-product formation of diazinon in water during UV and UV/H₂O₂ treatment. *Journal of Hazardous Materials*, B136, pp. 553-559, 2006.

Sozzi. D.A., Taghipour F.(2006), Computational and experimental study of annular photo-reactor hydrodynamics, *International journal of Heat and Fluid Flow* 27(2006), 1043-1053.

Ultraviolet Disinfection Guidance Manual (2003), United States Environmental Protection Agency, June 2003, Draft

USEPA(1998), Handbook on Advanced Photochemical Oxidation Processes, EPA/625/R-98/004, USEPA, December 1998

Versteeg, HK., Malalasekera W.(1995), An Introduction to Computational Fluid Dynamics : The Finite Volume Method, Longman Scientific and Technical, Harlow, Essex, UK, 3rd August 1995, ISBN 0-582-21884-5

Von Sonntag, C., and H.P. Schuchmann(1992). UV disinfection of drinking water and by-product formation—some basic considerations. *Journal of Water Supply Research and Technology* 41, no 2, pp67-74

Watts,R.J., Udell, M.D, and Laung, S. W. (1990), Treatment of pentachloro-contaminated soil using Fenton's reagent. *Hazard Waste Hazard*. Vol 7, pp335-345

Watts,R.J., Udell, M.D, and Laung, S. W. (1991), Treatment of contaminate soil using catalyzed hydrogen peroxide. In: *Proceeding of the First International Symposium Chemical Oxidation Technologies for the Nineties*, Echenfelder, W.W.,

Bowers, A.R, and Roth, J.A.(eds).Vanderbilt University, Nashville, Tennessee, USA, pp 37-50

Wols, B. (2007), Residence time distributions in ozone contactors, World congress on ozone and ultraviolet technologies, Los Angeles, 27-29 August 2007, in press

Wright, H. and Reddy, S.(2002), Reactor Design and Upscaling: The Use of CFD-Modeling, Workshop of UV in drinking water treatment, March 20-23,2002, Utrecht, the Netherlands

Yu, Ming-Ho (2005), Environmental toxicology : Biological and Health Effects of Pollutants, ISBN 1-56670-670-X, CRC press LLC

List of Appendixes

Appendix I. UV Dose Calculation Table.....	92
Appendix II	
Degradation of 4TBP with Different Initial H ₂ O ₂ Concentrations.....	93
Appendix III Velocity Measurement with Corrected Coordinates.....	98
Appendix V Salt Dose Experiment Output	118
Appendix VI Dye Dose Video.....	123
Appendix VII Comsol Flow Models	123
Appendix VIII UV Dose Model	123

Appendix I. UV Dose Calculation Table

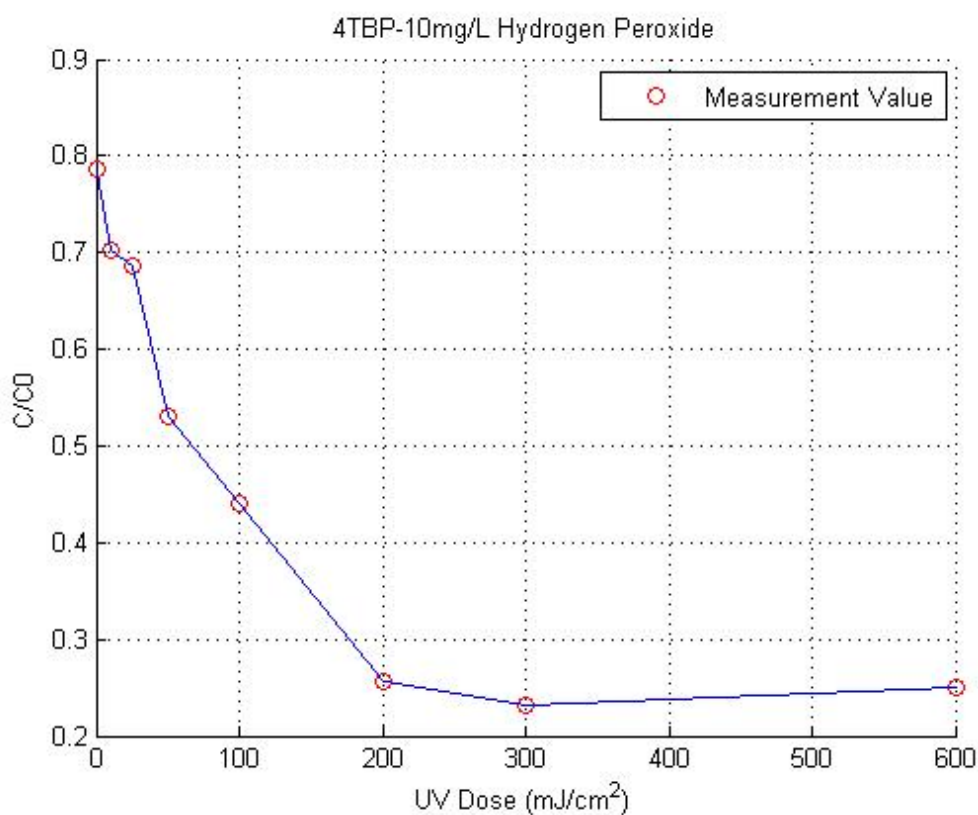
See the separate excel file with the DVD.

Appendix II

Degradation of 4TBP with Different Initial H₂O₂ Concentrations

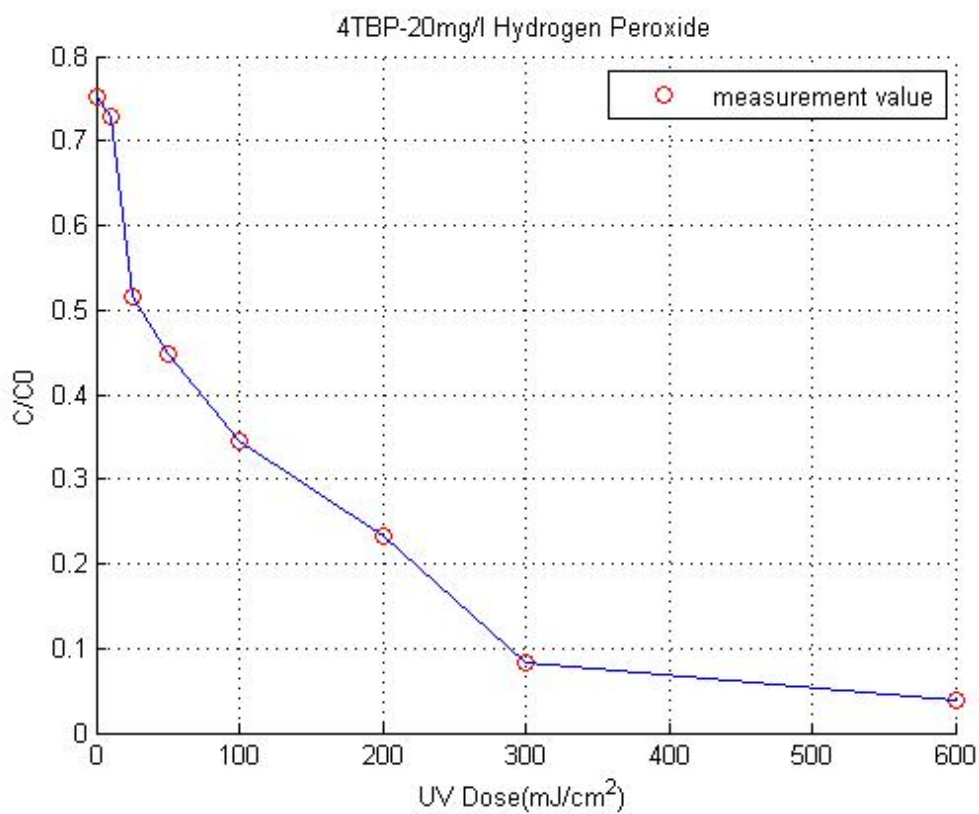
For dose of 10mg/l

UV Dose	C(μg/L)	C0(μg/L)	C/C0	Ln(C/C0)	Time(s)
0	309.038	392.528	0.7873018	-0.2391436	12.171
10	275.851	392.528	0.702755	-0.352747	121.7
25	269.307	392.528	0.6860835	-0.3767559	304.3
50	208.062	392.528	0.5300565	-0.6347718	608.6
100	172.66	392.528	0.4398667	-0.8212835	1217.1
200	100.753	392.528	0.2566772	-1.3599359	2434.2
300	90.604	392.528	0.2308218	-1.4661095	3651.4
600	98.567	392.528	0.2511082	-1.3818714	7302.7



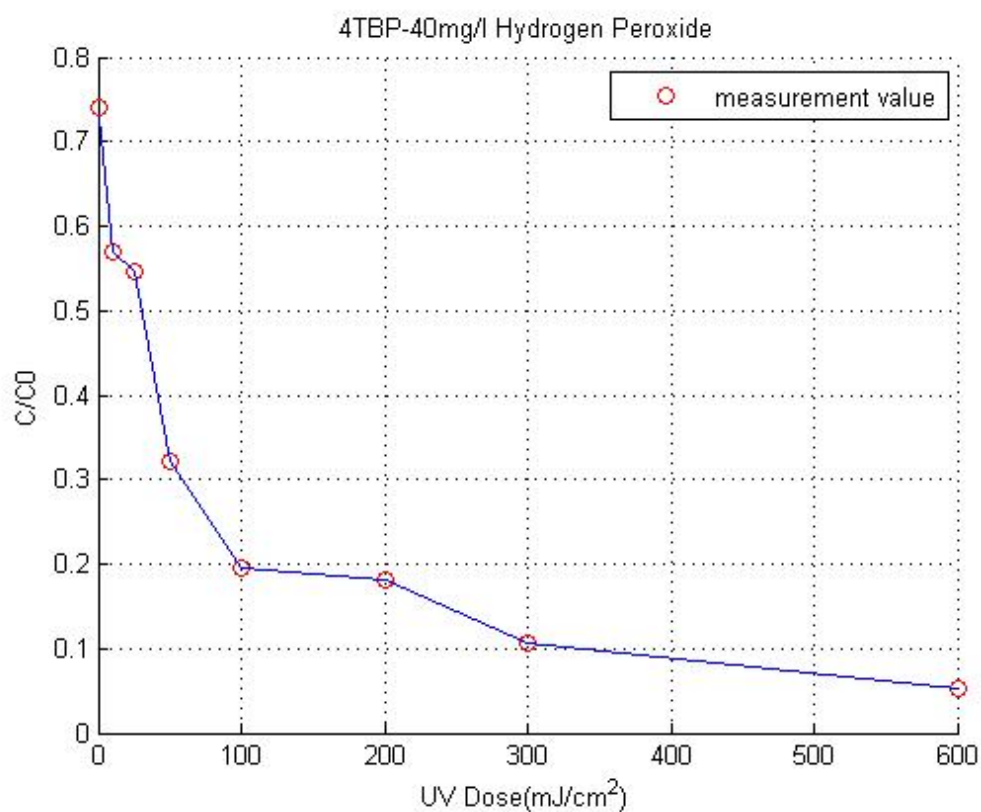
For dose of 20mg/l

UV Dose		C($\mu\text{g/L}$)	C0($\mu\text{g/L}$)	C/C0	Ln(C/C0)	Time(s)
0	mJ/cm^2	295.605	392.528	0.75308	-0.2835838	12.171
10	mJ/cm^2	286.462	392.528	0.7297874	-0.315002	121.7
25	mJ/cm^2	202.023	392.528	0.5146716	-0.6642263	304.3
50	mJ/cm^2	175.922	392.528	0.4481769	-0.8025672	608.6
100	mJ/cm^2	135.305	392.528	0.3447015	-1.0650764	1217.1
200	mJ/cm^2	91.81	392.528	0.2338941	-1.4528866	2434.2
300	mJ/cm^2	32.289	392.528	0.0822591	-2.4978813	3651.4
600	mJ/cm^2	15.065	392.528	0.0383794	-3.2602337	7302.7



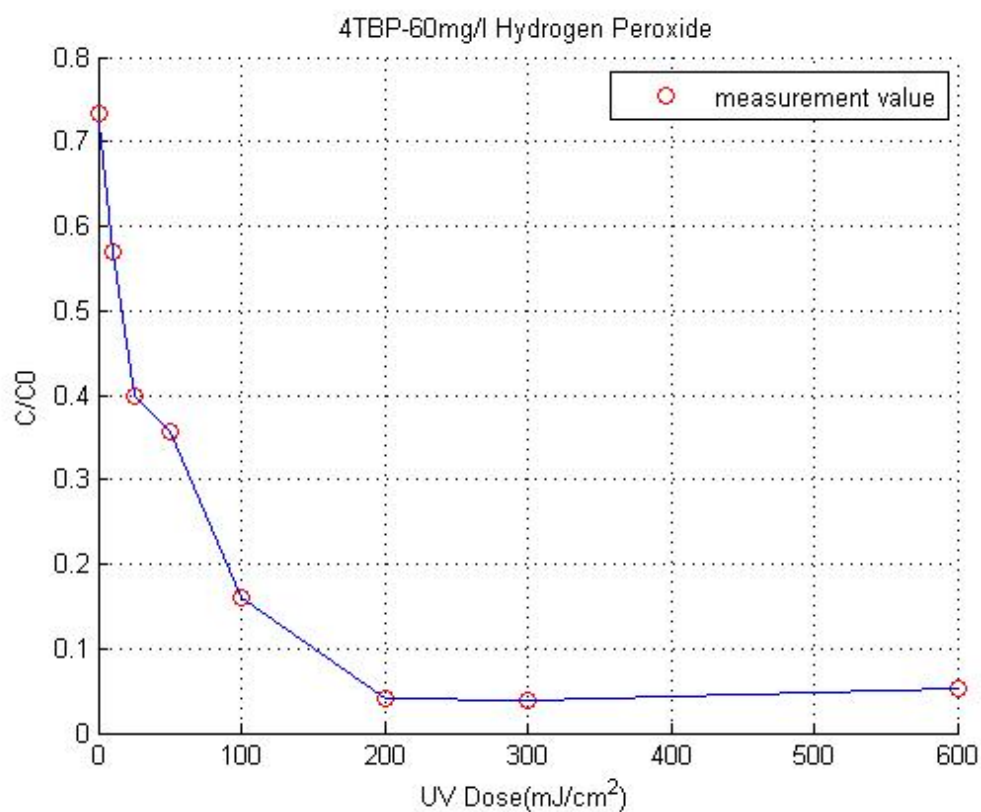
For dose of 40mg/l

UV Dose	C($\mu\text{g/L}$)	C0($\mu\text{g/L}$)	C/C0	Ln(C/C0)	Time(s)
0	290.203	392.528	0.73931796	-0.3020272	12.171
10	223.803	392.528	0.57015805	-0.5618417	121.7
25	214.188	392.528	0.54566298	-0.6057537	304.3
50	126.136	392.528	0.32134268	-1.1352472	608.6
100	77.04	392.528	0.19626625	-1.6282831	1217.1
200	71.408	392.528	0.18191823	-1.704198	2434.2
300	41.358	392.528	0.10536318	-2.250342	3651.4
600	20.495	392.528	0.05221284	-2.9524269	7302.7



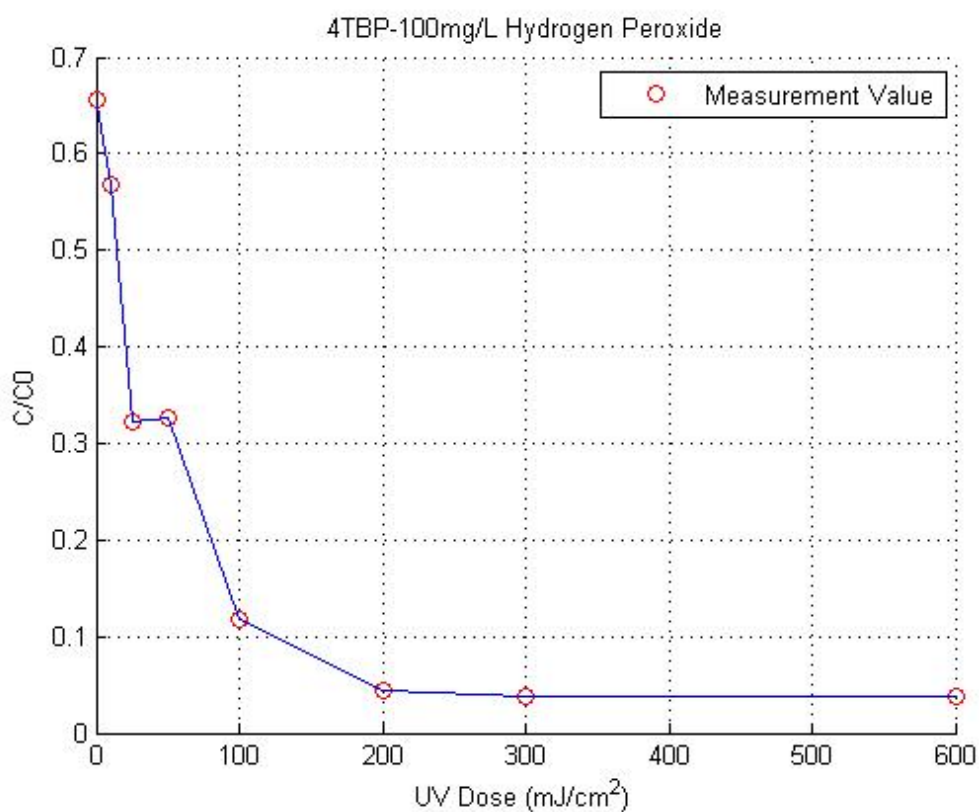
For dose of 60mg/l

UV Dose	C($\mu\text{g/L}$)	C0($\mu\text{g/L}$)	C/C0	Ln(C/C0)	Time(s)
0	287.939	392.528	0.73355022	-0.3098592	12.171
10	224	392.528	0.57065993	-0.5609618	121.7
25	156.654	392.528	0.39909	-0.9185683	304.3
50	140	392.528	0.35666245	-1.0309654	608.6
100	62.484	392.528	0.15918355	-1.8376973	1217.1
200	15.663	392.528	0.03990289	-3.2213066	2434.2
300	15.045	392.528	0.03832848	-3.2615622	3651.4
600		392.528			

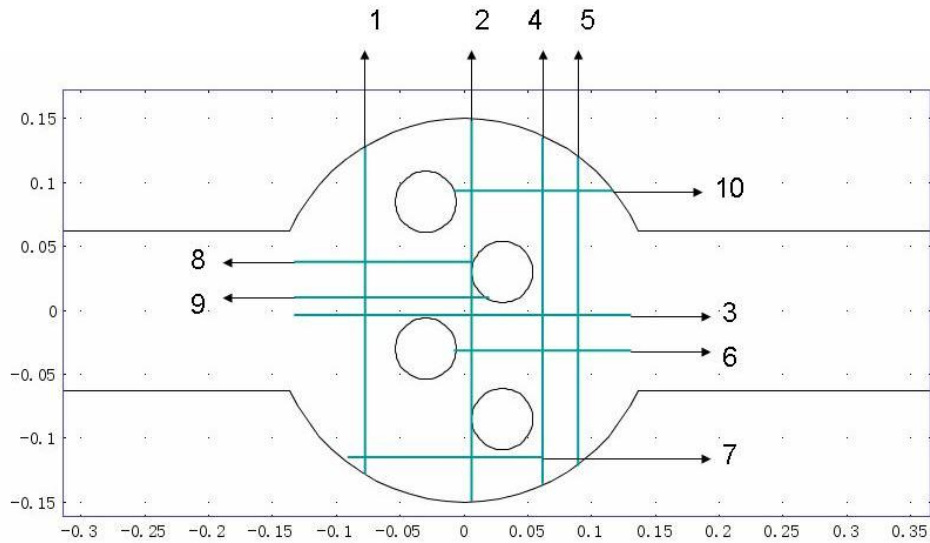


For dose of 100mg/l

UV Dose	C($\mu\text{g/L}$)	C0($\mu\text{g/L}$)	C/C0	Ln(C/C0)	Time(s)
0	257.156	392.528	0.6551278	-0.422925	12.171
10	223.008	392.528	0.5681327	-0.5654002	121.7
25	126.891	392.528	0.3232661	-1.1292794	304.3
50	128.013	392.528	0.3261245	-1.1204761	608.6
100	46.041	392.528	0.1172935	-2.1430756	1217.1
200	17.021	392.528	0.0433625	-3.13816	2434.2
300	14.663	392.528	0.0373553	-3.2872806	3651.4
600	14.586	392.528	0.0371591	-3.2925457	7302.7



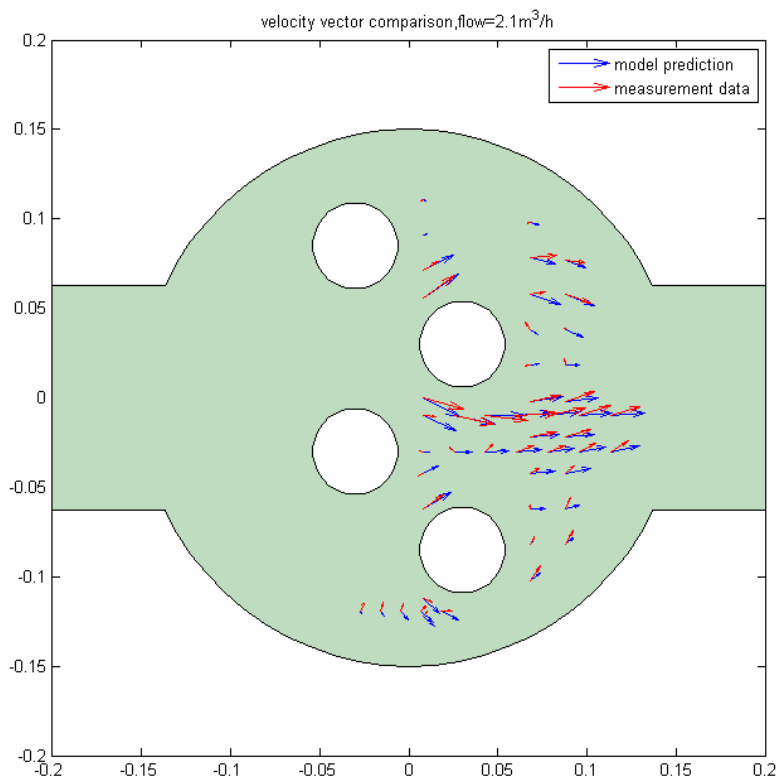
Appendix III Velocity Measurement with Corrected Coordinates

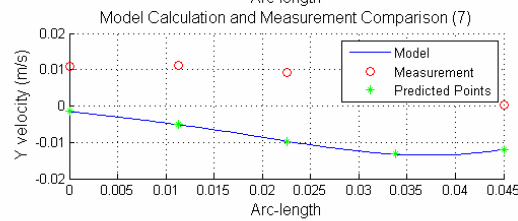
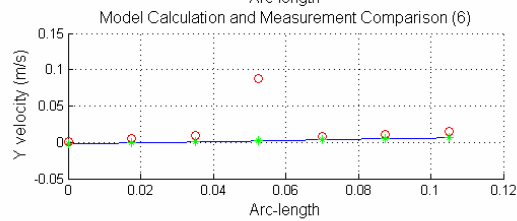
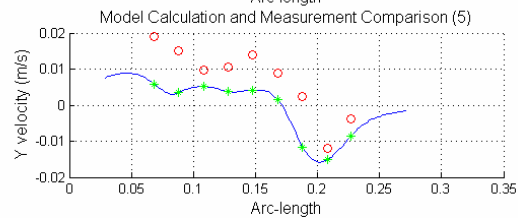
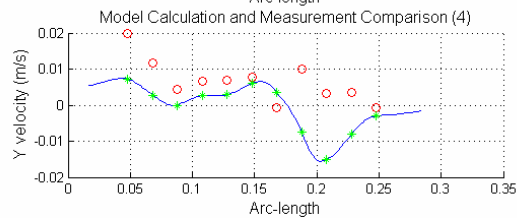
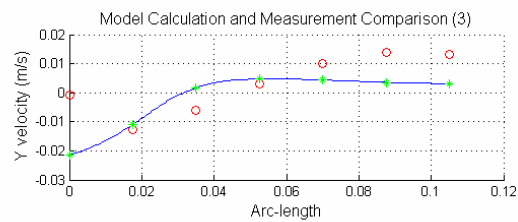
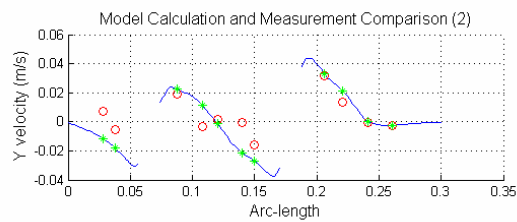
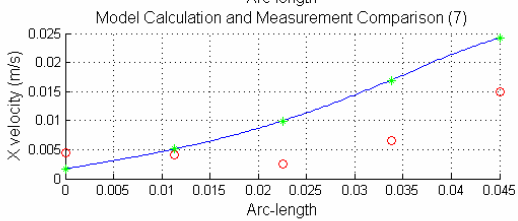
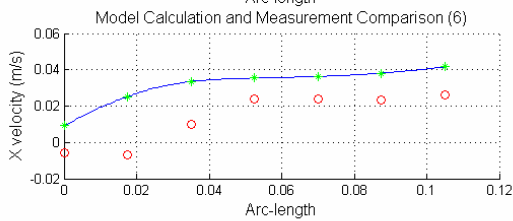
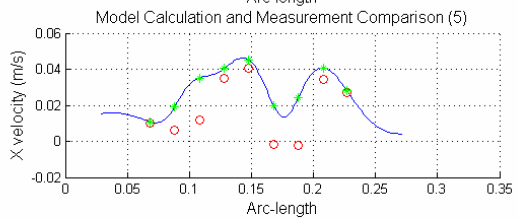
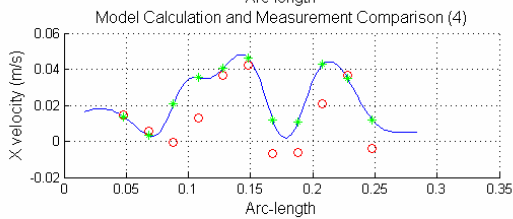
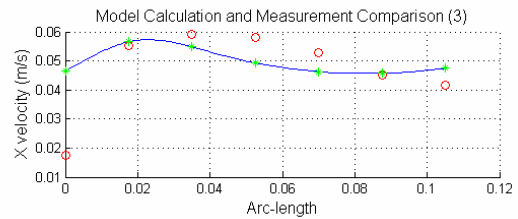
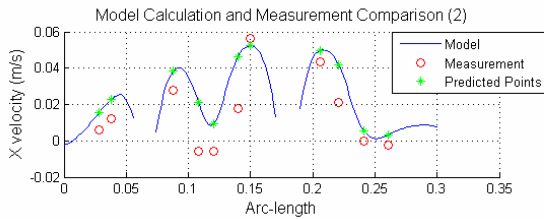


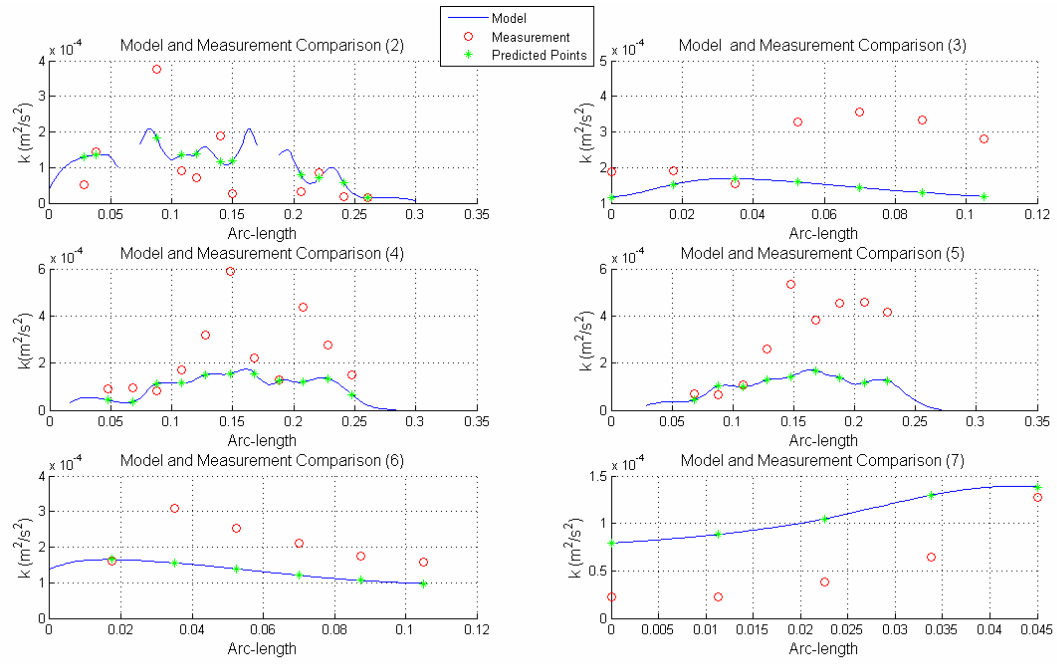
Detailed measurements see the separate excel files for both flows.

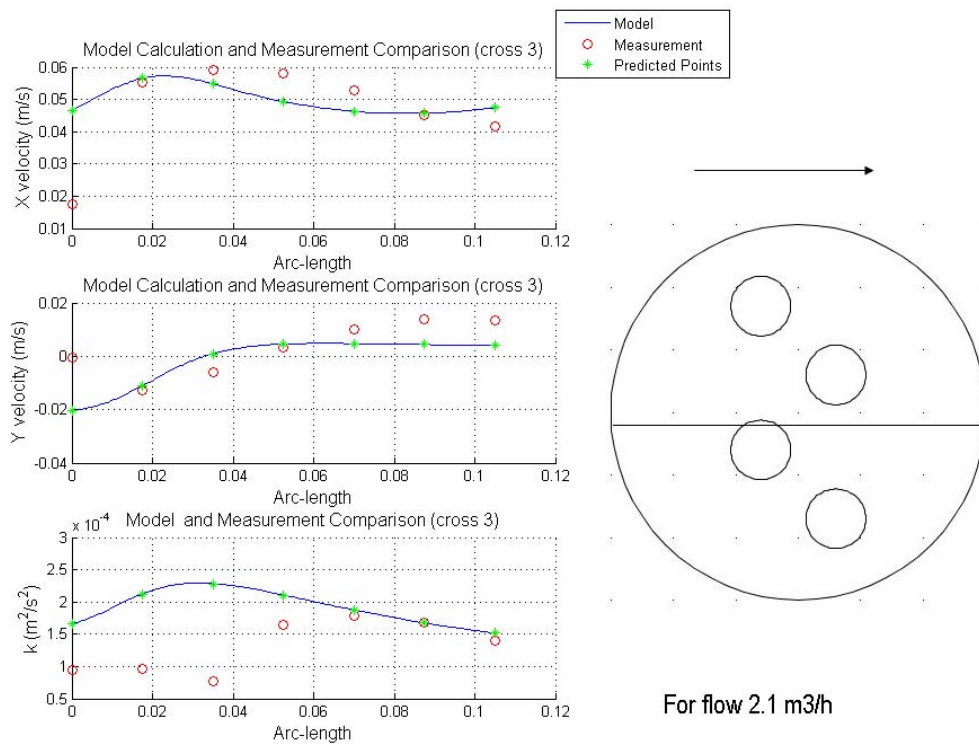
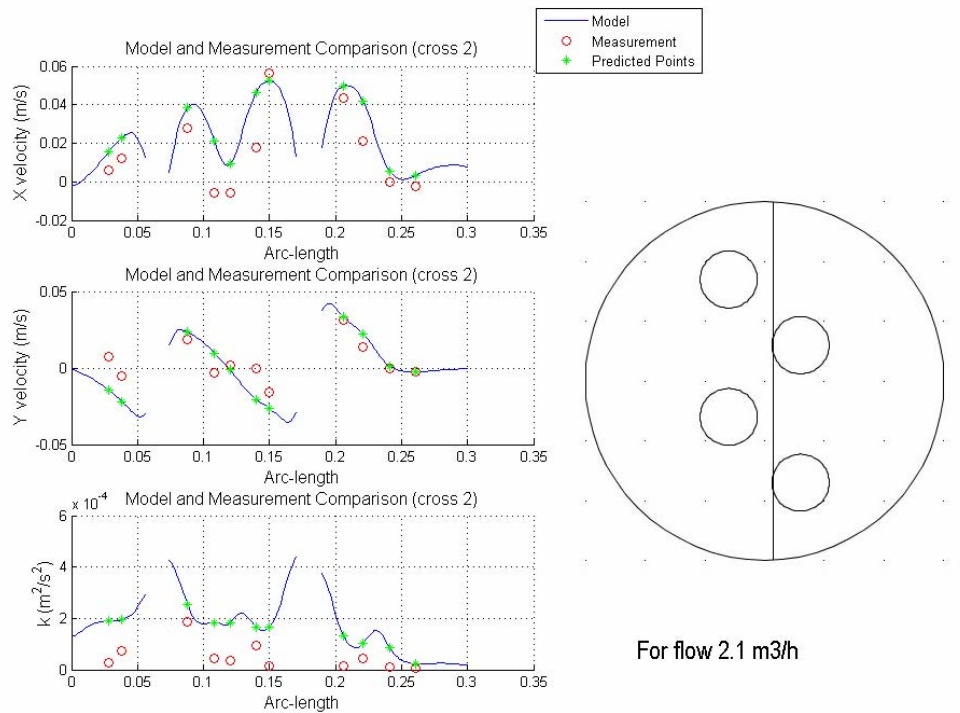
Cross Section Measurements and Model Comparison

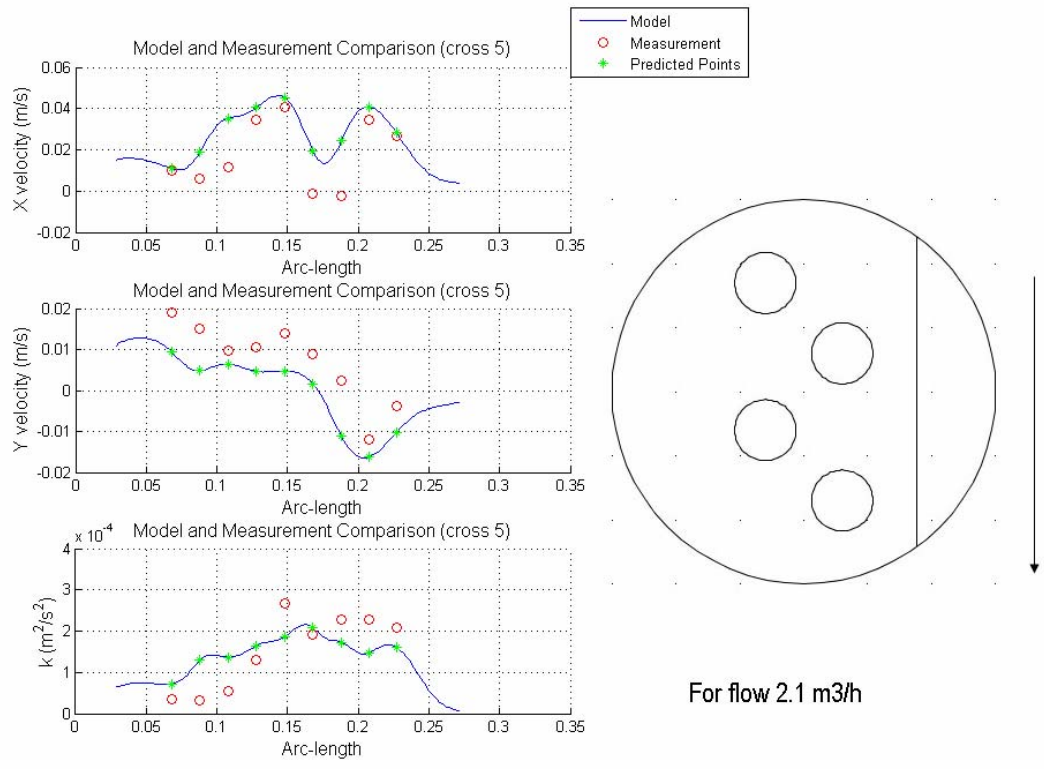
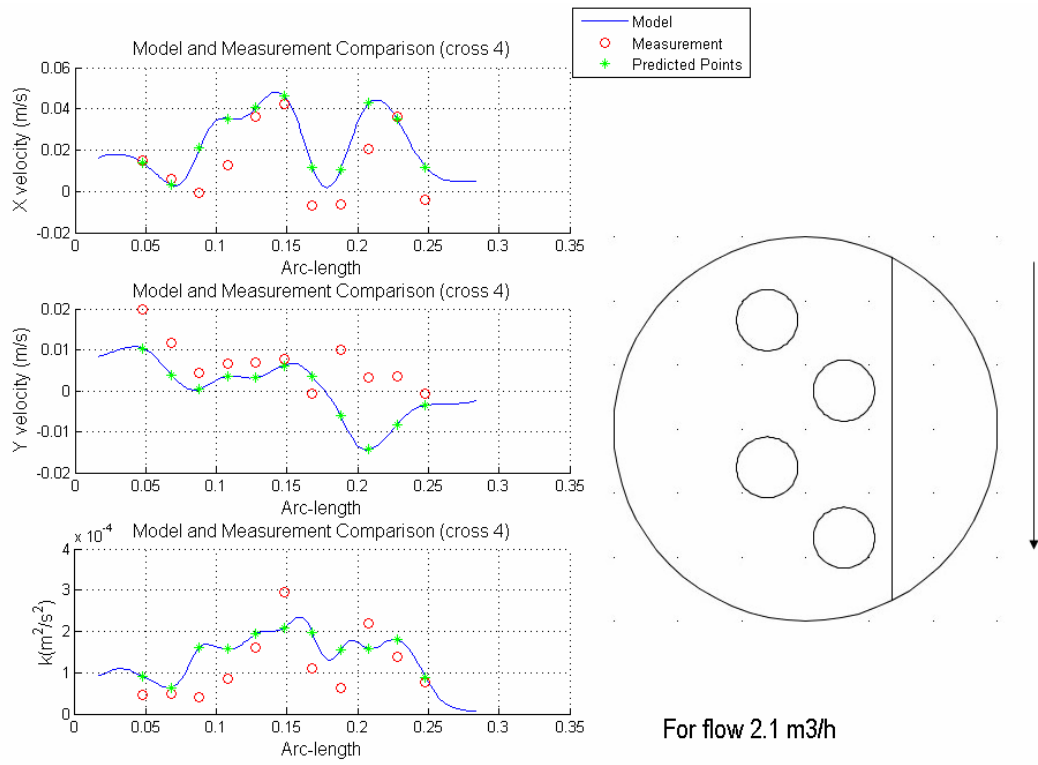
For $2.1\text{m}^3/\text{h}$ Flow

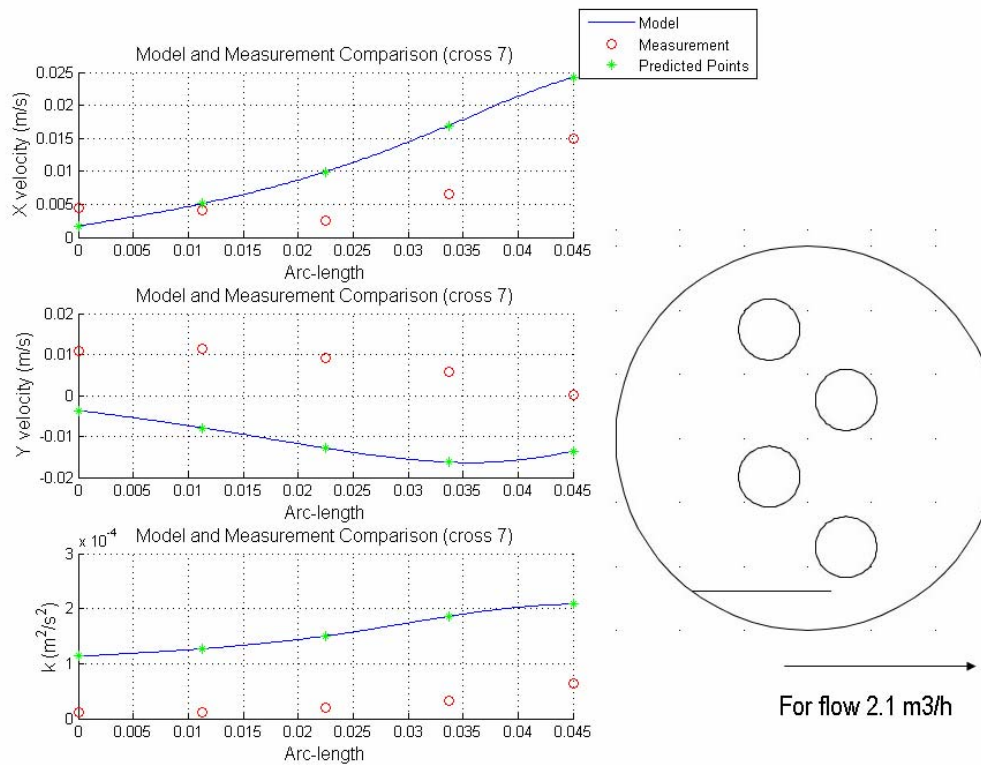
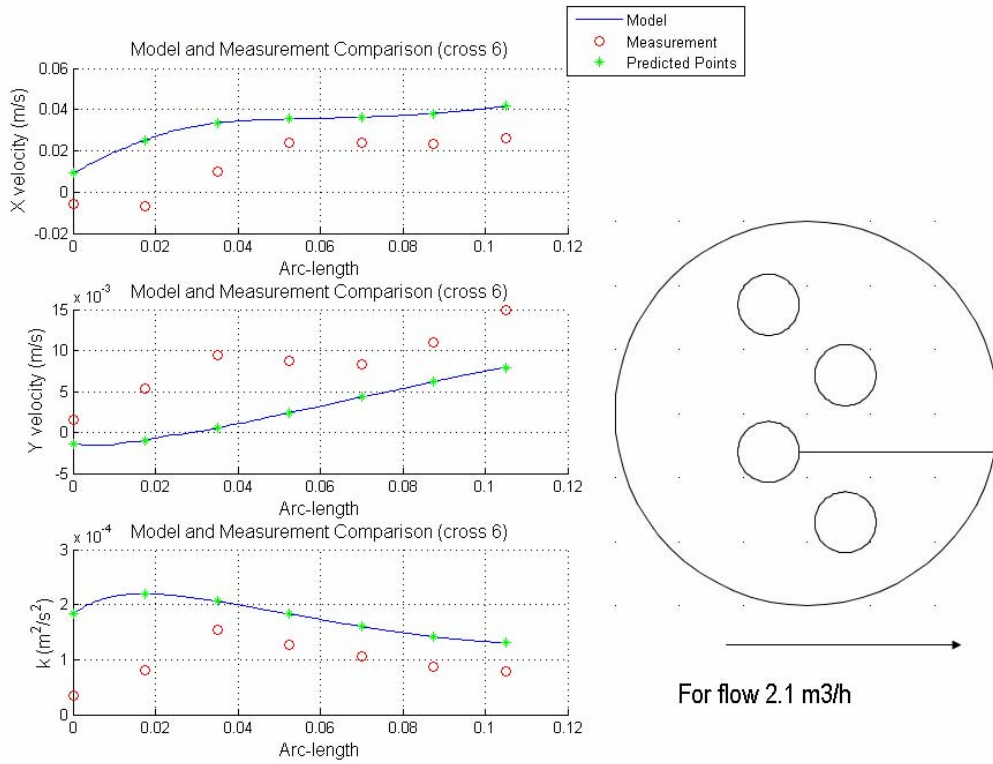




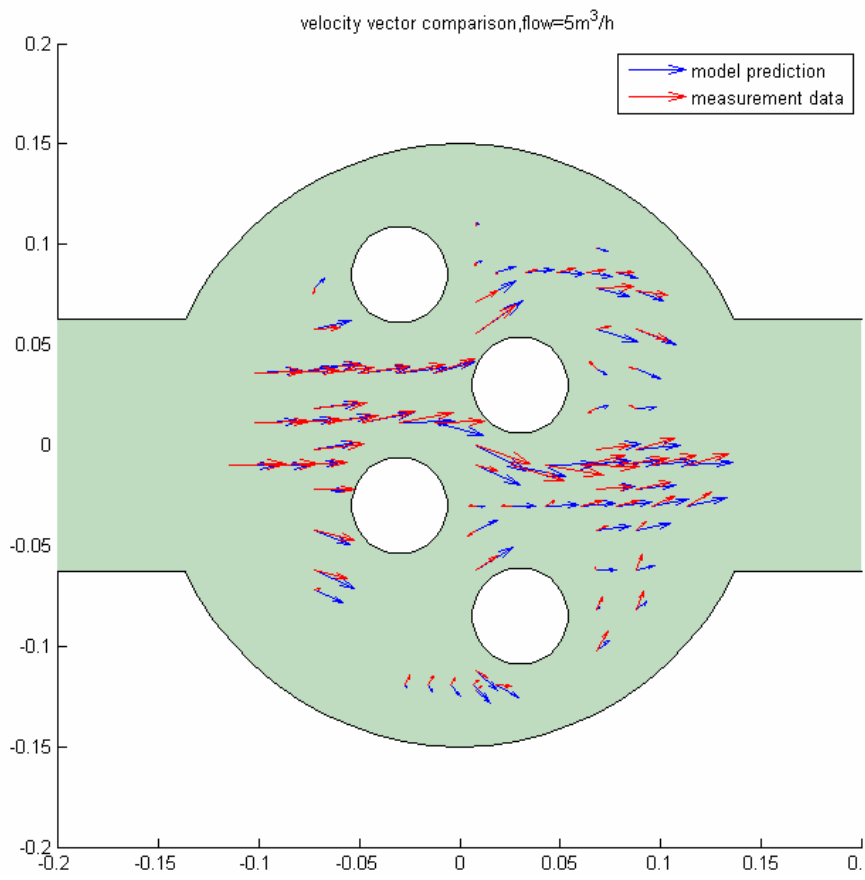


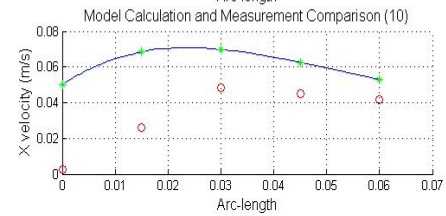
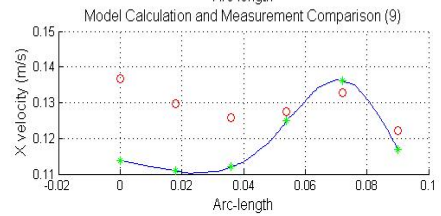
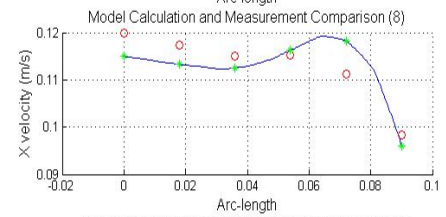
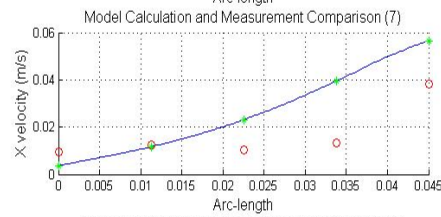
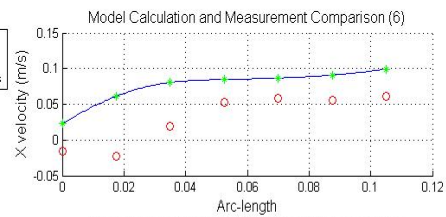
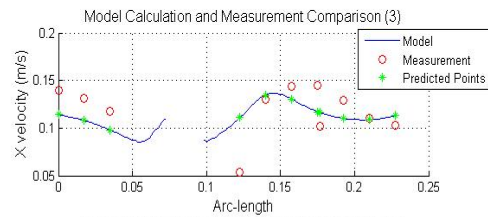
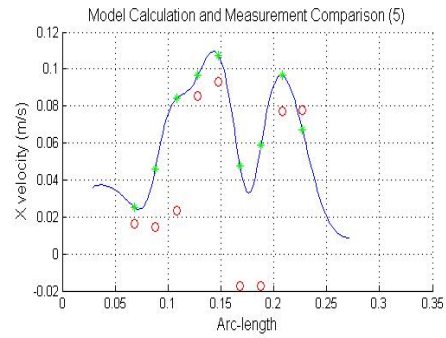
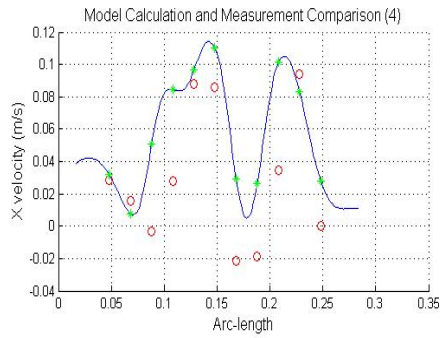
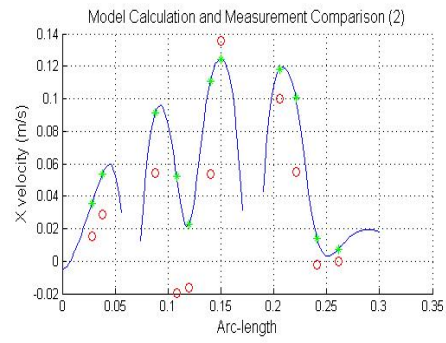
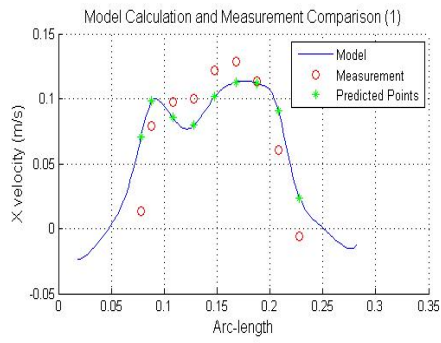


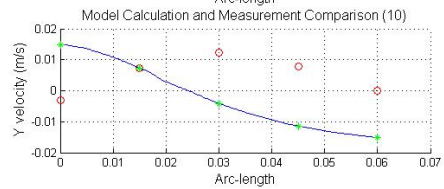
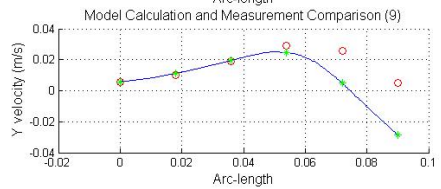
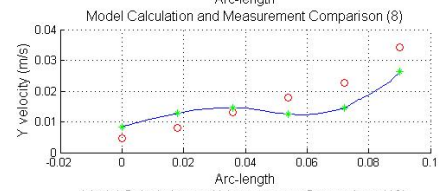
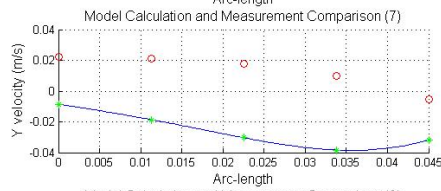
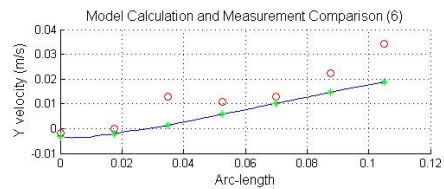
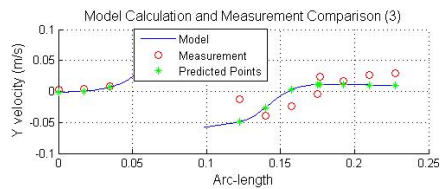
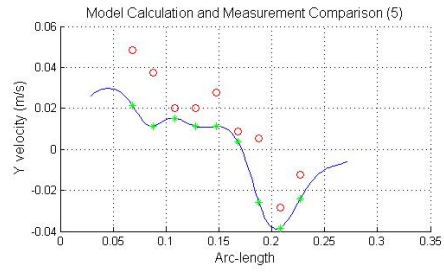
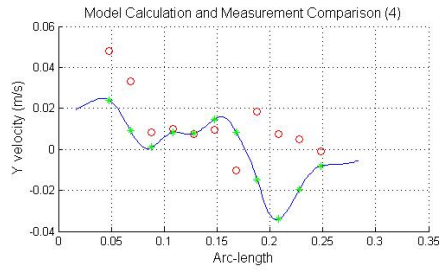
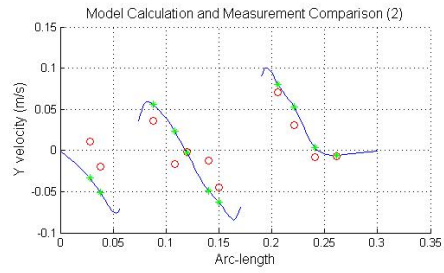
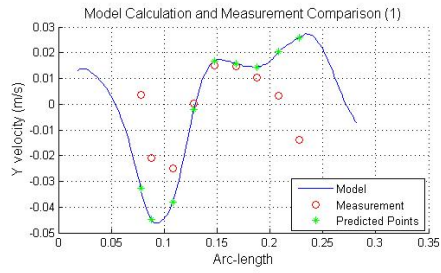


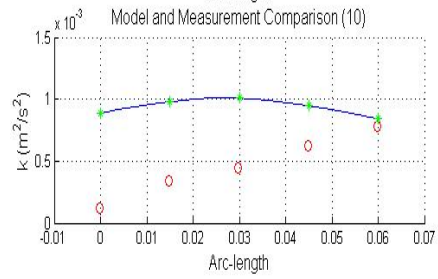
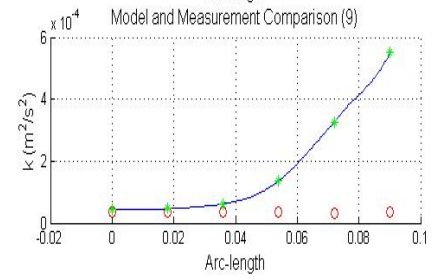
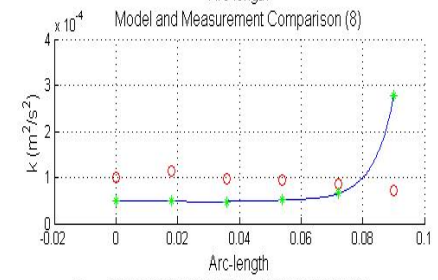
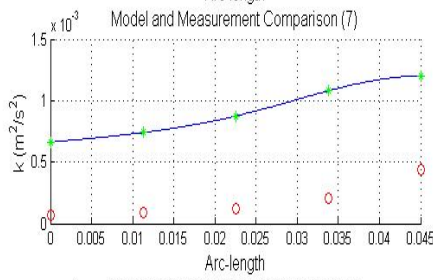
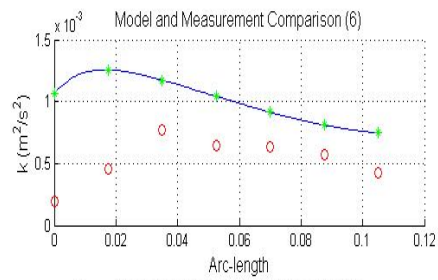
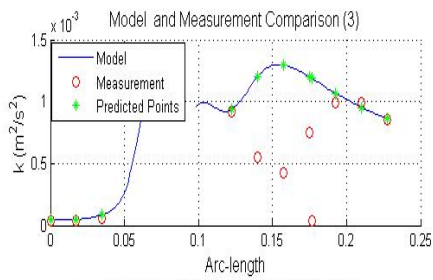
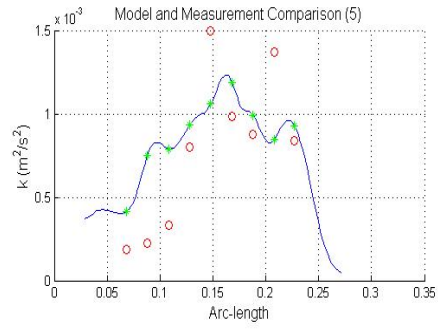
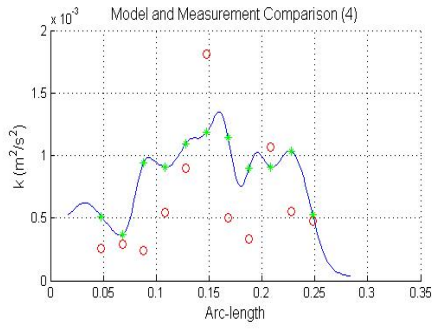
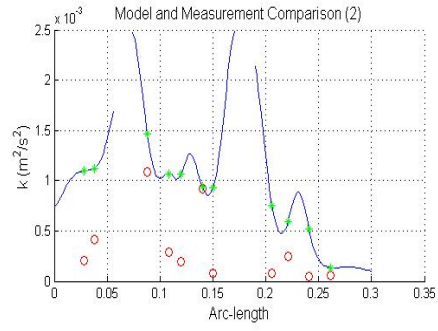
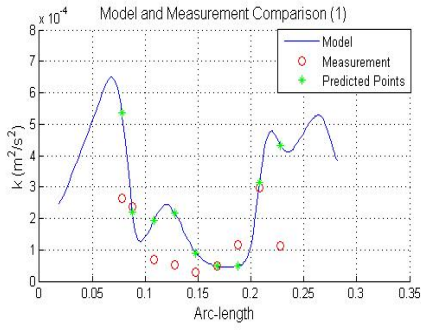


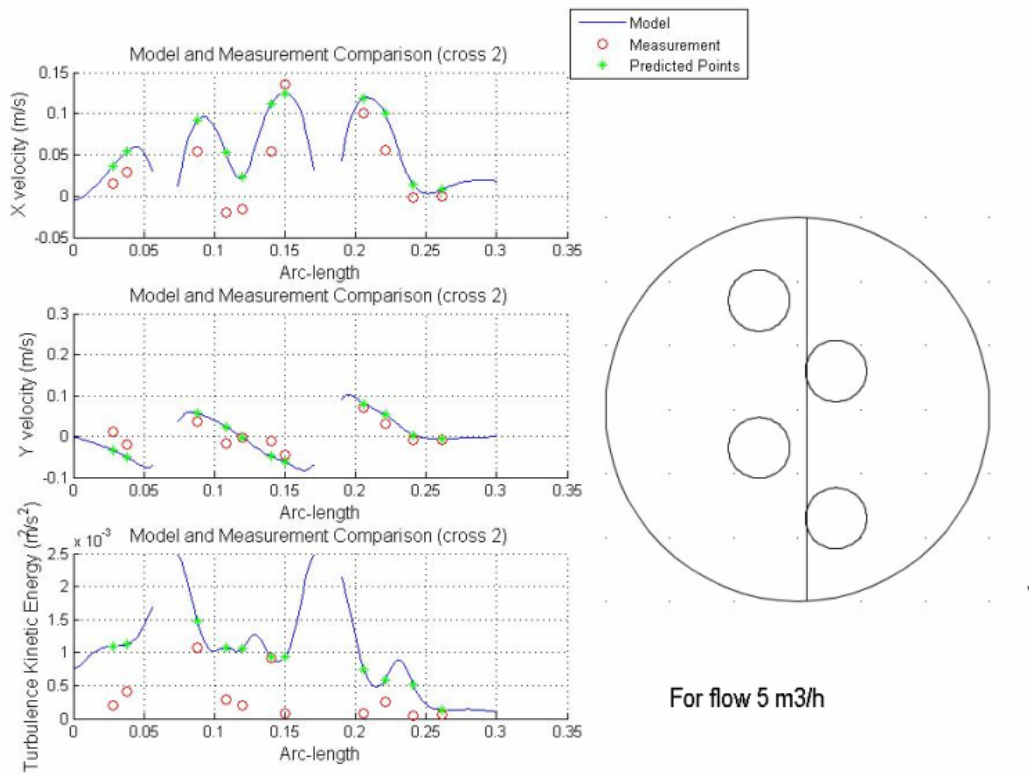
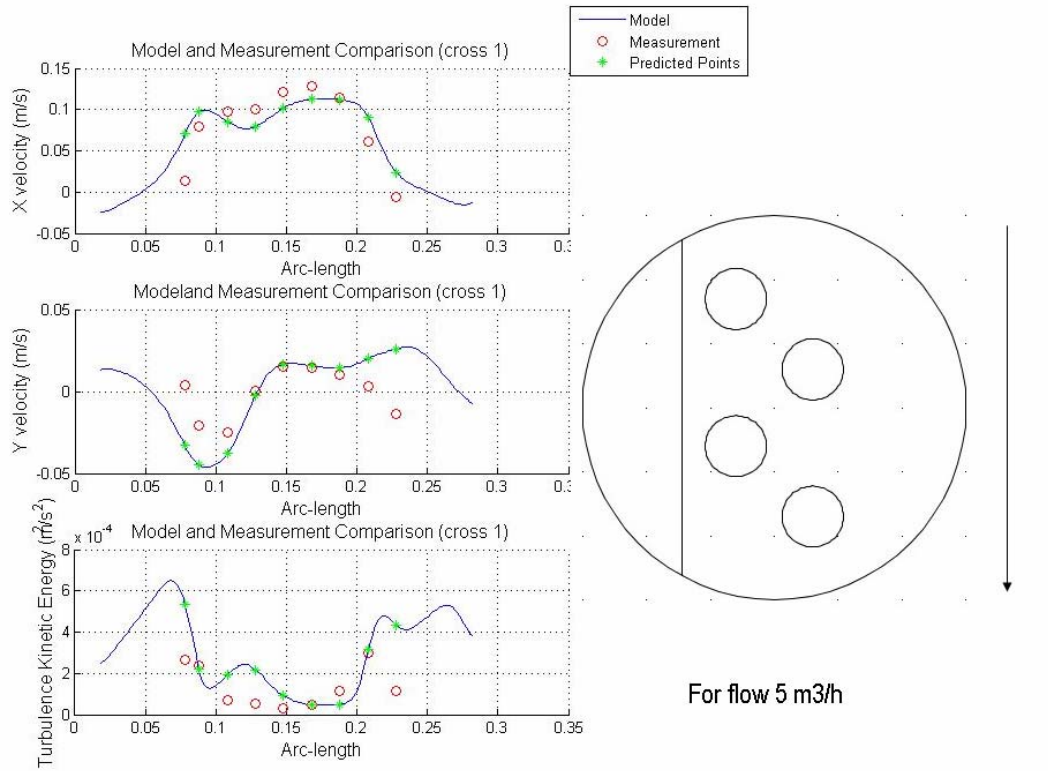
For $5\text{m}^3/\text{h}$ Flow

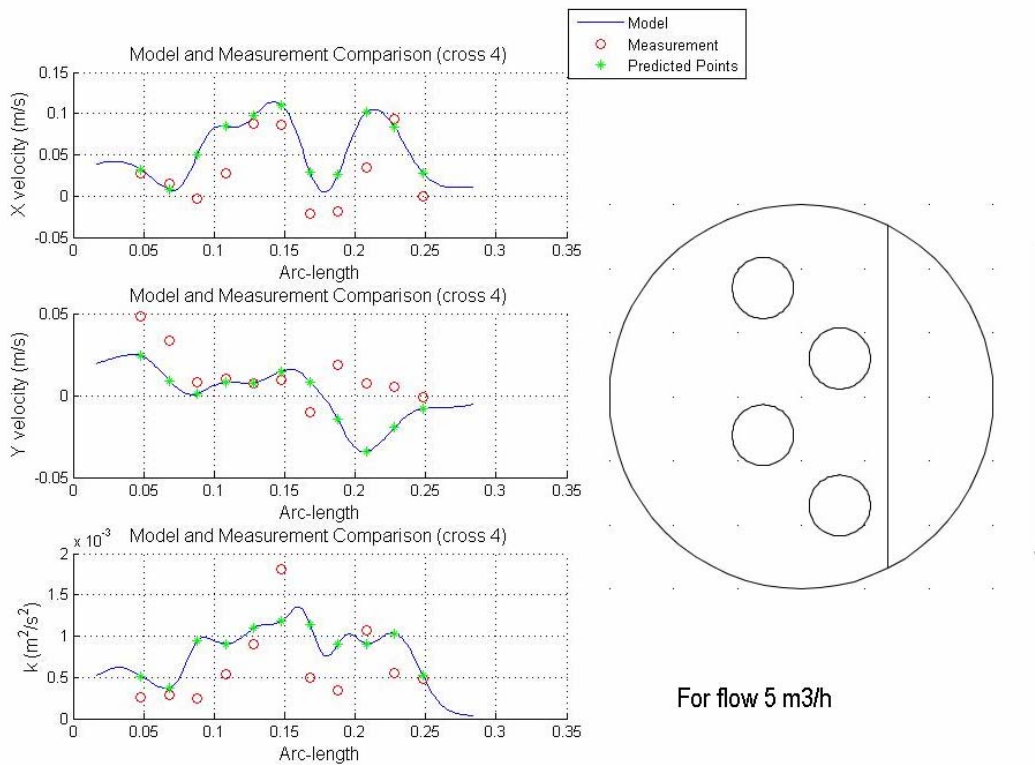
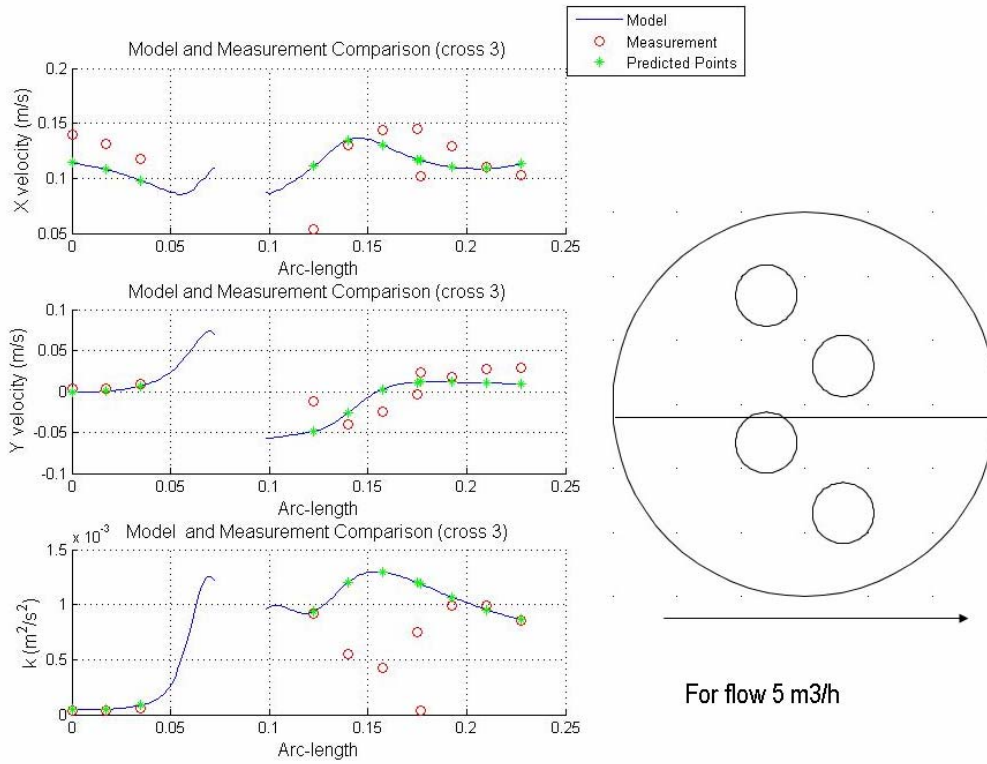


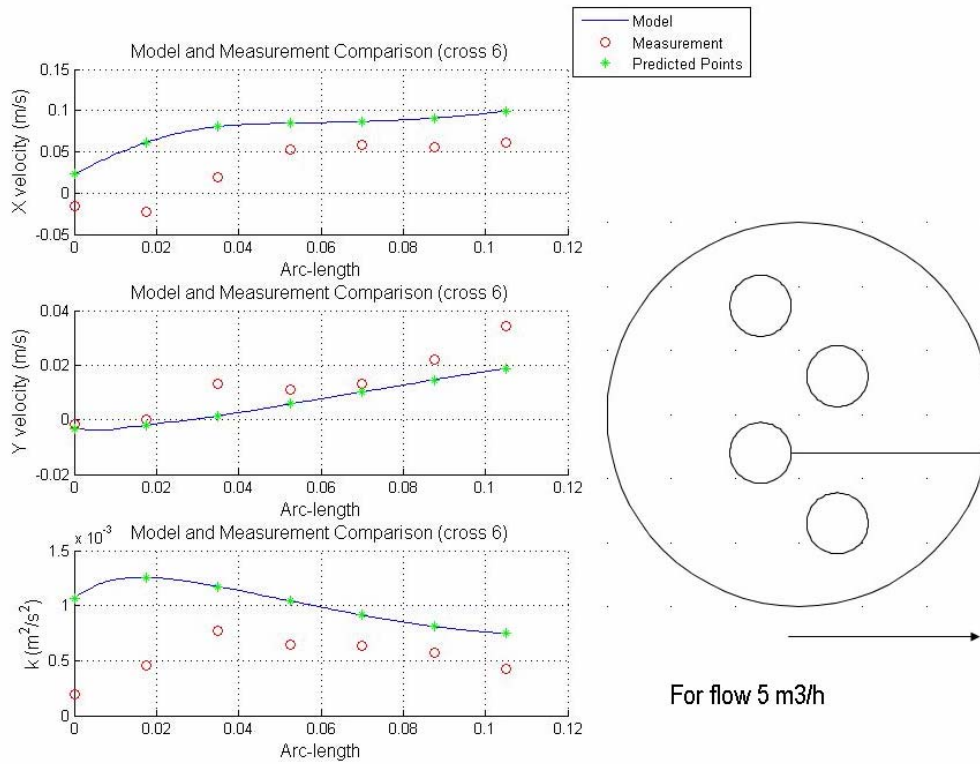
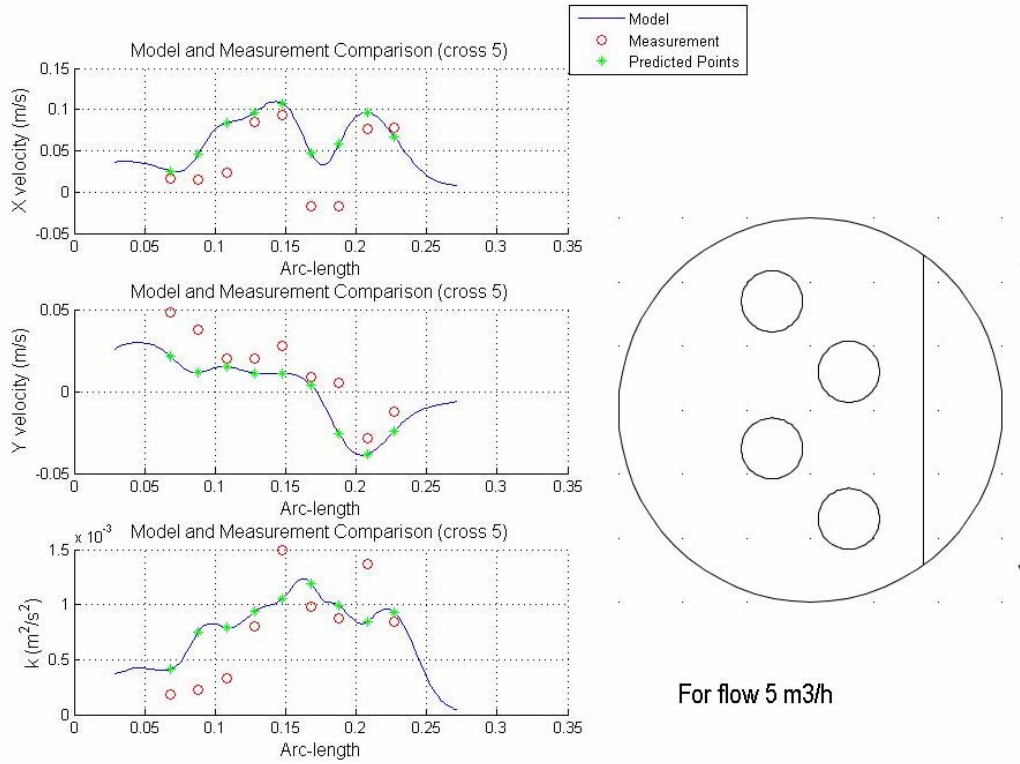


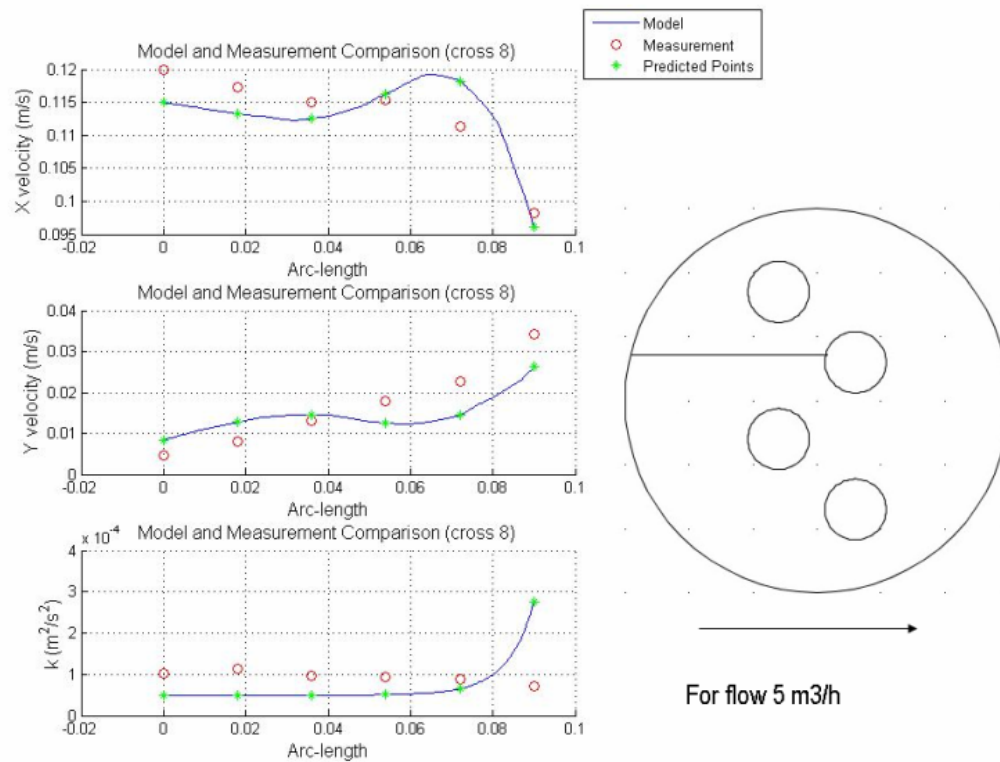
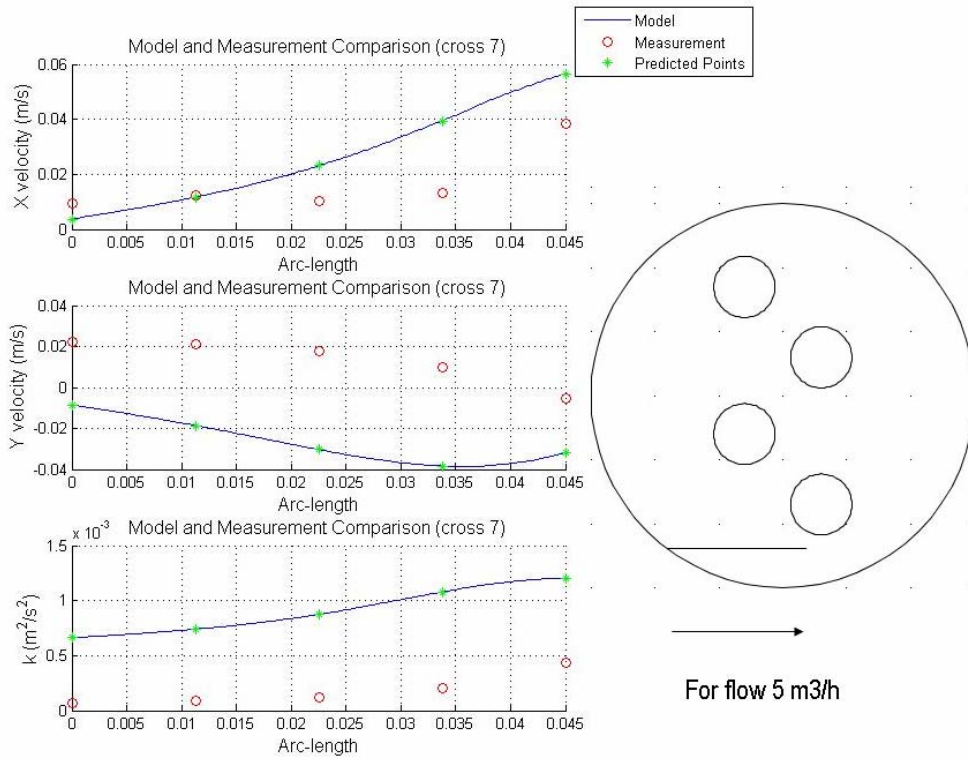


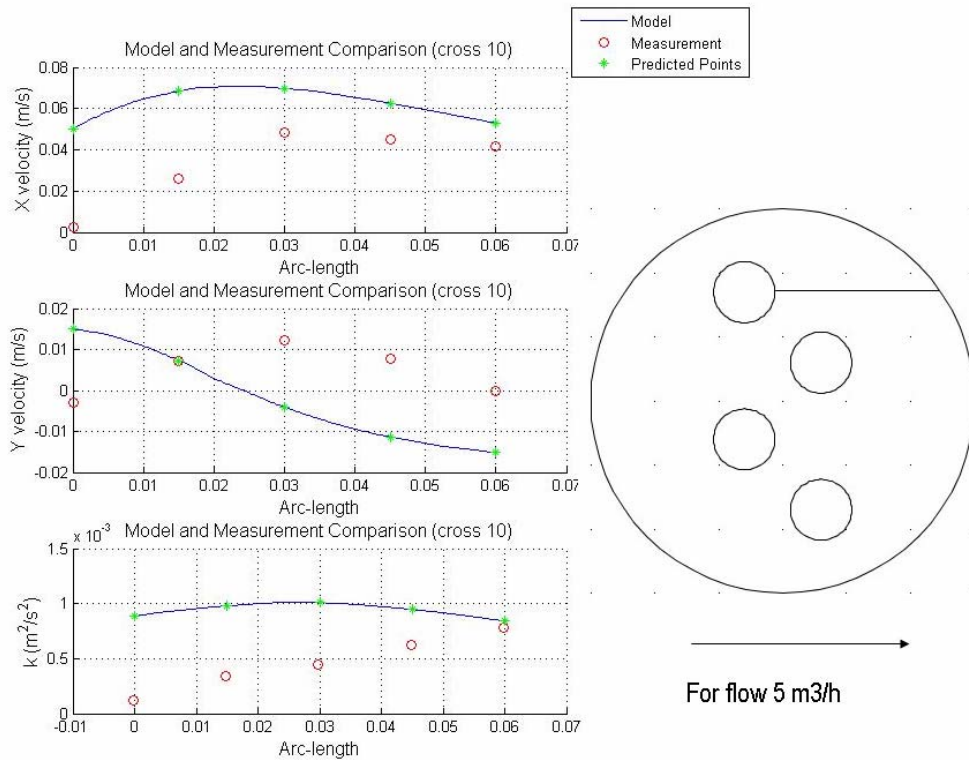
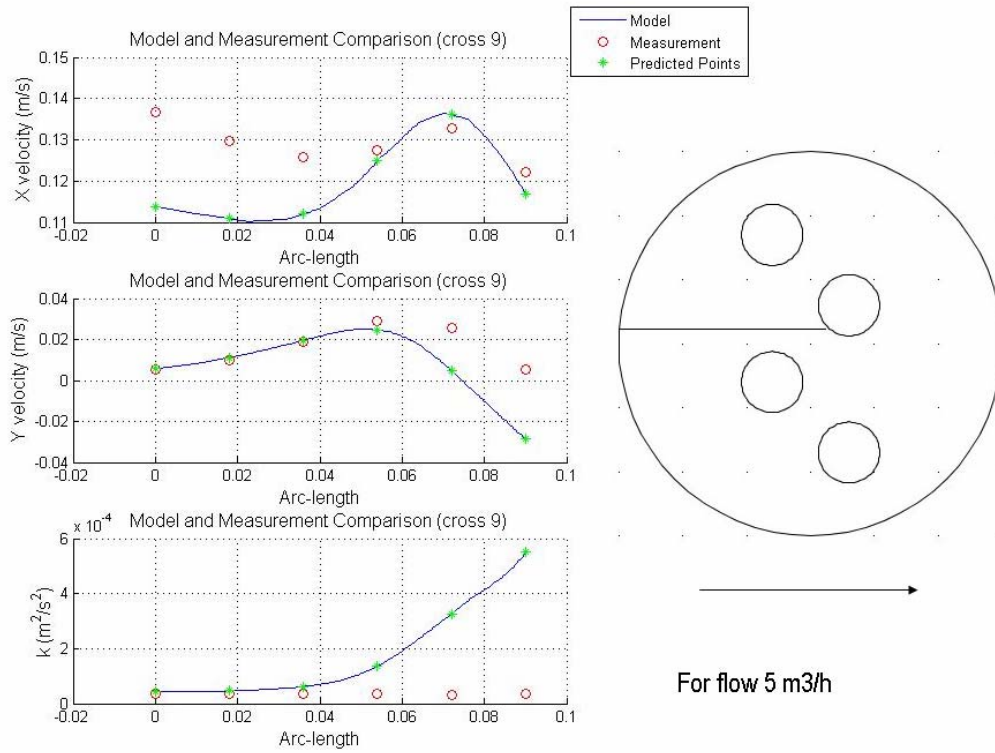




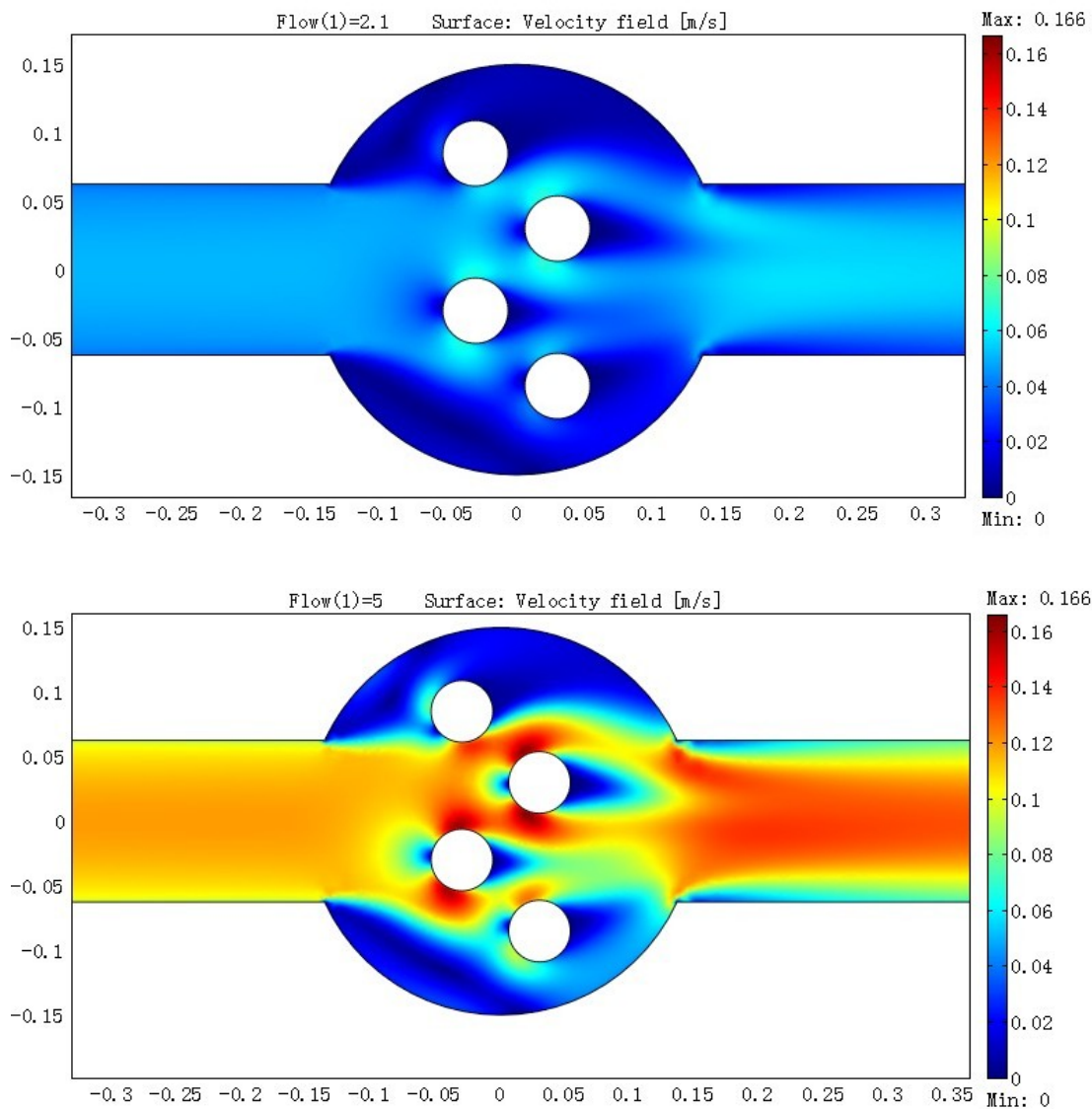




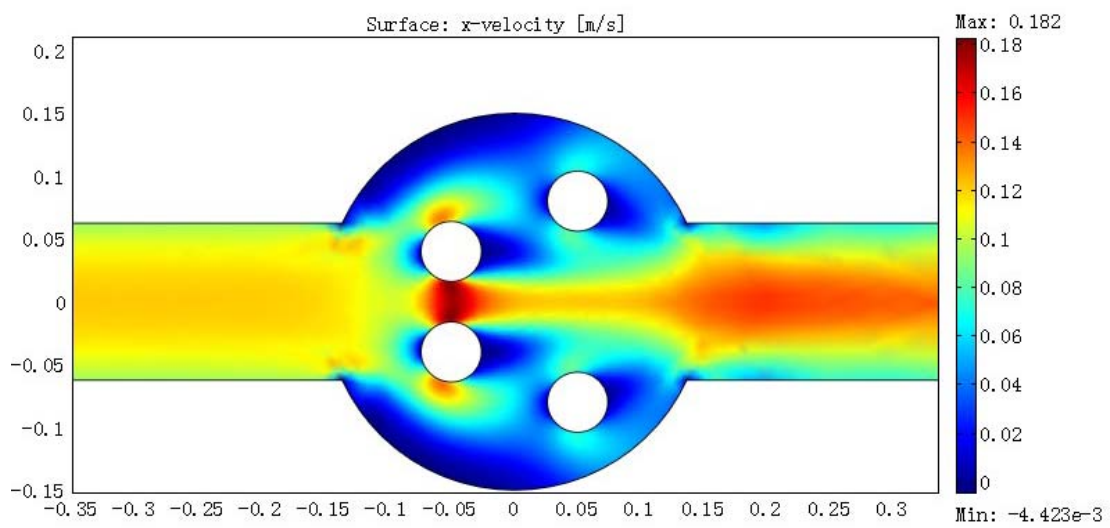
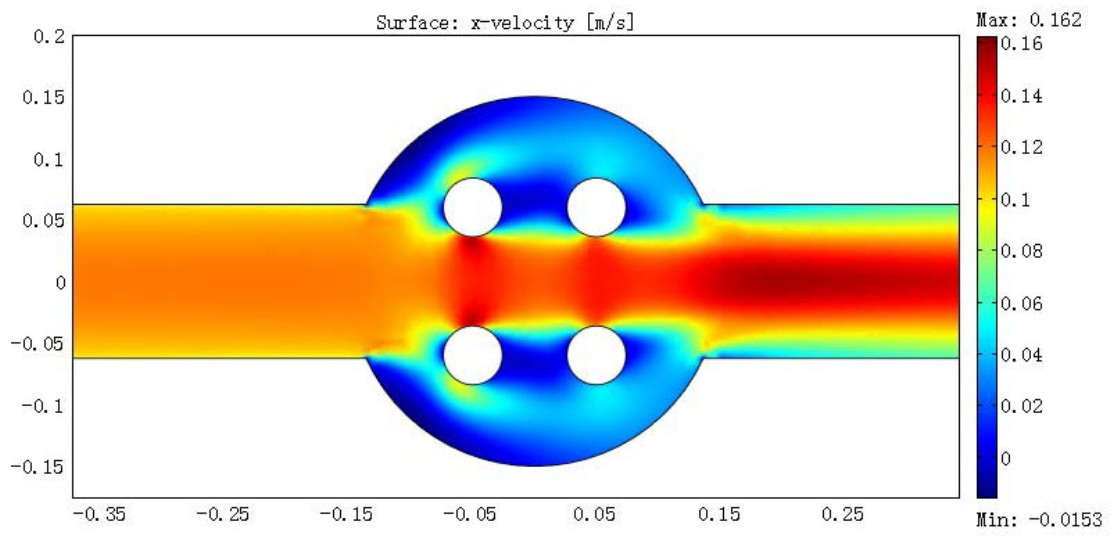
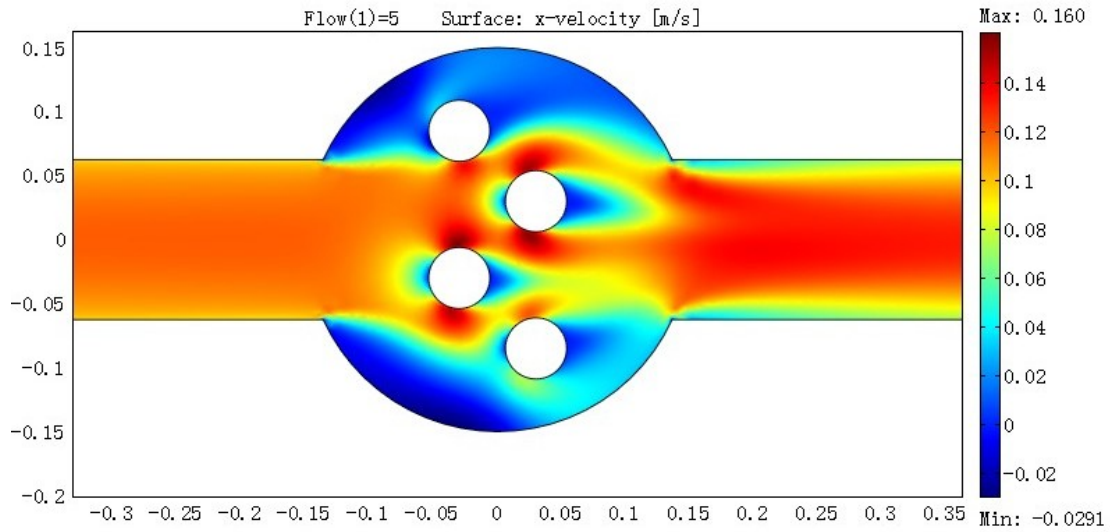




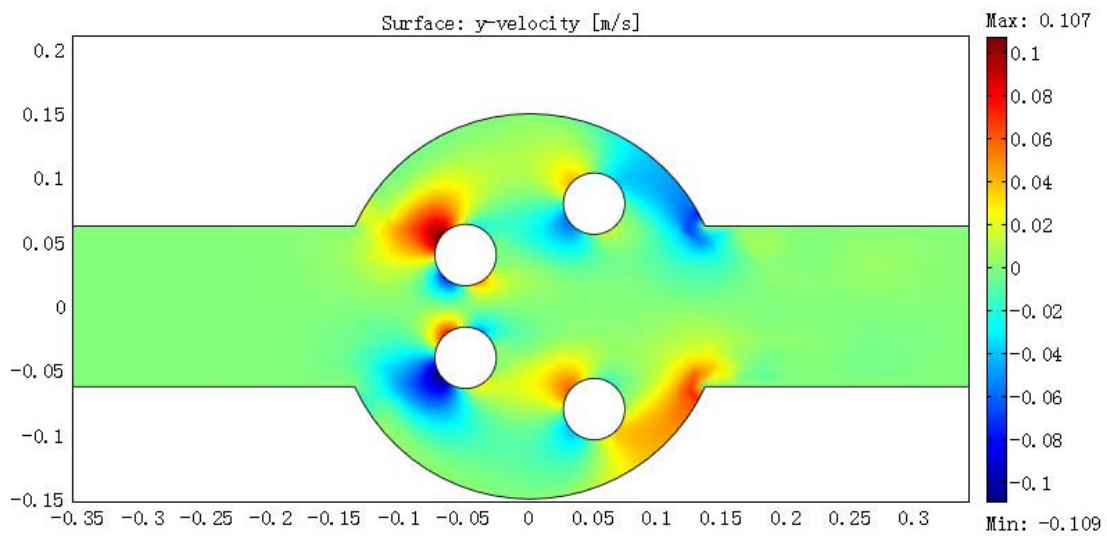
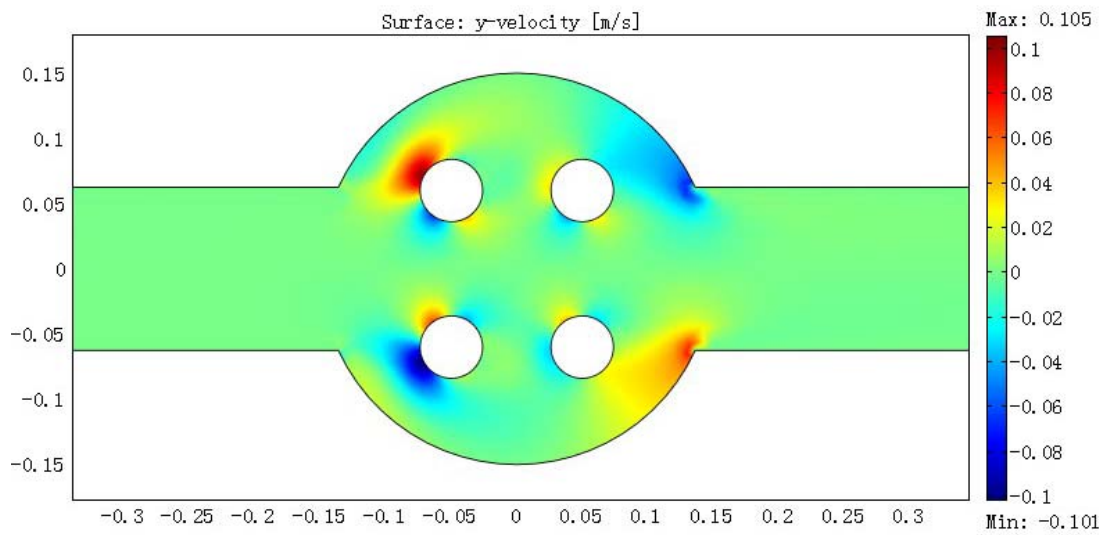
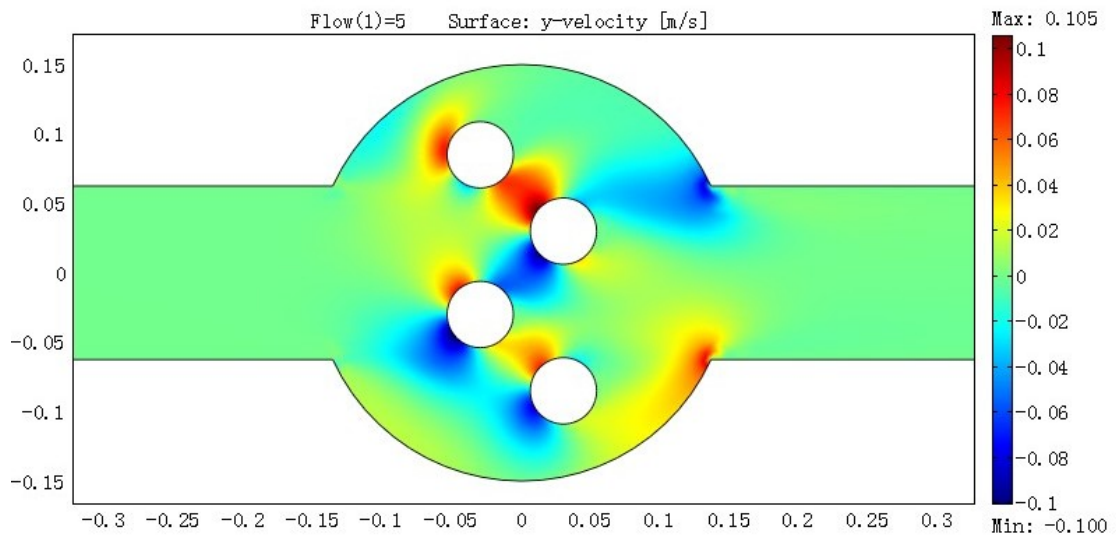
Appendix IV Other Flow Model Output



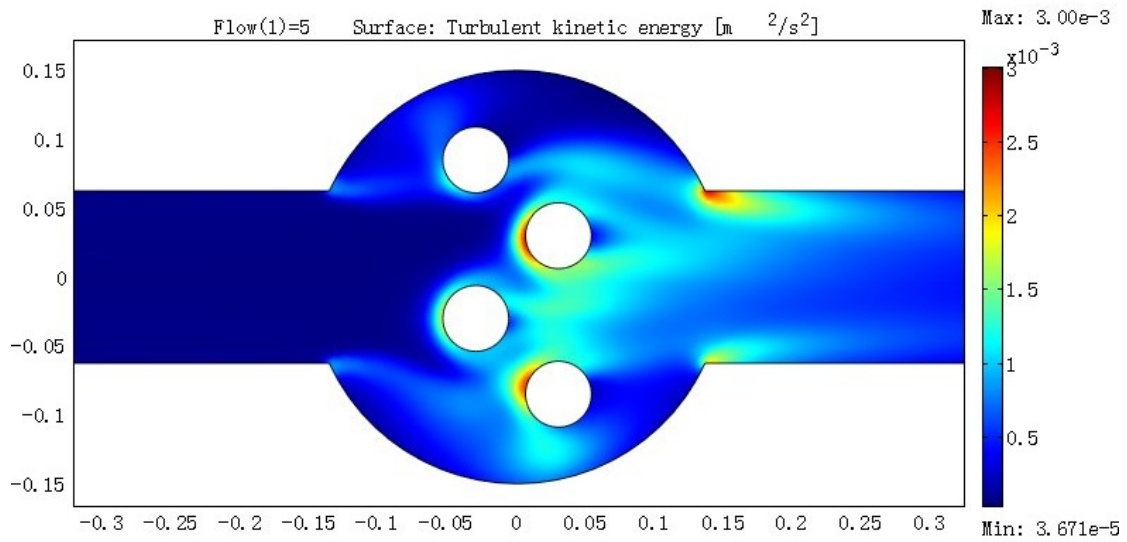
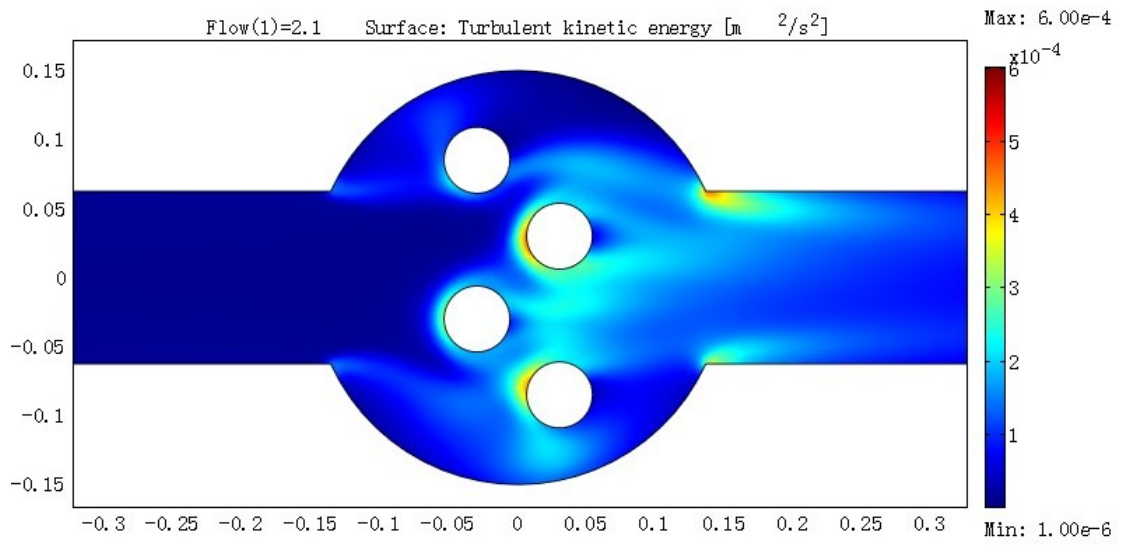
Velocity Field with Different flow rates, 2.1m³/h (top), 5m³/h (bottom)



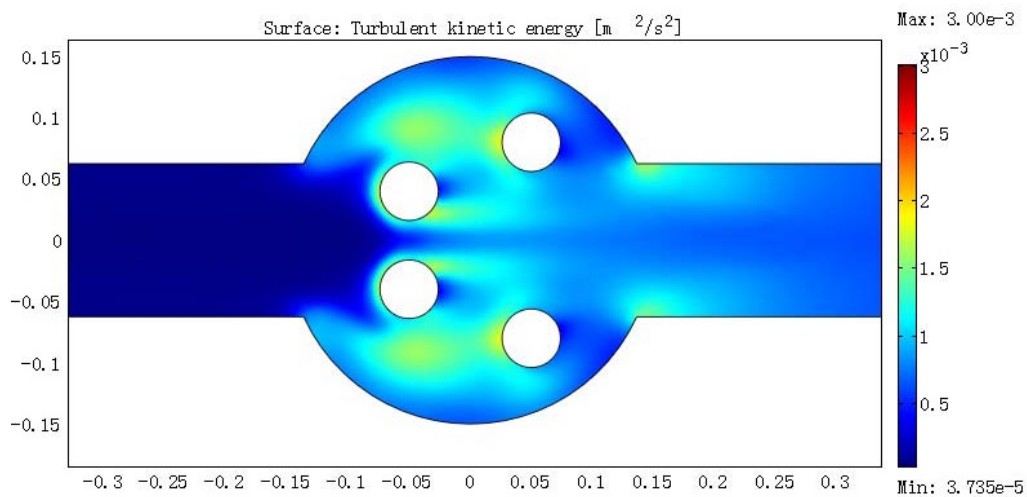
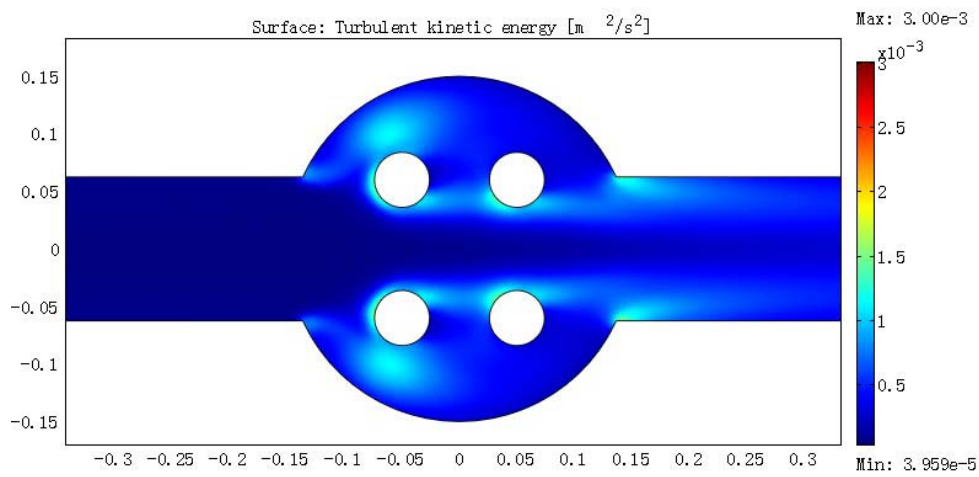
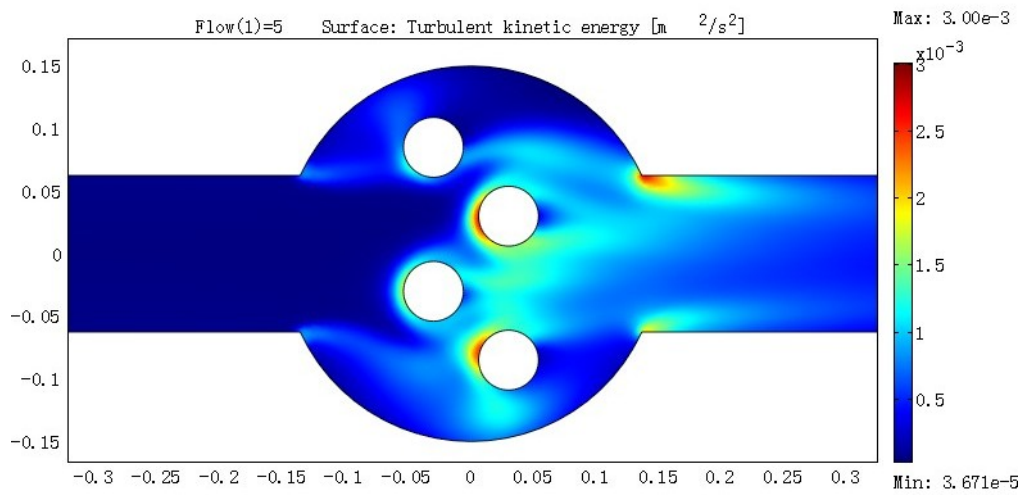
X Mean Velocity, position0(top), position 1(middle), position 2(bottom), $5\text{m}^3/\text{h}$



Y Mean Velocity, position0(top), position 1(middle), position 2(bottom), $5\text{m}^3/\text{h}$

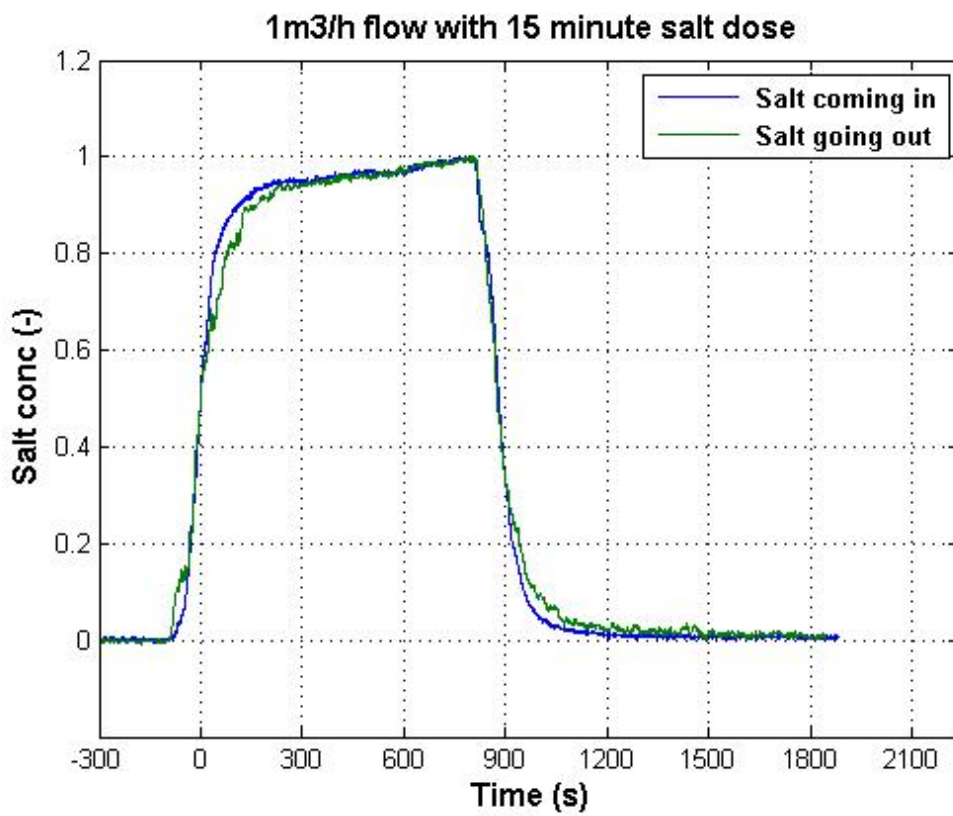
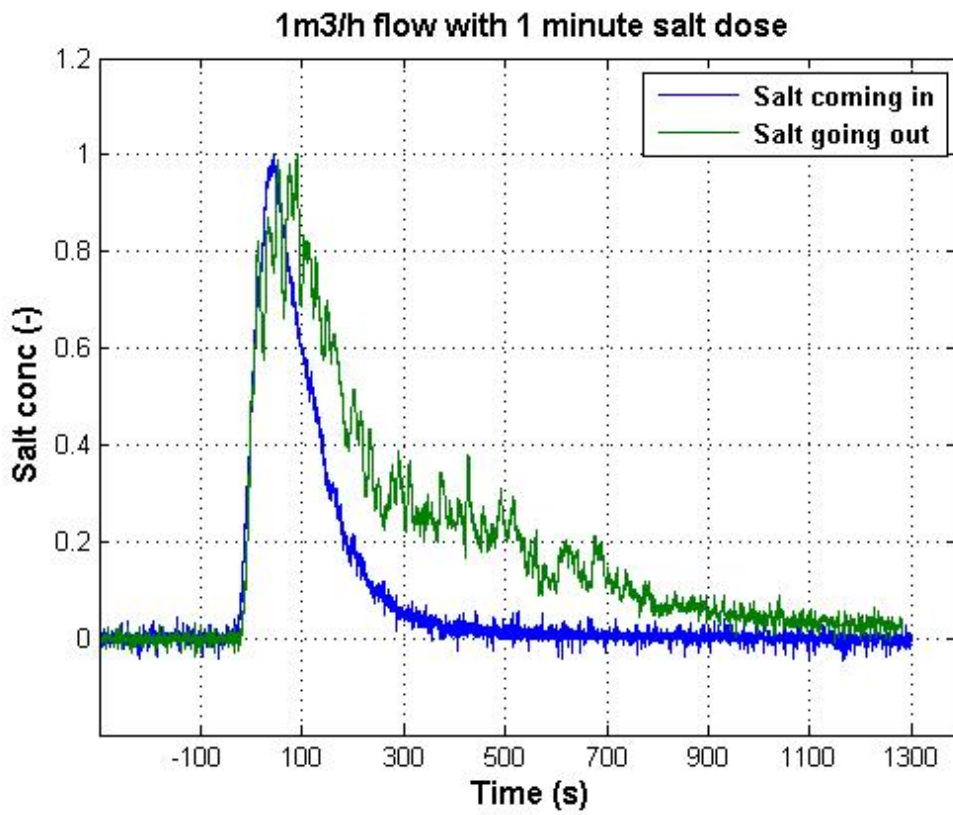


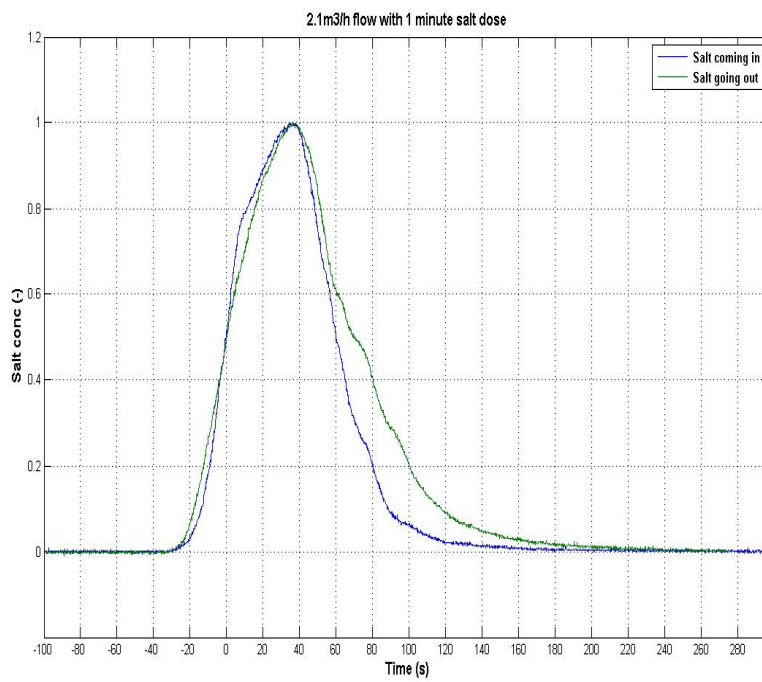
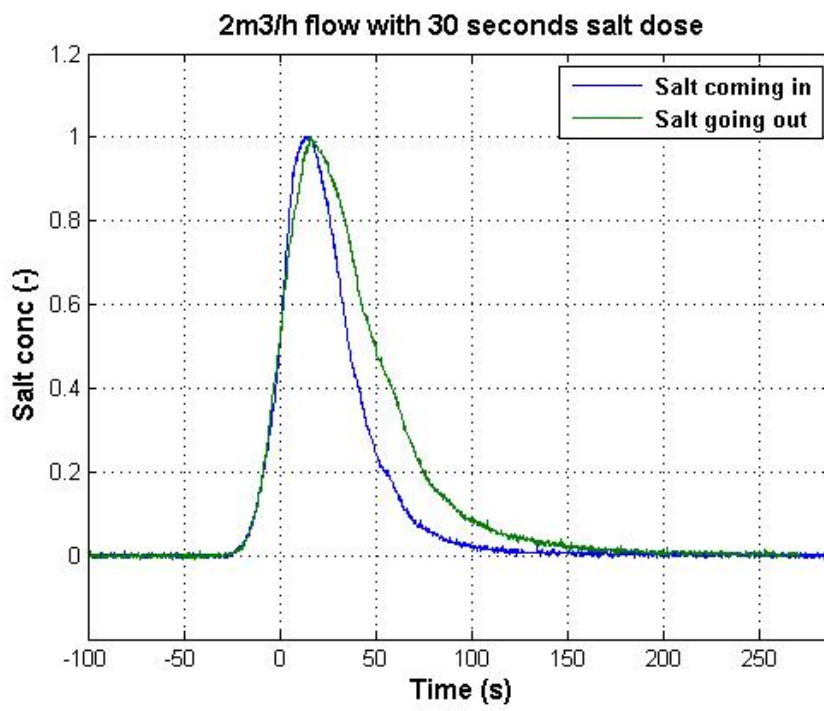
Turbulence Kinetic Energy, position0 , $2.1\text{m}^3/\text{h}$ (top) $5\text{m}^3/\text{h}$ (bottom)

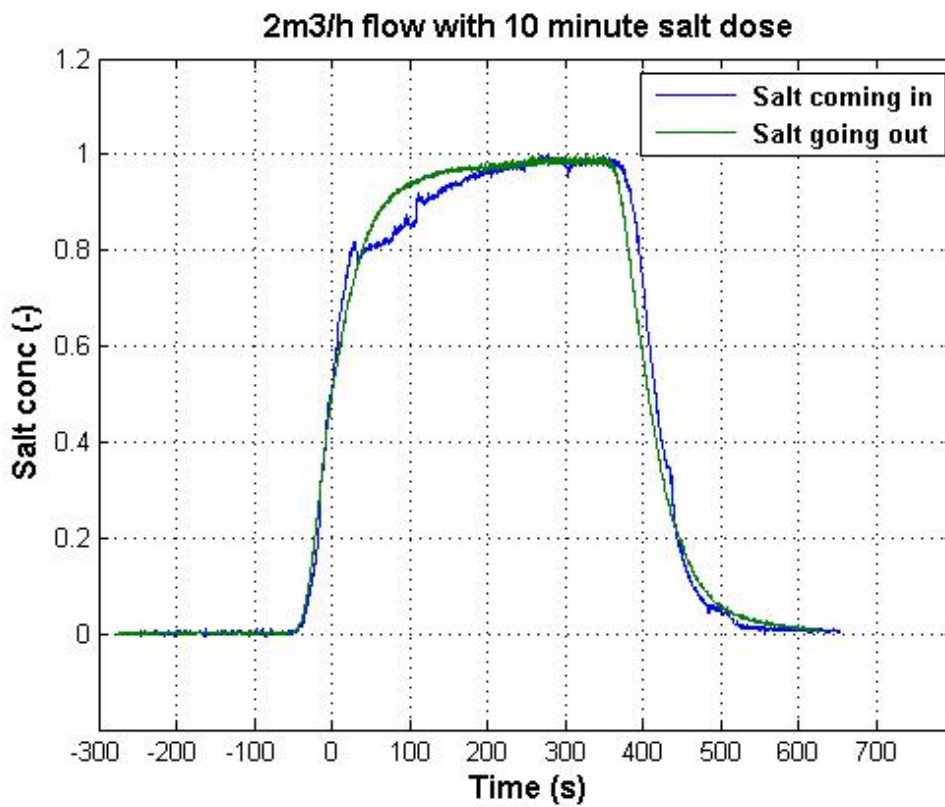
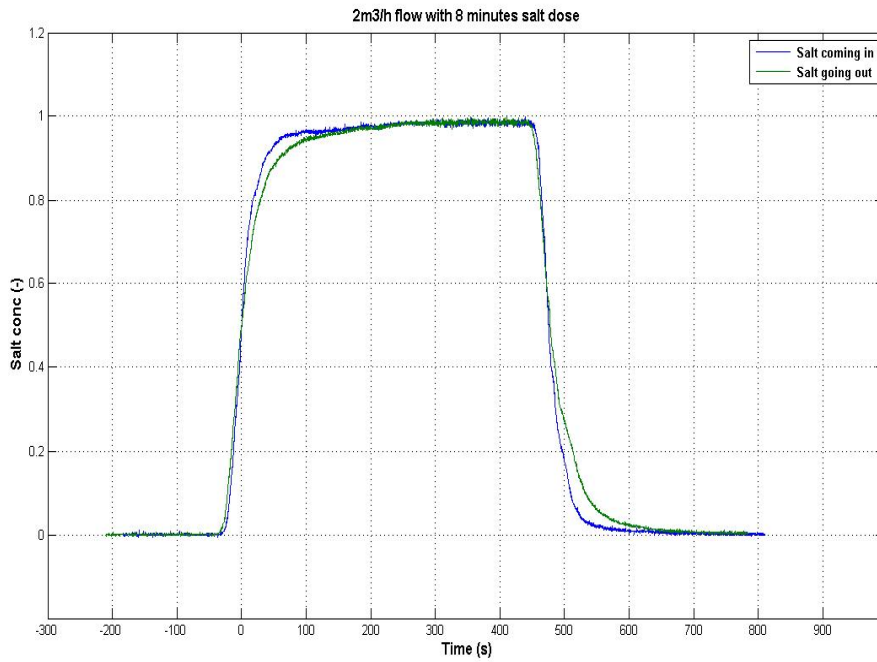


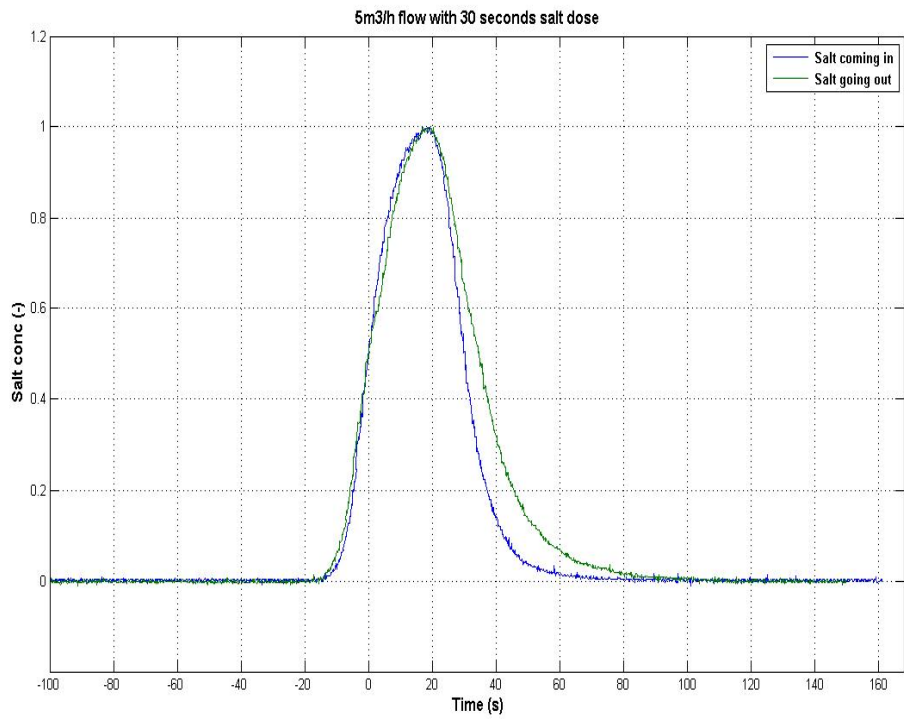
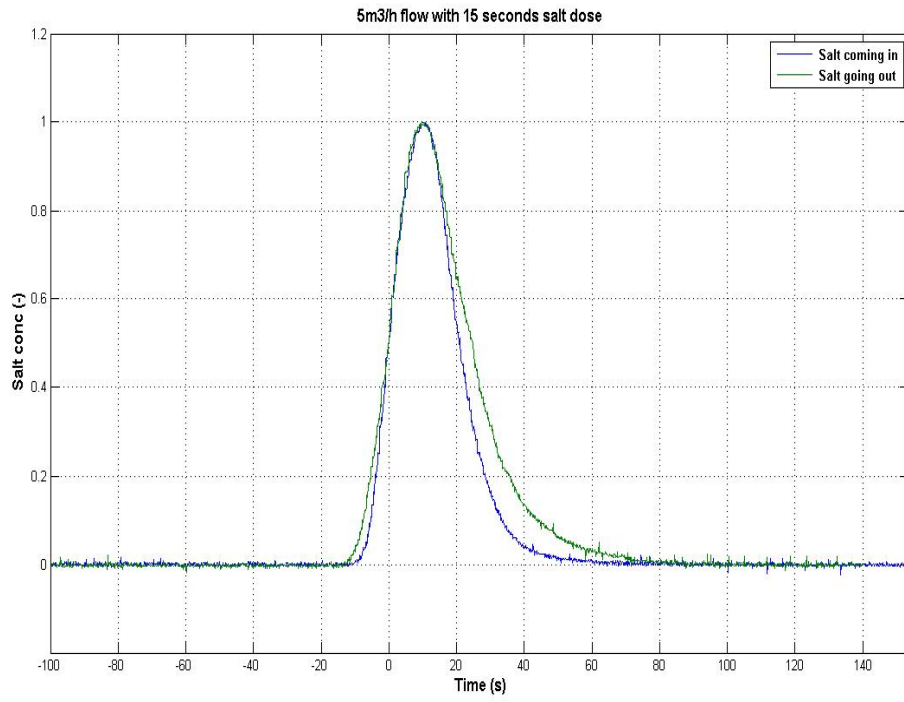
Turbulence Kinetic Energy, position0 (top) ,position 1(middle) , position 2 (bottom)
 $5 \text{m}^3/\text{h}$ (bottom)

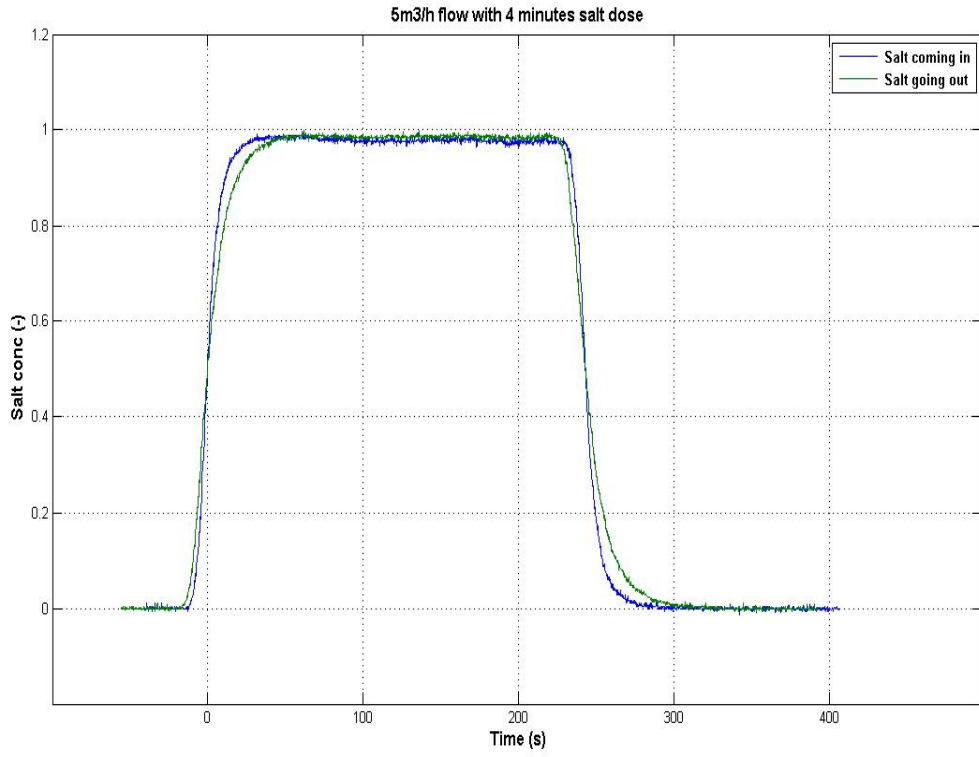
Appendix V Salt Dose Experiment Output











Appendix VI Dye Dose Video

Appendix VII Comsol Flow Models

Appendix VIII UV Dose Model

See the attached DVD

